**Faculty of Engineering and Computing**

# Vibration Frequencies of Whirling Rods and Rotating Annuli

**Wai Sun SHUM**

**This thesis is presented for the Degree of**
**Doctor of Philosophy**
**of**
**Curtin University of Technology**

**August 2005**

**Declaration**

This thesis contains no material which has been accepted for the award of any other degree or diploma in any university.

To the best of my knowledge and belief this thesis contains no material previously published by any other person except where due acknowledgment has been made.

Signature: 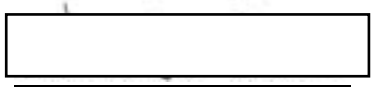

Date: 26 August 2005

**Acknowledgments**

This thesis is the result of a detailed and dedicated project by the author Wai Sun SHUM, who would like to thank his academic advisor Dr. Rodney D. Entwistle. The author is particularly grateful for the discussions with and suggestions from him on the vibration problems of static whirling rods and dynamic rotating annuli. Discussions include formulation of the proposed non-linear steady state model on whirling rods that involve the Poisson's effect in the deformation of rods. He also introduced the author to the rotating annuli vibration problem and suggested a non-linear formulation of the same problem. Throughout the course of studies, the author has received some financial and teaching relief from the Department of Mechanical Engineering, Curtin University of Technology.

Perth

Western Australia

## Abstract

*Static Whirling Rods*

Past researchers suggested that “static instabilities” exist at certain rotational speeds of whirling rods. This thesis shows these instabilities are an artefact of the material constitutive laws that are being used well outside their range of applicability. An alternative approach is developed where strains due to rotation are separated from the superimposed vibration. This enables the generally predicted lowering of longitudinal natural frequencies with rotational speed shown to be simply a result of the bulk changes in the geometry of whirling rods. Steady state equations of whirling rods are formulated in Lagrangian coordinates. Due to the non-linear nature of the governing equations, an original numerical method is applied to solve the problem. Numerical results are compared with analytical results obtained from the linearized uniaxial model. There is a close agreement between these two models at low angular velocities. However, at high angular velocities, discrepancies between them arise, confirming that the nonlinear strain-displacement relationship has significant effect on the results and the inferred “static instabilities”. This approach first solves the “static” problem of the deformed geometry of a highly strained whirling rod before longitudinal natural modes are determined by classical methods. Furthermore, conditions for existence and uniqueness of solutions are derived.

*Dynamic Rotating Annuli*

In-plane modes of vibration of annular plates are investigated. Two different models of equations one from Bhuta and Jones and the other from Biezeno and Grammel that govern the rotational motions of annuli will be studied. Since Biezeno and Grammel’s model was originally derived in Eulrian coordinates, their model will be transformed to the Lagrangian coordinates for the purpose of comparison with Bhuta and Jones’ model. The solutions of the equations assume small oscillations of vibration being superimposed on the steady state of the annulus while it is in rotation. Exact and approximate solutions are obtained for the Bhuta and Jones’ model, where the approximate solutions on in-plane displacements and natural frequencies are acquired by ignoring the Coriolis effect. A proposed numerical scheme is implemented to solve

the governing equations coupled with radial and circumferential displacements. Uniqueness of solutions will be mentioned although it will not be rigorously derived because it is out of the scope of this thesis. Approximate analytical results show that both radial and circumferential natural frequencies are decreasing when the rotational speed of an annulus is increasing. The exact and numerical results on both models that take the Coriolis effect into account show that radial natural frequencies are increasing and circumferential natural frequencies are decreasing when the rotational speed of an annulus is increasing.

## Contents

## Nomenclature

| | | |
|---|---|---|
| $a_i$'s | unknown constants to be determined with index $i$. | – |
| $a_r$ | radial acceleration of a rotating disc. | m/s$^2$ |
| $a_\theta$ | circumferential acceleration of a rotating disc. | m/s$^2$ |
| $A_0$ | uniform cross-sectional area of a non-rotating undeformed rod. | m$^2$ |
| $A(z)$ | cross-sectional area of a rod at $z$ of a deformed whirling rod. | m$^2$ |
| $A(x)$ | cross-sectional area of a rod at $x$ of a deformed whirling rod. | m$^2$ |
| $J_n(.)$ | Bessel function of the first kind of order $n$, | – |
| $C^1(0, L]$ | a class of functions that are continuously differentiable in $(0, L]$. | – |
| $C^2(R_1, R_2]$ | a class of functions that are twice continuously differentiable in $(R_1, R_2)$ and continuously differentiable at $R_2$. | – |
| $d_0$ | uniform diameter of a non-rotating undeformed rod. | m |
| $d(x)$ | diameter of a cross-sectional area at Lagrangian coordinate $x$. | m |
| $E$ | Young's modulus or modulus of elasiticity. | Pa |
| $f_i$'s | prescribed functions with index $i$. | |
| $f_N$ | axial natural frequencies obtained by the classical (receptance) approach. | rad/s |
| $F_R$ | radial body force in Eulerian coordinates | N |
| $F_\Theta$ | circumferential body force in Eulerian coordinates. | N |
| $F_r$ | radial body force in Lagrangian coordinates | N |
| $F_\theta$ | circumferential body force in Lagrangian coordinates. | N |
| $f_R$ | radial body force per unit volume in Eulerian coordinates | N/m$^3$ |
| $f_\Theta$ | circumferential body force per unit volume in Eulerian coordinates. | N/m$^3$ |
| $f_r$ | radial body force per unit volume in Lagrangian coordinates | N/m$^3$ |
| $f_\theta$ | circumferential body force per unit volume in Lagrangian coordinates. | N/m$^3$ |
| $G$ | shear modulus $G = \dfrac{E}{2(1+\upsilon)}$. | Pa |
| $g(.)$, $h(.)$ | known functions. | – |
| $L$ | length of a non-rotating undeformed rod. | m |
| $n$ | Size of the series in the proposed numerical solution. | – |

| | | |
|---|---|---|
| $N$ | An index with values of natural numbers. | – |
| $p_N$ | analytical axial natural frequencies for rotating deformed rod obtained by Bhuta and Jones (1963a). | rad/s |
| $P_r$ | amplitude of the radial excitation normal stress. | Pa |
| $P_c$ | amplitude of the torsional or circumferential excitation shear stress. | Pa |
| $R$ | Eulerian radial distance. | m |
| $r$ | Lagrangian radial distance. | m |
| $R_1$ | inner radius of a non-rotating annulus. | m |
| $R_2$ | outer radius of a non-rotating annulus. | m |
| $t$ | time variable. | s |
| $u(z)$ | longitudinal, axial or extensional displacement in Eulerian coordinate $z$. | m |
| $u(x)$ | longitudinal, axial or extensional displacement in Lagrangian coordinate $x$. | m |
| $u(R,t)$ | radial displacement at Eulerian $R$ and time $t$. | m |
| $u(r,t)$ | radial displacement at Lagrangian $r$ and time $t$. | m |
| $u_0(r)$ | static radial displacement of a rotating annulus. | m |
| $u_1(r)$ | dynamic radial displacement of a rotating annulus. | m |
| $v(R,t)$ | circumferential displacement at Eulerian $R$ and time $t$. | m |
| $v(r,t)$ | circumferential displacement at Lagrangian $r$ and time $t$. | m |
| $v_0(r)$ | static circumferential displacement of a rotating annulus. | m |
| $v_1(r)$ | dynamic circumferential displacement of a rotating annulus. | m |
| $x$ | Lagrangian coordinate $x = z - u(z)$. | m |
| $y_0$ | uniform thickness of a stationary undeformed annulus. | m |
| $y$ | thickness profile of a rotating deformed annulus. | m |
| $Y_n(.)$ | Bessel function of the second kind of order $n$. | – |
| $z$ | Eulerian coordinate $z = x + u(x)$. | m |
| $\alpha_{\xi\eta}$ | receptance for sub-structure $A$ with displacement at location $\xi$ and applied force at location $\eta$. | m/N |
| $\beta_{\xi\eta}$ | receptance for sub-structure $B$ with displacement at location $\xi$ and applied force at location $\eta$. | m/N |
| $\gamma_{\xi\eta}$ | receptance for sub-structure $C$ with displacement at location $\xi$ | m/N |

| | | |
|---|---|---|
| | and applied force at location $\eta$. | |
| $\gamma_{xy}$ | shear strain in Cartesian coordinates, i.e. change of angle in radian between the planes perpendicular to the $x$ and $y$ axes. | rad |
| $\gamma_{r\theta}$ | shear strain in Lagrangian coordinates, i.e. change of angle in radian between the planes perpendicular to the $r$ and $\theta$ axes. | rad |
| $\chi$ | the second order differential operator $\frac{d^2}{dr^2}+\frac{1}{r}\frac{d}{dr}-\frac{1}{r^2}$. | – |
| $\varepsilon_L(x)$ | lateral strain of a rod at the Lagrangian coordinate $x$. | – |
| $\varepsilon_z(x)$ | lateral strain of an annulus at the Lagrangian coordinate $x$. | – |
| $\varepsilon(z)$ | longitudinal, axial or extensional strain at $z$ of a deformed whirling rod. | – |
| $\varepsilon(x)$ | longitudinal, axial or extensional strain at $x$ of a deformed whirling rod. | – |
| $\varepsilon_R$ | radial normal strain in Eulerian coordinates. | – |
| $\varepsilon_\Theta$ | circumferential normal strain in Eulerian coordinates. | – |
| $\varepsilon_r$ | radial normal strain in Lagrangian coordinates. | – |
| $\varepsilon_\theta$ | circumferential normal strain in Lagrangian coordinates | – |
| $\upsilon$ | Poisson's ratio. | – |
| $\omega$ | excitation forcing circular frequency. | rad/s |
| $\omega_N$ | analytical axial natural frequencies for non-rotating undeformed rod. | rad/s |
| $\omega_{rN}^0, \omega_{rN}^{200\pi}$ | $N$th mode of radial natural frequencies of an annulus with no Coriolis forces predicted by the approximate solution in Subsection 4.2.2. Superscripts indicate the angular velocity of the annulus. | rad/s |
| $\omega_{cN}^0, \omega_{cN}^{200\pi}$ | $N$th mode of circumferential natural frequencies of an annulus with no Coriolis forces predicted by the approximate solution in Subsection 4.2.2. Superscripts indicate the angular velocity of the annulus. | rad/s |
| $\Omega$ | Angular velocity of a whirling rod or a rotating annulus. | rad/s |
| $\phi_{rN}^0, \phi_{rN}^{200\pi}$ | $N$th mode of radial natural frequencies of an annulus with Coriolis forces predicted by the exact solution in Subsection 4.2.3. Superscripts indicate the angular velocity of the annulus. | rad/s |

| | | |
|---|---|---|
| $\phi_{cN}^{0}, \phi_{cN}^{200\pi}$ | *N*th mode of circumferential natural frequencies of an annulus with Coriolis forces predicted by the exact solution in Subsection 4.2.3. Superscripts indicate the angular velocity of the annulus. | rad/s |
| $\Phi_{\Xi}^{1t}, \Phi_{\Xi}^{2t}$ | time-domain second order differential operators on interior of domain *r* and time *t*. | – |
| $\Phi_{\Xi}^{1\omega}, \Phi_{\Xi}^{2\omega}$ | frequency-domain second order differential operators on interior of domain *r* and frequency $\omega$. | – |
| $\Phi_{\partial\Xi}^{i}$ | frequency-domain differential operators at the boundary of domain *r*, $i$ = 1, 2, 3, 4. | – |
| $\varphi_{rN}^{0}, \varphi_{rN}^{200\pi}$ | *N*th mode of radial natural frequencies of an annulus with Coriolis forces predicted by Biezeno and Grammel's model using numerical method in Section 4.3. Superscripts indicate the angular velocity of the annulus. | rad/s |
| $\varphi_{cN}^{0}, \varphi_{cN}^{200\pi}$ | *N*th mode of circumferential natural frequencies of an annulus with Coriolis forces predicted by Biezeno and Grammel's model using numerical method in Section 4.3. Superscripts indicate the angular velocity of the annulus. | rad/s |
| $\Psi_{\Xi}$ | nonlinear integro-differential operator on interior of domain *x*. | – |
| $\Psi_{\Xi}^{1}, \Psi_{\Xi}^{2}$ | second order differential operators on interior of domain *r*. | – |
| $\Psi_{\partial\Xi}^{i}$ | differential operators at the boundary of a domain, $i$ = 1, 2, 3, 4. | – |
| $\rho_0$ | constant material density of a non-rotating undeformed rod. | kg/m$^3$ |
| $\rho(z)$ | material density at *z* of a deformed whirling rod. | kg/m$^3$ |
| $\rho(x)$ | material density at *x* of a deformed whirling rod. | kg/m$^3$ |
| $\sigma_R$ | radial normal stress in Eulerian coordinates. | Pa |
| $\sigma_\Theta$ | circumferential normal stress in Eulerian coordinates. | Pa |
| $\sigma_r$ | radial normal stress in Lagrangian coordinates. | Pa |
| $\sigma_\theta$ | circumferential normal stress in Lagrangian coordinates. | Pa |
| $\tau_{xy}$ | shear stress acting parallel to the *y*-axis on the surface perpendicular to the *x*-axis in Cartesian coordinates. | Pa |
| $\tau_{R\Theta}$ | circumferential shear stress acting in $\Theta$ direction and on the plane perpendicular to the *R*-axis in Eulerian coordinates. | Pa |
| $\tau_{r\theta}$ | circumferential shear stress acting in $\theta$ direction and on the plane | Pa |

| | | |
|---|---|---|
| | perpendicular to the $r$-axis in Lagrangian coordinates. | |
| $\Theta$ | Eulerian coordinate in the circumferential direction. | rad |
| $\theta$ | Lagrangian coordinate in the circumferential direction. | rad |
| $\vartheta(r,t)$ | angular displacement at Lagrangian $r$ and time $t$. | rad |
| $\vartheta_0(r)$ | static angular displacement of a rotating annulus. | rad |
| $\vartheta_1(r)$ | dynamic angular displacement of a rotating annulus. | rad |
| $\Xi$ | interior of a domain. | – |
| $\partial\Xi$ | boundary of a domain, | – |
| $\zeta_{rN}^{0}, \zeta_{rN}^{200\pi}$ | $N$th mode of radial natural frequencies of an annulus with Coriolis forces predicted by Bhuta and Jones' model using numerical method in Section 4.3. Superscripts indicate the angular velocity of the annulus. | rad/s |
| $\zeta_{cN}^{0}, \zeta_{cN}^{200\pi}$ | $N$th mode of circumferential natural frequencies of an annulus with Coriolis forces predicted by Bhuta and Jones' model using numerical method in Section 4.3. Superscripts indicate the angular velocity of the annulus in rad/s. | rad/s |

# Chapter 1

## Introduction

### *1.1 Scope and Background of the Investigation*

The aim of this thesis is to study the large strain deformation of steadily whirling rods, axial natural frequencies of steady whirling rods, in-plane natural frequencies of dynamic axisymmetric rotating annuli and solutions of complex coupled differential equations.

Application of whirling rod-like components can be found in the design of turbine blades that generate electrical power from wind power and helicopter blades that generate lift for air-borne vehicles (Figure 1.1).

Figure 1.1. Reprint from "Bramwell's helicopter dynamics (2nd edition)" by A. R. S. Bramwell, Oxford, England : Butterworth-Heinemann, ©2001, with permission from Elsevier.

At low angular velocity, axial displacements are relatively small compared to the original length of the rod. Hence a small strain analysis of the problem is adequate. As the angular velocity of a whirling rod increases, axial displacements of the rod increase due to the higher centripetal or centrifugal force. As a result, the linear strain-displacement relationships assumed in small strain analyses may be no longer valid. In order to better approximate vibration problems under large strain deformation, nonlinear strain-displacement relationships should be employed. For some machinery designs, accurate estimations of the extension of a rod-like object to provide room for clearance while it is rotating at high angular velocity are required. Moreover, axial natural frequencies of whirling rods will be scrutinized due to the deformed shape caused by the centripetal force of rotation.

Additionally, in-plane vibrations of annular plates are of interest in applications in a number of areas such as circular saws for wood cutting, grinding wheels with thousands of hard and tough abrasive grains distributed throughout the wheels that move against the workpiece to cut away tiny chips of material such as diamond, steam turbine discs and compact discs or digital versatile discs for storage of digital information such as music or movies (Figure 1.2).


Figure 1.2. Photograph of a compact disc with digital data being retrieved into music while rotating in a CD−ROM.

In rotating annulus problems, studies are carried out to investigate if there is a link between the rotational speed $\Omega$ and the in-plane natural frequencies of the annulus. The significance of studying the natural frequencies of rod-like and disc-like objects while they are rotating is to prevent a catastrophic failure of material. When the frequency of an external excitation coincides with one of the natural frequencies of vibration of an object, resonance occurs. At resonance, the amplitude of vibration of the object becomes large with associated stresses leading to material fatigues, fractures or loss of functions. Therefore, an accurate prediction of natural frequencies becomes crucial for the design of structures that consist of rotating rod-like and/or disc-like components.

For in-plane vibrations of rotating annuli at low angular velocities, motion is governed by a system of differential equations coupled with radial and circumferential displacements. Because of the difficulty of solving coupled differential equations both analytically and numerically, they are usually decoupled under the assumption that the Coriolis effect is small. However, such an assumption might give rise to an erroneous estimate of the natural frequencies of vibration of rotating annuli.

### *1.2 Preliminaries of Previous Work*

Practical vibration problems are limited to the linear elastic region of the stress-strain relationships of elastic materials. In general, the physical rule that governs this linear elastic region is the Hooke's law. However, some previous published work (Kinkaid *et al*. (2001)) has given results with strains well beyond the applicability of Hooke's law for existing material.

When an axial stress is applied to a rod, the cross-sectional area of the rod is altered due to Poisson's effect. As volume is not conserved, local density alters. That is, the material of the rod no longer remains isotropic. A similar physical phenomenon happens to an annulus. As a result, when rods and annuli are rotating, the cross-sectional areas of rods and thicknesses of annuli will be altered as well as the material density. In most of the previous work[1] involving whirling rods and rotating annuli, such variations have not been taken into account.

[1] Chapter 2: Literature Review.

In previous work by other researchers, most assumed small strain deformation. That is material is not deformed by a large amount compared to the dimension of the object which implies linear strain-displacement relationships [2] could be adopted. This simplified the analysis of solving linear governing differential equations that made the analytical solution possible. Nonetheless, such a small strain assumption did not take the Poisson's effect into account. Previous work in determining the natural frequencies has a common feature. The predictions were dependent on allowing incorrect large strain deformation and they excluded the Poisson's effect. Furthermore, controversy has occurred as to whether natural frequencies of rotating components are increasing or decreasing as the angular velocity of rotation is increasing.

### *1.2.1 Eulerian and Lagrangian Formulations*

In this thesis, a whirling rod is taken to be an initially prismatic rod that is rotating about an axis passing through one end and perpendicular to the longitudinal axis of the rod. Similarly, when a disc or an annulus is rotating at its centre about a centroidal axis perpendicular to the plane of rotation, it is referred to as a disc or an annulus under rotating motion. Vibration problems on whirling rods and rotating annuli have been formulated in both Eulerian and Lagrangian coordinates. When an observer is fixed at a location while an object is vibrating, the observer will see the vibration motion of the object. By definition, the observer is using the Eulerian coordinate system to reference the motion of the object. On the other hand, if an observer is moving along with a point on a vibrating object, the observer will see no motion of that particular point at all time. Such a referencing system is known as the Lagrangian coordinate system. Mathematically, Eulerian coordinates and Lagrangian coordinates for rods are related by

$$z = x + u(x, t)$$

or

$$x = z - u(z, t),$$

where $z$ is the Eulerian coordinate, $x$ is the Lagrangian coordinate, $u(z, t)$ and $u(x, t)$ are the longitudinal, axial or extensional displacement of a rod at location $z$ and $x$

[2] Fung, Y.C., 1994, "A First Course in Continuum Mechanics (Third Edition)", Prentice Hall.

respectively at time *t*. Eulerian coordinates and Lagrangian coordinates for axisymmetric discs or annuli are related by

$$R = r + u(r, t)$$

or

$$r = R - u(R, t),$$

where $R$ is the radial Eulerian coordinate, $r$ is the radial Lagrangian coordinate, $u(R, t)$ and $u(r, t)$ are the radial displacement of a disc or an annulus at location $R$ and $r$ respectively at time $t$. Both coordinate systems had been pursued in previous work.[3] Although it is more convenient to use Eulerian coordinates, it has difficulties when imposing boundary conditions at the free end of a rod and the free edge of a disc or an annulus. On the contrary, problems formulated in Lagrangian coordinates enjoy the ease of imposing the free end or free edge boundary conditions, however, issue of existence and uniqueness of solution arises.

### *1.2.2 Whirling Rods*

Derivations of governing equations using 1-D Hooke's law on both Eulerian and Lagrangian coordinates by excluding the Poisson's effect have been performed.[4] In order to relate the stress to displacement $u$ during the derivation of the governing equations, strain-displacement relationships are mandatory because 1-D Hooke's law is a relationship between stress and strain. According to Fung,[2] Eulerian axial strain $\varepsilon_E$ and Lagrangian axial strain $\varepsilon$ for rods are known to be

$$\varepsilon_E = \frac{\partial u}{\partial z} - \frac{1}{2}\left(\frac{\partial u}{\partial z}\right)^2 \text{ and } \varepsilon = \frac{\partial u}{\partial x} + \frac{1}{2}\left(\frac{\partial u}{\partial x}\right)^2.$$

For small strain analysis, $\varepsilon_E$ and $\varepsilon$ are approximated by

$$\varepsilon_E \approx \frac{\partial u}{\partial z} \text{ and } \varepsilon \approx \frac{\partial u}{\partial x}.$$

[3] Bhuta, P.G. and Jones, J.P., 1963b, "Symmetric Planar Vibrations of a Rotating Disk", *The Journal of the Acoustical Society of America*, **35**, pp. 982 – 989.

[4] Bhuta, P.G. and Jones, J.P., 1963a, "On Axial Vibrations of a Whirling Bar", *The Journal of the Acoustical Society of America*, **35**, pp. 217 – 221.

It is clear from the above expressions that for small strain analysis, where $\left|\frac{\partial u}{\partial z}\right| << 1$ and $\left|\frac{\partial u}{\partial x}\right| << 1$, the nonlinear square terms are being ignored to form the linear approximations. After the governing equations were obtained in terms of the axial displacement *u* either in Eulerian or Lagrangian coordinate, they can be solved analytically and numerically.

From previous work,[4] governing equations that excluded the Coriolis effect generally predict the lowering of natural frequencies as the whirling speeds of rods were increasing. On the contrary, there are speculations on governing equations that include the Coriolis effect will predict a different result for natural frequencies.

### *1.2.3 Rotating Discs or Annuli*

Similar to the rod problems, previous derivations[3] of governing equations using 2-D Hooke's law on rotating annuli had not included the Poisson's effect. Thus, thickness and density variations of annular plates while they are rotating have been disregarded. Again, in order to relate the stress to displacement *u* in the derivation of the governing equations, strain-displacement relationships are mandatory because 2-D Hooke's law are relationships between stresses and strains. According to Fung,[2] Eulerian radial normal strain $\varepsilon_R$ and Eulerian circumferential normal strain $\varepsilon_\Theta$ for small strain analysis are given by

$$\varepsilon_R = \frac{\partial u}{\partial R} \text{ and } \varepsilon_\Theta = \frac{u}{R},$$

Lagrangian radial normal strain $\varepsilon_r$ and Lagrangian circumferential normal strain $\varepsilon_\theta$ for small strain analysis are given by

$$\varepsilon_r = \frac{\partial u}{\partial r} \text{ and } \varepsilon_\theta = \frac{u}{r},$$

Eulerian circumferential shear strain $\gamma_{R\Theta}$ and Lagrangian circumferential shear strain $\gamma_{r\theta}$ for small strain analysis are given by

$$\gamma_{R\Theta} = \frac{\partial v}{\partial R} - \frac{v}{R} \text{ and } \gamma_{r\theta} = \frac{\partial v}{\partial r} - \frac{v}{r},$$

where $v = v(R, t)$ is the circumferential displacements in Eulerian coordinates $(R, \Theta)$ at time $t$ and $v = v(r, t)$ is the circumferential displacements in Lagrangian coordinates $(r, \theta)$ at time $t$.

The resulting governing equations constitute a system of differential equations that are coupled with the radial and circumferential displacements through the Coriolis effect. Due to the difficulty of solving the coupled equations, the Coriolis effect was usually assumed to be small[3] and has been ignored in order to obtain an analytical solution. The result from such an assumption in general resembled those for steadily whirling rods in that they predicted the lowering of natural frequencies when the rotating speed was increasing.

Although results for natural frequencies of decoupled equations for rotating discs or annuli by ignoring the Coriolis effect had been obtained,[3] none of the papers in the previous work have given a method, either theoretically or numerically, that generate the natural frequencies for rotating discs or annuli that take the Coriolis effect into account. Similar to rods, there are speculations on governing equations that include the Coriolis effect will predict a different result for natural frequencies.

## *1.3 Current Work*

This thesis aims to make a contribution towards the improvement of the models and predictions of natural frequencies of whirling rods and rotating annuli by including some of the parameters previously neglected. In addition, Poisson's effect will be included in the models to account for the variations of cross-sectional areas of whirling rods, thicknesses of rotating annuli and material densities for both whirling rods and rotating annuli.

### *1.3.1 Steady Whirling Rods*

It is known that elastic instabilities occur at or beyond certain angular velocity of rotation. The existence of elastic instabilities has been debated for over 40 years and is still not resolved. This thesis approaches the steady whirling rods problem by

concentrating on the geometrical deformation of the rods due to rotational strains. Non-linear integro-differential governing equations are formulated that include the Poisson's effect into the steady rotation of rods. This means the nonlinear strain-displacement relationships discussed in Subsection 1.2.2 are incorporated into the governing equations. These equations are solved by the proposed numerical method. Results obtained from the deformed geometry that included the variations of cross-sectional area and material density are used to calculate the axial natural frequencies by the classical approach. Elastic instabilities will be shown to be equivalent to the issue of existence and uniqueness of solution in Chapter 3.

### *1.3.2 Dynamic Rotating Annuli*

Two existing models of rotating annuli including vibration dynamics, one from Bhuta and Jones[3] and the other one from Biezeno and Grammel[5], will be scrutinized. Poisson's effect is added into the steady rotation of Biezeno and Grammel's model. Solutions are achieved by separating the deformation of the annular plates due to rotational strains from the superimposed vibrational motions. Analytical solutions are acquired for the coupled system of differential equations on the Bhuta and Jones' model. These analytical solutions will be compared with the results drawn from the proposed numerical method. Frequency response approach, which identifies the relationship between displacements and excitation forcing frequency spectrum, will be called upon to search for the natural modes of rotating annuli with Coriolis effect. Approximate solution extracted from the decoupled governing equations by excluding the Coriolis effect will be shown to have a slight difference in estimating the natural frequencies of vibration. Finally, comparisons between the analytical and numerical results of the Bhuta and Jones' model on radial and circumferential mode shapes will be presented in Chapter 4.

[5] Biezeno, C.B. and Grammel, R., 1954, "Engineering Dynamics, Volume 3 Steam Turbines (Translated from the original German (1939, 1953) by E.F. Winter and H.A. Havemann)", Blackie and Son Ltd, pp. 34.

### *1.3.3 Proposed Numerical Method*

In Chapter 3 and Chapter 4, numerical solutions are computed from the proposed numerical method. This method resembles collocation, Galerkin and Rayleigh-Ritz methods,[6] although not exactly the same. All these methods assume the unknown solution of governing equations to be represented by a linear combination of prescribed functions, namely $\sum_{i=0}^{n} a_i f_i$ , where $a_i$'s are the unknown coefficients to be determined, $f_i$'s are the prescribed functions and $n$ is a non-negative integer. In the end, a non-linear algebraic system of equations is generated to be solved by the Newton's method for the unknowns $a_i$'s. Collocation, Galerkin and Rayleigh-Ritz methods belong to the family of projection methods. The prescribed functions $f_i$'s are often called the basis functions. These basis functions could be orthogonal to each other. One of the choices of these basis functions is the Chebyshev polynomials of first and second kind. Nonetheless, the prescribed functions embraced in the proposed numerical method are demanded to be a complete representation of the unknown solution in Newton's sense. Completeness of a solution in Newton's sense simply means that the numerical solutions produced by the Newton's iteration method converge to the true solution. This criterion might not be satisfied if the chosen prescribed functions are not otherwise complete in the Newton's sense. For instance, the Chebyshev polynomials might not be a complete representation of the unknown solution in Newton's sense. Recently, there is another similar approach that chooses the prescribed functions as radial basis functions. The representation of an unknown solution has the form $\sum_{i=0}^{n} a_i f(|\mathbf{r} - \mathbf{r_i}|)$, where $\mathbf{r}$ and $\mathbf{r_i}$ represent variable points and chosen fixed points respectively in the computational domain. Some of the well-known radial basis functions are:

Generalized multiquadric: $f(r) = (r^2 - c^2)^m$

Gaussian: $f(r) = \exp(-cr^2)$

Generalized thin-plate spline: $f(r) = r^m \ln(r)$

[6] mathworld.wolfram.com

where *c* and *m* are predefined constants. Readers may refer to Chantasiriwan,[7,8] who recently demonstrated the application of radial basis functions to unveil the solutions for the multidimensional problems of Poisson, Helmholtz and diffusion-convection equations.

### *1.4 Thesis Outline*

This chapter has provided an overview of the current and past approaches on whirling rods and rotating annuli. Chapter 2 gives a thorough literature review of the past papers that are related to current work. Chapter 3 addresses the steady whirling rods and their vibration frequencies at steady rotation. Moreover, "static instabilities" are shown to be same as an issue of the existence and uniqueness of solution. Chapter 4 presents the dynamic rotating annuli problems that include the Corislis effect with results on dynamic natural frequencies and mode shapes. Chapter 5 provides critiques of the mathematical models, boundary conditions, cross-sectional area of rods and thickness of annuli, analytical solutions, proposed numerical method, results and the implications for machine design. Chapter 6 summarizes the results obtained from the studies of steady whirling rods and dynamic rotating annuli with some suggested future work. Lastly, the appendices include all the related physical laws, previously derived equations of motion, classical substructuring receptance approach for natural frequencies and general theorem on the existence and uniqueness of solution.

[7] Chantasiriwan, S., 2004a, "Investigation of the Use of Radial Basis Functions in Local Collocation Method for Solving Diffusion Problems", *International Communications in Heat and Mass Transfer*, **31**, pp. 1095 – 1104.

[8] Chantasiriwan, S., 2004b, "Cartesian Grid Methods Using Radial Basis Functions for Solving Poisson, Helmholtz and Diffusion-Convection Equations", *Engineering Analysis with Boundary Elements*, **28**, pp. 1417 – 1425.

# Chapter 2

## Literature Review

### *2.1 Whirling Rods*

The study of axial, longitudinal or extensional vibration frequencies of a rod rotating at one end has been of interest for over a century. Beginning at the end of 18th century, researchers had already looked into the vibration of different stationary objects. Pochhammer (1876) investigated certain modes of vibration of circular cylinders (also see Love (1944)). Chree (1889) obtained results for longitudinal vibration of an isotropic elastic non-rotating straight bar with non-circular cross section. Not until the middle of the 19th century, researchers started to formulate the constitutive laws and governing equations of motion for whirling bars and rods. Methods of estimating the frequencies have been published since 1963 (see Bhuta and Jones (1963a)). The problem remains unresolved, as disagreement ('controversy', Venkatesan and Nagaraj (1981)) exists on whether the natural frequencies are increasing or decreasing with increasing rotational speed. Furthermore, it is generally agreed that static longitudinal strain becomes unbounded when a certain rotational speed is reached. This phenomenon has been called a ‘static resonance’ or ‘static instability’.

Chronologically, the work has been developing as follows. Bhuta and Jones (1963a) were exploring problems involving small strains where the use of Lagrangian coordinates (undeformed) yielded improved models compared to the use of Eulerian (deformed) coordinates. While they identified the possibility of a critical speed, it followed the assumption of small strains but did not recognise that the strains near critical speeds were well beyond being 'small' (see Hodges and Bless (1994)). As Brunelle (1971) did not cite Bhuta and Jones (1963a), he appears to have discovered this instability independently. Anderson (1975) reconsidered the problem by incorporating the non-linear strain equations and separated the analysis by superimposing the 'initial stress' (static equilibrium) problem onto the 'deformed motion' (dynamic) problem of linearised small amplitude vibrations. Although such an

assumption for nonlinear equations did not seem to be appealing, he asserted that the longitudinal natural frequencies increased with rotational speed and excluded the possibility of static instability. Hodges' (1977) analysis suggested that the sign of the frequency shift with rotation depended on the hardening or softening characteristic of the strain-displacement property of the material. Venkatesan and Nagaraj (1981) claimed that Hodges' (1977) equations contained an error and suggested that premature ordering “completely changed” the characteristic of the behaviour of the longitudinal natural frequencies with rotational speed. Hodges (1983) refuted these conclusions by maintaining that an unknown material parameter (the coefficient of the nonlinear strain term) governed the response. A decade later Hodges and Bless (1994) further reinforced the earlier findings by proposing simple non-linear strain energy models that included a cubic term in the displacement gradient. They showed that instability existed only when the coefficient of this term was less than one, signifying a softening stiffness. They noted that instability only occurred at strains well beyond the range of elastic action for most materials. The question of longitudinal natural frequencies was not addressed. O'Reilly and Turcotte (1997a, 1997b) approached the problem using the theory of a Cosserat rod and superimposed the small vibrational deformations on large static deformations using a non-linear rod theory. However, they left the specific form of the strain energy function unspecified and no solutions were offered. None of the models outlined above had included the Poisson’s effect of lateral contraction of the bar. However, in O'Reilly and Turcotte’s later paper with Kindaid (2001), they did include lateral contraction of the bar and showed that instability coincided with the condition of the cross-sectional area of the bar somewhere reducing to zero. They concluded that this lateral contraction had a significant influence on the displacement. Some numerical solutions were offered where a whirling bar is fixed at one end. To enforce this boundary condition, they also constrained the lateral contraction at the axis of rotation, leading to a lateral strain profile that they termed a 'boundary layer'.

Meanwhile, there were another group of researchers who worked on transverse vibration of rotating beams without coupling to longitudinal vibration. Although transverse vibration is not of primary interest in the current work, it is mentioned to interested readers and indicating the condition that causes a transverse vibration. Bhat (1986) predicted the transverse vibration of a rotating beam with tip mass by beam characteristic orthogonal polynomials with Rayleigh-Ritz method. Results on natural

frequencies and mode shapes had been presented. Lo and Renbarger (1951) formulated the integro-differential equation for the bending vibrations of rotating beams, they showed that vibration modes are independent of the angle that the plane of vibration made to the plane of rotation. Lo (1952) cracked the bending vibration of a rotating beam in a plane not perpendicular to the plane of rotation with the conclusion that Coriolis effect on natural frequencies was negligible in most applications. Schilhansl (1958) investigated the stiffening effect of the centrifugal force on the first mode bending frequency by successive approximation. He demonstrated this effect was dependent on the angle of the beam made with the direction of circumferential velocity. In terms of finding the natural frequencies, Rubinstein and Stadter (1972) provided lower and upper bounds for the bending frequencies of rotating beams and Pnueli (1972) offered three methods of finding transverse natural frequencies of rotating beams. All of these studies on transverse vibration of rotating beams, without coupling to longitudinal vibration, assumed a small strain analysis without large strain longitudinal deformations. Hence the longitudinal displacements played no role in interacting with the transverse vibrations of rotating beams.

A library of references on theory of rods includes the following work. Carnegie (1959, 1967) used Hamilton's principle and variational method to build equations of motion of cantilever blades with small vibrations mounted at the root on the periphery of a rotating disc. In addition, an equation for fundamental frequency under certain conditions was established. Green and Laws (1966) derived the theory of rods according to theories from thermodynamics. Green *et al*. (1974a, 1974b) derived the constitutive equations for elastic rods of isotropic material with variable cross-section. From these constitutive equations, a system of differential equations on flexural displacement of a beam with circular cross-section was developed. Berdichevskii (1981) split the 3-D theory of elasticity of a rod into nonlinear 1-D and linear 2-D problems to be solved. Dentsoras and Dimarogonas (1983) incorporated the Paris-Erdogan equation to study the fatigue crack propagation at or near resonance of a beam under longitudinal vibrations. Naghdi and Rubin (1984, 1989) formulated the non-linear constrained theories of rods based on Cosserat curve with two directors for certain modes of motion or deformation of rods. Moreover, they compared the solutions of four different linear theories on a straight, homogeneous, isotropic elastic beam of rectangular cross section with part of the lower surface in contact with a

stationary rigid flat surface. Shield and Im (1986) employed a theory for linear elastic behaviour in which strains were small but displacement and rotations could be large to the bending and twisting of a rod or beam by end loads and its own weight. Papadopoulos and Dimarogonas (1987) investigated the free and forced longitudinal and transverse vibrations of a rotating shaft with an open crack. Krishnaswamy and Batra (1998) constructed a coupled system of partial differential equations that related the longitudinal and cross-sectional displacement of a bar based on the concept developed by Green *et al*. (1974a, 1974b). All the work mentioned in this paragraph basically established theories on rods and beams but offered no results and comparisons.

In terms of numerical work, methods such as finite-difference, finite element, Rayleigh-Ritz, Ritz, Galerkin, perturbation, transfer matrix and Laplace transform methods had been applied. Bertholf (1967) applied a finite difference scheme to solve the governing equations for axial and radial displacements of a cylindrical bar. Cherukuri and Shawki (1996) ran a finite-difference scheme to solve the second order partial differential equations coupled with axial and radial displacements. Abbas (1979) constructed two finite element models for the dynamic analysis of thick pre-twisted blades. Matins and Oden (1983) used finite element method for spatial discretization and Newmark's or central-difference method for time discretization to study a class of problems in elastodynamics with variational formulation. Langley (1989) applied finite element method to the equations of motion of an aircraft panel derived by dynamic stiffness method. Akoz *et al*. (1991) obtained the mixed finite element equations based on a new functional by Gateaux differential to solve 3-D bar problems. Dawson (1968) applied Rayleigh-Ritz method that used orthogonal approximating functions to determine the natural frequencies and mode shapes of vibration of pre-twisted rectangular cross-section beams. Rao and Carnegie (1970, 1972, 1973) presented a solution on a uniform untwisted rotating cantilever blade mounted on the periphery of a disc vibrating in the plane of rotation by using Ritz method. Oh *et al*. (2003) developed a structural model that encompassed features such as anisotropy and transverse shear warping restraint, and pretwist and presetting angles. Extended Galerkin method was employed to solve the model. Lakin (1974) undertook the method of matched asymptotic expansions to solve a fourth order differential equation that arose from the transverse vibrations of a slender rod rotating at a constant angular velocity. Lakin and Nachman (1978, 1979) solved the fourth order boundary value problems associated with small vibrations or

buckling of a rotating uniform rod clamped at one end by singular perturbation methods. The fourth order partial differential equations governing the free vibrations of the rotation of a rod was deciphered by uniform approximations with results involving Airy and Scorer functions. Bapat (1995) used a transfer matrix method and a closed form solution of a uniformly tapered rod to solve for the natural frequencies. Sankin. and Yuganova (2001) deployed a frequency method of Laplace transform to crack the problem of longitudinal vibrations of elastic rods with stepwise variable cross-section when collided with a rigid obstacle. An outcome of this survey of all these numerical works shows that none of the previous work used the numerical method proposed in this thesis to solve the problems.

Some other researchers have embraced either analytical solutions or other numerical solutions for beams and rods vibration problems. Hutchinson (1972) determined the axisymmetric vibrational characteristics of an elastic circular rod of finite length with stress-free boundaries and the analytical solution was expressed in terms of Bessel functions. Results on frequencies are compared with the Pochhammer-Chree solution. Subrahmanyam *et al*. (1981) compared the numerical results using Reissner and potential energy methods on a pre-twisted cantilever blade executing coupled bending-bending vibrations. Natural frequencies and mode shapes were displayed. Bathe and Dvorkin (1985) discussed a 4-node plate-bending element for linear elastic analysis obtained from a general nonlinear continuum mechanics based on a 4-node shell element formulation. Eisenberger (1991) determined the axial stiffness of a variable cross-sectional rod by exact element method. Longitudinal vibration natural frequencies were found when the axial stiffness was set to zero and were compared with the finite element results. Mizusawa (1993) predicted the natural frequencies of vibration of rectangular Mindlin plates by spline strip method. Kumar and Sujith (1997) performed appropriate transformations to the governing equation of axial vibration of a rod with varying cross-section. Solvable differential equations were obtained with the solutions being expressed in terms of Bessel and trigonometric functions. Chen (1997) evaluated the transverse deflection and natural vibration frequency of a bar in axial compression loading by shooting method. Results on natural frequencies had been presented. Hestermann *et al*. (1996) developed axial and torsional receptances of tapered circular shafts. Axial natural frequencies were calculated from the derived receptance and results agreed well with experimental data.

Although results of computations on natural frequencies have been offered, the question whether natural frequencies are rising or falling while rotational speed is increasing remains unanswered.

## *2.2 Rotating Discs*

Biezeno & Grammel (1954) and Bhuta & Jones (1963b) had suggested that the Coriolis coupling forces should be included in the equations of motion. Some previous researchers had made various assumptions to decouple the governing equations in order to achieve an analytical solution. This thesis offers results that show the differences on the natural frequencies of vibration between equations with and without such a simplification.

Formulation of the governing equations of rotating discs can be established in Eulerian or Lagrangian coordinates. In the work that involved the Eulerian coordinates (Bhuta and Jones (1963b)), free edge boundary conditions were applied by presuming that rotation did not impose a large radial and circumferential strains on the plates. In contrast, boundary conditions applied on a free edge in Lagrangian coordinates would eliminate such an undesirable presumption. However, issues of existence and uniqueness of solutions formulated in Lagrangian coordinates arise.

Much of the current work on rotating annuli is based on the governing equations formulated earlier by Biezeno & Grammel (1954) and Bhuta & Jones (1963b). Biezeno and Grammel (1954) set up the governing equations of in-plane vibrations of rotating annular plates with variable thickness in Eulerian coordinates involving the coupling of radial and circumferential displacements. In Subsection 4.1.2, their governing equations will be transformed into Lagrangian coordinates in order to avoid the difficulty of imposing the free edge boundary condition in Eulerian coordinates and for the purpose of comparing the results obtained from the Bhuta and Jones' model formulated in Lagrangian coordinates. Furthermore, Poisson's effect is introduced into the Biezeno and Grammel's static model. This enhances the accountability of the static model with material density and plate thickness variations. Bhuta and Jones (1963b) created the governing equations similar to Biezeno and Grammel (1954) of a rotating parallel annulus with radial and circumferential displacements coupled in both Eulerian

and Lagrangian coordinates. These governing equations were linear systems of equations without incorporating the Poisson's effect. Although attempts had been made to solve the governing equations for in-plane displacements and natural frequencies, their solutions did not take any specific boundary conditions into considerations. Moreover, the analytical results obtained appeared to be awkward and were different from what has been obtained in Section 4.2 of this thesis, where an analytical solution for the linear coupled system of equations will be offered.

There is other work that involved the Coriolis coupling effect. Doby (1969) had considered the dynamical instabilities, which existed because of the coupling between the radial and tangential motion, of a thin rotating disc under the influence of Coriolis and centrifugal forces. His results showed that Coriolis force was increasingly important as the rotational speed was increasing. Lessen and Gangal (1970) illustrated the effects on extensional and torsional vibration frequencies where Coriolis acceleration was either included or excluded using dynamic equations with Lame constants. Results on the first two natural frequencies were given at different rotational speeds. Luo and Mote Jr. (2003) invented the governing equations for asymmetric mode, which included the symmetric case, of vibration of rotating discs. Results were achieved by perturbation together with Galerkin methods and were compared with results from linear von Karman models.

Work that coupled the radial and transverse vibrations can be found as well. Lin (1995) obtained an analytical solution for coupled radial and transverse vibration of cylinders or discs by introducing a mechanical coupling coefficient, predictions on natural frequencies had good agreements with experimental data. Huang and Al-Khattat (1977) transformed the axisymmetric free and forced governing equations of a rotating circular plate coupled with transverse and radial displacements into an eigenvalue problem, their solution was compared with Berger assumption which showed that Berger assumption was only accurate at small amplitude of vibration. Recently, Heo & Chung (2004) and Chung *et al*. (2000) had studied rotating discs by coupling all three modes of transverse, radial and circumferential vibrations together. Results showed that both vibration periods and amplitudes were decreasing as the rotating speed was increasing.

Many researchers have obtained solutions for the in-plane natural frequencies. Although results have not been confirmed experimentally due to the difficulty of taking measurements while the plates were rotating, natural frequencies were often calculated from the assumed harmonic solution for the unknown displacements of the governing equations. Lee and Ng (1995) developed the equations of motion for rotating isotropic annular plates by variational method to calculate the natural frequencies. They produced results on frequency parameters, which were related to natural frequency through a constant, with comparisons to other work. Farag and Pan (1999) attained the resonance frequencies and mode shapes of rectangular plates with comparisons to finite elements methods, although the rectangular plates were non-rotating. In their other work (Farag and Pan (2003)), they studied the in-plane natural frequencies of non-rotating circular plates clamped at the free edge. Srinivasan and Ramamurti (1980) evaluated the frequencies of a rotating annulus with clamped-free boundaries by using Lame potentials to represent the in-plane displacements. Results on natural frequencies and steady state stress response were computed. Irie *et al*. (1984) applied the transfer matrix method to locate the natural frequencies of annular plates with clamped or free boundary conditions at inner and outer edges of the plates. They presented results on axisymmetric and asymmetric vibration of natural frequencies. In all the work described in this paragraph, only Farag and Pan (1999) produced mode shapes for in-plane vibrations of non-rotating rectangular plates. To the best knowledge of the author of this thesis, a robust theoretical or numerical methodology that seeks natural frequencies of vibration of objects, with arbitrary shapes and applied oscillation force at any location, has not yet been devised. In Subsection 4.4.3, a proposed frequency response approach will be presented to solve for the natural frequencies of vibration of rotating annuli.

Other references on the theory of rotating discs or annuli can be found. Carrier (1945) formulated the dynamic equations of free and forced vibrations of a rotating ring with rigid or elastic supports. Analytical solutions with different boundary conditions were obtained. Berger (1955) derived simplified nonlinear equations for flat plates to calculate the deflections and stresses by neglecting strain energy due to the second invariant of the middle-surface strains. Although he claimed that there was good agreement between the approximation and the exact solution whenever comparisons were possible, no data from the calculations were given. Tobias (1957) deduced the

equations of motion of imperfect circular discs by considering the kinetic energy, bending strain energy and extensional strain energy of vibrating discs. The nonlinear formulation of the problem eventually boiled down to analyse the Mathieu equation, where analytical expressions on natural frequencies were presented. Mindlin and Medick (1959) inferred a system of two-dimensional equations of extensional motion of isotropic elastic plates. Series solutions were obtained for the governing equations as well as frequency spectra were explored and compared with the corresponding solution of the three-dimensional equations. Gazis and Mindlin (1960) decoded the equations of extensional motion of elastic plates for the case of axially symmetric vibrations of a circular disc. The frequency equation was solved and results were compared with experiments performed by E.A.G. Shaw. Kirkhope (1977) derived the dynamic stiffness matrices for the in-plane vibration of thick circular rings by including transverse shear and rotary inertia. Numerical results on in-plane frequencies were compared with experimental data. Bickford and Reddy (1985) demonstrated the rotatory inertia and shear deformation effect on the bending frequencies of rotating rings. Results showed that by including rotatory inertia and shear deformation in the governing equations, natural frequencies decreased at all rotational speeds. Adams (1987) determined the critical speeds of a spinning elastic disc in the range of rotational speeds relevant to floppy disc magnetic recording applications. Burdess *et al*. (1987) created and solved the steady state free or forced equations of motion with radial and circumferential displacements with solutions expressed in terms of scalar potential and vector function. Hutton *et al*. (1987) analysed the response of free and forced vibrations of a rotating guided circular saw. Natural frequencies subjected to applied stationary point loads at the outer edge of a saw were investigated. In addition, effects of spring stiffness, number of springs and spring locations on frequency characteristics of a rotating disc were studied. Leung and Pinnington (1987) formulated the responses of a rotating disc subjected to a stationary in-plane force at its rim or its centre. They found that resonance occurred whenever the excitation frequencies of any of the two counter-rotating vector coincided with the natural frequencies of the rotating disc. Luo (2000) constructed an approximate nonlinear thin plate theory based on the exact geometry of the deformed middle surface. By imposing certain conditions on the involved parameters, his theory reduced to other existing plate theories. He also claimed that his theory was applicable to all deformation processes of thin plates such as elasticity, plasticity and others.

In terms of numerical work, finite element, Rayleigh's, Galerkin, Rayleigh-Ritz and transfer matrix methods had been sought. Farag and Pan (1998) attained the resonance frequencies and mode shapes of rectangular plates with comparisons to finite elements methods. In addition, input power and structural intensity were also presented. Lamb and Southwell (1921) solved for the transverse displacement of a spinning disc by Rayleigh's method with the assumption that in-plane displacements were unaffected by small transverse motion. Wah (1963) devised the dynamic case of large deflection theory of plates proposed by Berger by adding a transverse inertia term. Galerkin method was applied to obtain a solution with simply supported or clamped boundary conditions. Irons and Kennedy (1989) applied Galerkin's method to unravel the transverse displacement of non-axisymmetric vibration of centrally clamped with variable thickness thin discs. Ramaiah (1981) analysed the transverse vibrations equations of spinning annular plates derived from variation principle using Rayleigh-Ritz method for different boundary conditions. Like the survey on rotating rods, none of these works on rotating discs applied the same numerical methods as that proposed in this thesis.

Some researchers solved rotating discs or annuli problems by analytical or other numerical means. Eversman and Dodson (1969) found a series solution for the transverse displacement of a centrally clamped spinning circular disc. Wahed and Bishop (1976) found an analytical solution for the free and forced linear vibration theory with inertia, damping and stiffness matrix terms. Chen and Jhu (1996) investigated the effect of clamping ratio on natural frequencies and critical speeds of an annulus, where clamping ratio is the ratio of inner radius to outer radius of an annulus. Numerical results showed that asymptotic critical speed depends on Poisson's ratio but not clamping ratio. Shen and Song (1996) predicted the transverse vibration of a rotating circular plate excited by stationary in-plane edge loads. Niordson (1997) worked out the problems of axisymmetric and non-axisymmetric in-plane vibration of annular discs with non-uniform thickness to find an optimal shape for the design of thin axisymmetrical discs.

# Chapter 3

## Strain and Axial Vibration of Whirling Rods[9]

This chapter discusses axial strain and natural axial frequencies of static prismatic whirling rods. Poisson's effect will be incorporated into the governing equations. This effect was excluded in previous work by other researchers (Bhuta & Jones (1963a)). The inclusion of the Poisson's effect will give a better mathematical model because variations of material density and cross-sectional area while rods are rotating are taken into account. Since there is a controversy on whether axial natural frequencies are rising or falling while the angular velocity is increasing, this chapter offers an alternative approach to find the axial natural modes of a steadily whirling rod. The geometric configuration of such a rod is shown in Figure 3.1.

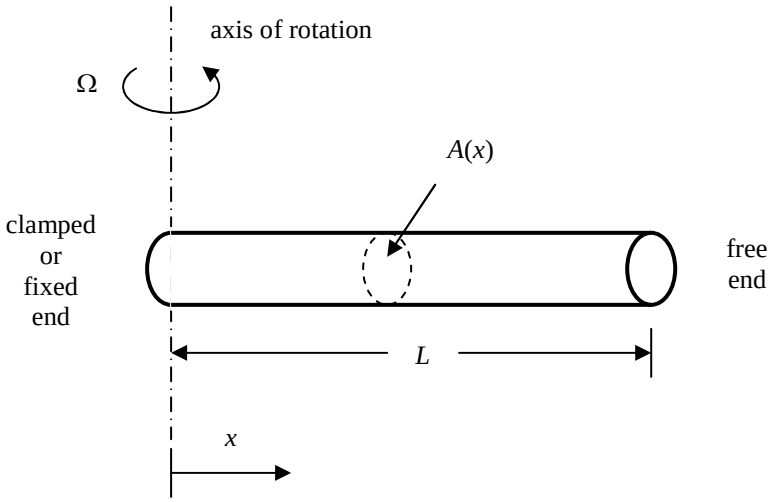


Figure 3.1. Geometric configuration in Lagrangian coordinate $x$ of a rod statically rotating about the axis of rotation at an angular velocity $\Omega$. $A(x)$ is the cross-sectional area of the rod. $L$ is the original length of the non-rotating rod.

The rod in Figure 3.1 is rotating at one of its ends about the axis of rotation. This end is a fixed or clamped end because no axial displacement occurs at $x = 0$. At the other end of the rod, it is a free end because no axial stress or strain occurs at $x = L$.

[9] Part and all of the work in this chapter had been published as references 4 and 3 mentioned on p.98 respectively. In addition, proof of Theorem 3.1 had been modified and is slightly different from the version published in reference 3 mentioned on p.98.

## *3.1 Linear Uniaxial Model*

Some previous work (Bhuta and Jones (1963a)) had applied free end boundary condition of whirling rods in Eulerian coordinates. But this free end position in Eulerian coordinate is exactly the same as the free end of the rod when it is not rotating. However, this is obviously not true, because when the rod is rotating, that free end in Eulerian coordinate under axial strain must be different from the free end position of the non-rotating rod. Therefore, problems formulated in Lagrangian coordinate are better modelled than those in Eulerian coordinate because of the proper implementation of the free end boundary condition. Formulation of steady whirling rods governing equations in Lagrangian coordinates will be performed in this thesis.

### *3.1.1 Governing Equations of Motion*

Previously, it had been shown that at low angular velocity $\Omega$, rotational motion of the rod at steady state could be described in Lagrangian coordinate $x$ by a linear uniaxial model with clamped-free boundary conditions (Kinkaid *et al*. (2001)),

$$E\frac{d^2u}{dx^2} = -\rho_0 (x + u)\Omega^2. \tag{3.1a}$$

For a clamped rod, no axial displacement at $x = 0$,

$$u(0) = 0. \tag{3.1b}$$

From 1-D Hooke's law, axial stress $\sigma(x) = \dfrac{F(x)}{A_0} = E\varepsilon(x)$, $F(x) = EA_0\varepsilon(x)$. By applying the linear strain-displacement relationship $\varepsilon(x) = \dfrac{du}{dx}$ in Lagrangian coordinate together with the fact that $F(x) = 0$ at the free end,

$$EA_0\left[\frac{du}{dx}\right]_{x=L} = 0, \tag{3.1c}$$

where $0 < x < L$, $E$ is Young's modulus or modulus of elasticity, $F(x)$ is the axial force at $x$ along the whirling rod, $A_0$ is the uniform cross-sectional area of a non-rotating rod, $\rho_0$ is the material density of the non-rotating undeformed rod, $u(x)$ is the axial, longitudinal or extensional displacement at $x$ and $L$ is the length of a non-rotating undeformed rod. Equations (3.1) assume small strain analysis with linear strain-displacement relationship. In addition, Poisson's effect is neglected by keeping the

material density and cross-sectional area constant. The full derivation of Equations (3.1) is attached in Appendix B of this thesis.

### *3.1.2 Exact Solution*

The analytical solution for Equations (3.1) according to Bhuta and Jones (1963a) is

$$u(x) = \frac{\sin(kx)}{k\cos(kL)} - x,$$

where $k = \sqrt{\frac{\rho_0}{E}}\,\Omega$. It is apparent from the above solution that $u(x)$ is undefined when

$$\Omega = \sqrt{\left[\frac{(2N-1)\pi}{2L}\right]^2 \frac{E}{\rho_0}},$$

for $N$ = 1, 2, 3, … . This means that solution obtained in Lagrangian coordinates does not exist at certain angular velocities Ω. However, before reaching the lowest angular velocity Ω when $N$ = 1, material could already fail at yield point as the strain occurs at these angular velocities are so large that the small strain analysis for the linear uniaxial model becomes invalid. As a result, this model is limited to small strains as no allowance is made for the reduction in $A(x)$ due to transverse Poisson's strain. Also, changes in $A(x)$ due to Poisson's strain necessarily imply density redistribution. Hence, the linear uniaxial model is not a representative of the situation at larger strains due to higher angular velocity Ω.

## *3.2 Proposed Non-Linear Model*

In this section, a nonlinear model will be formulated by allowing the variation of material density and cross-sectional area of a strained steadily whirling rod due to Poisson's effect.

### *3.2.1 Derivation of Governing Equations of Motion*

Assuming the rod material is isotropic with only axial normal stress $\sigma(z)$ presents, the one-dimensional Hooke's law in Eulerian coordinate can be written as

$$E\varepsilon(z) = \sigma(z),$$

where $z$ is the Eulerian coordinate and $\varepsilon(z)$ is axial normal strain at $z$ of a deformed rod. But from physical law,

$$\sigma(z) = \frac{F(z)}{A(z)},$$

where $F(z)$ is the axial force at $z$ along the deformed rod and $A(z)$ is the cross-sectional area of the rod at $z$ of a deformed rod. Notice that the relationship between the Eulerian coordinate $z$ and the Lagrangian coordinate $x$ in the previous section is $z = x + u(x)$. Substituting the expression for $\sigma(z)$ into the 1-D Hooke's law,

$$F(z) = EA(z)\varepsilon(z). \tag{3.2}$$

But the centripetal force $F(z)$ at any location is the summation of the centripetal forces due to all the differential elements at a greater radius. Thus

$$F(z) = \int_{x+u(x)}^{L+u(L)} \rho(z)A(z)z\Omega^2 dz, \tag{3.3}$$

where $\rho(z)$ is the material density at $z$ of an deformed rod. Substituting Equation (3.2) into Equation (3.3),

$$EA(z)\varepsilon(z) = \int_{x+u(x)}^{L+u(L)} \rho(z)A(z)z\Omega^2 dz. \tag{3.4}$$

In order to impose the free end boundary condition properly as mentioned in the previous section, Equation (3.4) will be transformed into the Lagrangian coordinate $x$. By conservation of mass, the mass of each of the differentially small segment in Lagrangian coordinate of a stationary rod is equivalent to the mass of the same differentially small segment in Eulerian coordinate while the rod is steadily rotating. Hence

$$\int_0^{s+u(s)} \rho(z)A(z)dz = \int_0^s \rho_0 A_0 dx,$$

where $A_0$ is the uniform cross-sectional area of a non-rotating undeformed rod and $s$ is any arbitrary position on the rod. Changing $z$ to $x$ and the order of integration in the above equation,

$$\int_0^s \left( \rho(x)A(x)\frac{dz}{dx} - \rho_0 A_0 \right) dx = 0,$$

where $A(x)$ is cross-sectional area of a rod at $x$ of a undeformed rod. Since this integration is true $\forall s \in [0, L]$, it must follow that the integrand of the above integral must be zero. Thus,

$$\rho(x)A(x)\frac{dz}{dx} = \rho_0 A_0 .$$

Changing $z$ to $x$ and the order of integration in Equation (3.4),

$$EA(x)\varepsilon(x) = \int_x^L \rho(x)A(x)\frac{dz}{dx}(x+u)\Omega^2 dx,$$

where $u = u(x)$ and $0 \le x \le L$. By applying the previous identity to this equation,

$$EA(x)\varepsilon(x) = \int_x^L \rho_0 A_0 (x+u)\Omega^2 dx . \tag{3.5}$$

From Poisson's relation of uniaxial stress,

$$\varepsilon_L(x) = -\upsilon\varepsilon(x),$$

where $\upsilon$ is Poisson's ratio, $\varepsilon_L(x)$ is the lateral strain at the Lagrangian coordinate $x$ and $\varepsilon(x)$ is the axial normal strain along the Lagrangian coordinate $x$. Consider a prismatic bar with circular cross-section,

$$\varepsilon_L(x) = \frac{d(x) - d_0}{d_0} = -\upsilon\varepsilon(x),$$

where $d(x)$ is the diameter of a cross-sectional area along Lagrangian coordinate $x$ and $d_0$ is the uniform diameter of an non-rotating undeformed rod, it follows that

$$d(x) = d_0 [1 - \upsilon\varepsilon(x)].$$

As a result,

$$A(x) = \frac{\pi}{4}[d(x)]^2 = \frac{\pi}{4} d_0^2 [1 - \upsilon\varepsilon(x)]^2. \tag{3.6}$$

Putting Equation (3.6) into Equation (3.5) and using

$$A_0 = \frac{\pi}{4} d_0^2$$

gives

$$E[1 - \upsilon\varepsilon(x)]^2\varepsilon(x) = \int_x^L \rho_0 (x+u)\Omega^2 dx . \tag{3.7}$$

By inserting the strain-displacement relation

$$\varepsilon(x) = \frac{du}{dx} + \frac{1}{2}\left(\frac{du}{dx}\right)^2$$

discussed in Subsection 1.3.1 into Equation (3.7),

$$E\left[1-\upsilon\left(\frac{du}{dx}+\frac{1}{2}\left(\frac{du}{dx}\right)^2\right)\right]^2\left[\frac{du}{dx}+\frac{1}{2}\left(\frac{du}{dx}\right)^2\right]=\int_x^L \rho_0(x+u)\Omega^2 dx\,, \qquad (3.8a)$$

where $0 < x < L$. For clamped boundary condition at $x = 0$ with no axial displacement on the whole cross sectional area $A(0)$,

$$u(0) = 0. \qquad (3.8b)$$

For free end boundary condition at $x = L$ with no axial strain $\varepsilon(L)$ occurs on the whole cross sectional area $A(L)$,

$$\left[\frac{du}{dx}+\frac{1}{2}\left(\frac{du}{dx}\right)^2\right]_{x=L} = 0. \qquad (3.8c)$$

Equations (3.8) are the steady state integro-differential equations for axial displacement $u(x)$ in Lagrangian coordinate $x$ that govern the strain of a whirling prismatic rod. Although this derivation is being done on a rod with circular cross-section, beams with non-circular cross sectional area can be derived in a similar fashion by including the cross-sectional area profile into the governing equation. This proposed model improves upon Equations (3.1) because the Poisson's effect, which accounts the variations of material density and cross-sectional area, has been included. Similar to the linear uniaxial model, the nonlinear governing equation is only valid in the linear elastic region that is governed by the 1-D Hooke's law. Beyond the end of this linear elastic region, which is the yield point, the validity of the governing equations does not apply. This proposed model is deduced by including all three variations of axial displacement, material density and cross-sectional area. Thus, it is suitable for large strain analysis. Furthermore, no previous papers reviewed in Chapter 2 had given a similar establishment in nonlinear steady whirling rods.

### *3.2.2 Proposed Numerical Solution*

Since it is very difficult, although not impossible, to obtain an analytical solution for nonlinear integro-differential equations, numerical solutions are sought here. This proposed numerical method has briefly been mentioned in Subsection 1.3.3. The difference between this method and the collocation type of methods is that this proposed numerical method chooses the prescribed functions $\{f_i(x)\}_{i=0}^{\infty}$ to be valid

representation of the unknown solution. This simply means the prescribed functions are chosen in such a way that the unknown solution can be approximated closely by a finite number of terms in $\{f_i(x)\}_{i=0}^{\infty}$. Assuming $\{f_i(x)\}_{i=0}^{\infty}$ is an infinite sequence with linear combinations of the functions representing an unknown variable $u(x)$, then

$$u(x) = \sum_{i=0}^{\infty} a_i f_i(x),$$

where $x \in [0, L]$ and $a_i$'s are unknown constants to be determined. For the current study, $\{f_i(x)\}_{i=0}^{\infty}$ is chosen to be $\{x^i\}_{i=0}^{\infty}$. Consider the following equations

$$\Psi_{\Xi}\ (u(x)) = g(x),\ x \in \Xi, \tag{3.9a}$$

$$\Psi_{\partial\Xi}^{1}\ (u(x)) = g_1(x),\ x \in \partial\Xi, \tag{3.9b}$$

$$\Psi_{\partial\Xi}^{2}\ (u(x)) = g_2(x),\ x \in \partial\Xi, \tag{3.9c}$$

where $\Psi_{\Xi}$ is a non-linear integro-differential operator on interior of domain $x$, $\Psi_{\partial\Xi}^{1}$, $\Psi_{\partial\Xi}^{2}$ are non-linear differential operators at the boundary of domain $x$, $\Xi$ represents the interior of domain $x$, $\partial\Xi$ represents the boundary of domain $x$, $u(x)$ is an unknown function of variable $x$ and $g(x)$, $g_1(x)$ and $g_2(x)$ are known functions of variable $x$. In order to implement a numerical solution in a computer, $u(x)$ can only be approximated by a finite number of terms in the complete set $\{f_i(x)\}_{i=0}^{\infty}$. Therefore,

$$u(x) \approx \sum_{i=0}^{n} a_i f_i(x)$$

are approximate solutions of Equations (3.9), where $n$ is a finite non-negative integer, $f_i$'s are prescribed functions and $a_i$'s are unknown constants to be determined. By choosing $x_j \in \Xi$, $j = 1, 2, \ldots n-1$, $x_0$ , $x_n \in \partial\Xi$, Equations (3.9) can be approximated by

$$\Psi_{\Xi}\left(\sum_{i=0}^{n} a_i f_i(x_j)\right) \approx g(x_j),\ x_j \in \Xi,\ j = 1, 2, \ldots n-1, \tag{3.10a}$$

$$\Psi_{\partial\Xi}^{1}\left(\sum_{i=0}^{n} a_i f_i(x_0)\right) \approx g_1(x_0),\ x_0 \in \partial\Xi, \tag{3.10b}$$

$$\Psi_{\partial\Xi}^{2}\left(\sum_{i=0}^{n} a_i f_i(x_n)\right) \approx g_2(x_n),\ x_n \in \partial\Xi, \tag{3.10c}$$

Equations (3.10) are a system of $n + 1$ nonlinear algebraic equations with $n + 1$ unknowns $a_0$ , $a_1$ , …, $a_n$ which can now be solved by Newton's method. Defining

$$e_j = \begin{cases} \Psi_{\partial\Xi}\left(\sum_{i=0}^{n} a_i f_i(x_0)\right) - g_1(x_0), \; j = 0, \\ \Psi_{\Xi}\left(\sum_{i=0}^{n} a_i f_i(x_j)\right) - g(x_j), \; j = 1,2,\ldots n-1, \\ \Psi_{\partial\Xi}\left(\sum_{i=0}^{n} a_i f_i(x_n)\right) - g_2(x_n), \; j = n, \end{cases}$$

then the stopping criterion for the Newton's iteration is when the error tolerance $\sum_{j=0}^{n} e_j^2$ << 1. For the particular problem in Equations (3.8), it is required that $u(x) \in C^1(0, L]$, where $C^1(0, L]$ is a class of functions that are continuously differentiable $\forall x \in (0, L]$.

### *3.3 Numerical Experiment and Model Comparisons*

Numerical experiments are performed on a rod made of steel with arbitrarily chosen parameters. Relevant parameters are diameter $d_0$ = 0.035 m, density $\rho_0$ = 7850 kg/m$^3$, Young's modulus $E$ = 200 GPa, Poisson's ratio $\upsilon$ = 0.29 and length of the rod $L$ = 1 m.

#### *3.3.1 Axial Displacements and Axial Stresses*

Comparisons between the analytical results of the uniaxial model in Equations (3.1) and the numerical results of the proposed non-linear model in Equations (3.8) are plotted in Figures 3.2 for axial displacements and Figures 3.3 for axial stresses. Size of the series $n$ in Equations (3.10) is chosen to be ten as the error tolerance is approximately $O(10^{-30})$ in the stopping criterion of the Newton's method. For $n$ = 20, there are no significant difference on the results compared to $n$ = 10. For $n$ > 20, the error tolerance of $O(10^{-30})$ is not achievable due to significant round off errors. Both models agree well at a low angular velocity $\Omega = 200\pi$ rad/s (6000 rpm) but only qualitatively agree at high angular velocity $\Omega = 1000\pi$ rad/s (30000 rpm).

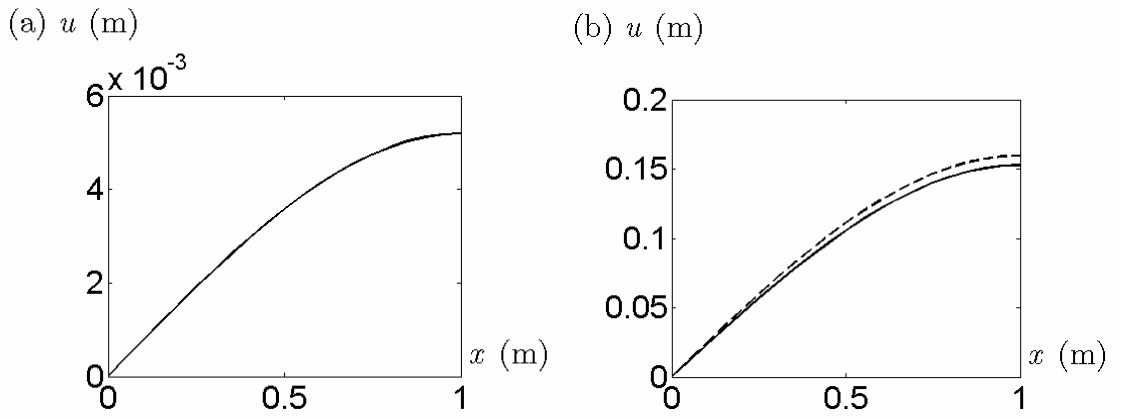


Figures 3.2. Plot of axial displacement $u(x)$ against Lagrangian coordinate $x$. Solid line — represents results from Equations (3.1). Dashed line –– represents results from Equations (3.8). $\rho_0$ = 7850 kg/m$^3$, $E$ = 200 GPa, $\upsilon$ = 0.29 and $L$ = 1 m. (a) $\Omega = 200\pi$ rad/s. (b) $\Omega = 1000\pi$ rad/s.

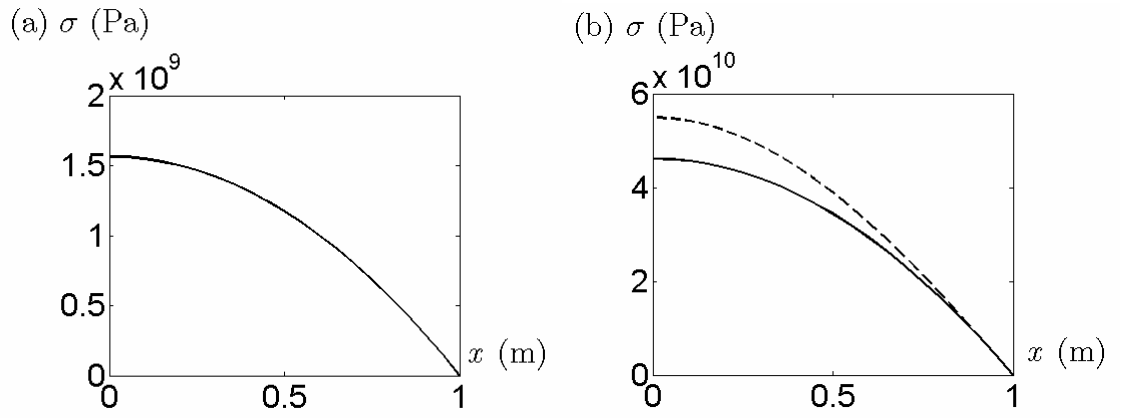


Figures 3.3. Plot of axial stress $\sigma(x)$ against Lagrangian coordinate $x$. Solid line — represents results from Equations (3.1). Dashed line –– represents results from Equations (3.8). $\rho_0$ = 7850 kg/m$^3$, $E$ = 200 GPa, $\upsilon$ = 0.29 and $L$ = 1 m. (a) $\Omega = 200\pi$ rad/s. (b) $\Omega = 1000\pi$ rad/s.

Although there are computational results beyond $\Omega = 200\pi$ rad/s, numerical results show that material of rods that made of steel with the above given parameters will fail at the yield point before reaching $\Omega = 200\pi$ rad/s. Thus the results in Figures 3.2 and Figures 3.3 are only displayed for the purpose of comparisons between the two models. Although the comparisons are beyond the yield point of the material, results show that the differences between the linear uniaxial model and the proposed nonlinear model become apparent at high angular velocities. If a rod with a material that has a linear elastic region that follows the Hooke's law at high angular velocities, the proposed nonlinear model prevails. Defining

$$e = \frac{\sigma_{NL} - \sigma_L}{\sigma_L},$$

where $\sigma_{NL}$ is the axial stress predicted by Equations (3.8) at $x$ = 0 and $\sigma_L$ is the axial stress predicted by Equations (3.1) at $x$ = 0, then from Figure 3.3a, $e \approx 0.39\%$ at $\Omega = 200\pi$ rad/s and from Figure 3.3b, $e \approx 19\%$ at $\Omega = 1000\pi$ rad/s. When $e$ = 1% and 10%, the corresponding angular velocities are at $\Omega = 294\pi$ rad/s and $812\pi$ rad/s respectively.

### *3.3.2 Material Density and Diameter of the Whirling Rod*

Although there are no analytical or experimental data to compare with, results obtained from the proposed numerical method on Equation (3.8) for the density and diameter of the rod while it is in rotation is shown in Figures 3.4 and Figures 3.5 respectively.

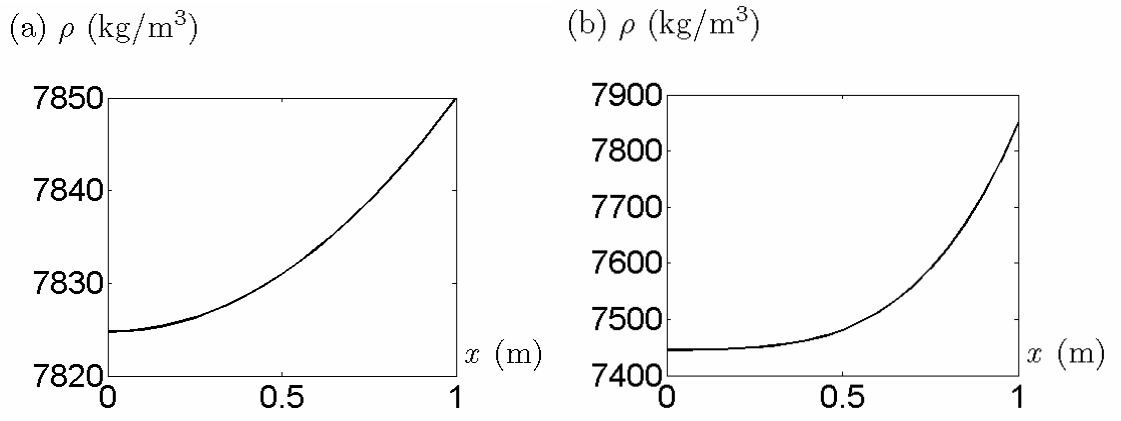


Figures 3.4. Plot of density $\rho(x)$ of the rotating rod against Lagrangian coordinate $x$. Solid line — represents results obtained by the proposed numerical method from Equations (3.8). $d_0$ = 0.035 m, $\rho_0$ = 7850 kg/m$^3$, $E$ = 200 GPa, $\upsilon$ = 0.29 and $L$ = 1 m. (a) $\Omega = 200\pi$ rad/s. (b) $\Omega = 1000\pi$ rad/s.

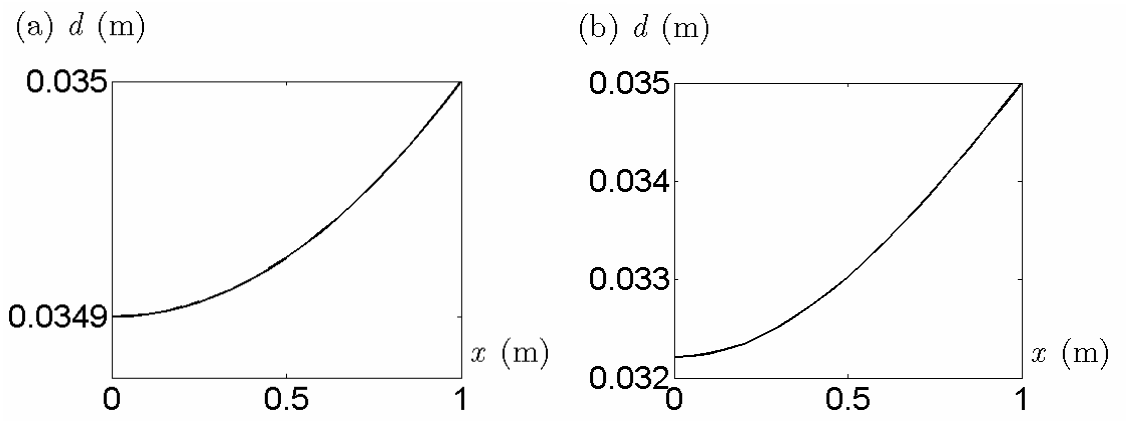


Figures 3.5. Plot of diameter $d(x)$ of the rotating rod against Lagrangian coordinate $x$. Solid line — represents results obtained by the proposed numerical method from Equations (3.8). $d_0$ = 0.035 m, $\rho_0$ = 7850 kg/m$^3$, $E$ = 200 GPa, $\upsilon$ = 0.29 and $L$ = 1 m. (a) $\Omega = 200\pi$ rad/s. (b) $\Omega = 1000\pi$ rad/s.

From Figures 3.4, material density of the whirling rod is redistributed compared to the constant density $\rho_0$ = 7850 kg/m$^3$ of the stationary rod. Similarly, from Figures 3.5, the diameter of the whirling rod varies along $x$ compared to the uniform diameter $d_0$ = 0.035 m of the stationary rod. In view of Figures 3.5, it can be concluded that the steady whirling rod has a trumpet-like shape.

### *3.3.3 Axial Natural Frequencies by Classical Method*

This thesis contends that the axial natural frequencies of a steadily whirling rod depend primarily on the geometry of the deformed rod, not on the rotary motion per se. Hence, having determined the deformed geometry, the determination of the axial vibration frequencies can be pursued via classical methods. A classical sub-structuring (receptance) method is employed to compute the axial natural frequencies of the deformed rod according to the results obtained from Equations (3.8). Readers may refer to Hestermann *et al*. (1996) for the full description of this method.

In the tables below,

$$\omega_N = \sqrt{\left[\frac{(2N-1)\pi}{2L}\right]^2 \frac{E}{\rho_0}},$$

where $N$ = 1, 2, 3, … , is the analytical axial natural frequencies for non-rotating undeformed rod. Moreover,

$$p_N = \sqrt{\left[\frac{(2N-1)\pi}{2L}\right]^2 \frac{E}{\rho_0} - \Omega^2}\ ,$$

where $N$ = 1, 2, 3, … , is the analytical axial natural frequencies for the rotating deformed rod obtained from Bhuta and Jones (1963a). Since small strain analysis is assumed, $p_N$ is only applicable to rods rotating at low angular velocities. $f_N$ , where $N$ = 1, 2, 3, … , represents axial natural frequencies obtained by the classical (receptance) approach on the results of model Equations (3.8). All axial natural frequencies in the tables below are rounded to the nearest integer. Results and comparisons are displayed in Table 3.1 to Table 3.3.

Table 3.1. First five axial natural frequencies of a fixed-free non-rotating isotropic rod with uniform circular cross-sectional area

| | $N = 1$ | $N = 2$ | $N = 3$ | $N = 4$ | $N = 5$ |
|---|---|---|---|---|---|
| $\omega_N$ (rad/s) | 7929 | 23786 | 39643 | 55501 | 71358 |
| $f_N$ (rad/s) | 7929 | 23786 | 39643 | 55501 | 71358 |

Table 3.2. First five axial natural frequencies of a rotating rod at angular velocity $\Omega = 200\pi$ rad/s

| | $N = 1$ | $N = 2$ | $N = 3$ | $N = 4$ | $N = 5$ |
|---|---|---|---|---|---|
| $p_N$ (rad/s) | 7904 | 23778 | 39638 | 55497 | 71355 |
| $f_N$ (rad/s) | 7886 | 23685 | 39479 | 55272 | 71064 |

Table 3.3. First five axial natural frequencies of a rotating rod at angular velocity $\Omega = 1000\pi$ rad/s

| | $N = 1$ | $N = 2$ | $N = 3$ | $N = 4$ | $N = 5$ |
|---|---|---|---|---|---|
| $p_N$ (rad/s) | 7280 | 23578 | 39519 | 55412 | 71289 |
| $f_N$ (rad/s) | 6713 | 20858 | 34857 | 48836 | 62808 |

The methods by Bhuta and Jones (1963a) and the classical approach both predict generally lowered axial natural frequencies if angular velocity is increased. However, the discrepancies between these two methods widen as angular velocity $\Omega$ increases further. These discrepancies are attributed to the $p_N$ predictions using the linear model that ignores the variations of material density and cross-sectional area while the $f_N$ predictions using the proposed nonlinear model take these two factors into account. It can be imagined that when a rod becomes longer, the wavelength of a near sinusoidal wave that is required to create a resonance is larger. If the wave speed remains constant, then the natural frequencies must be smaller accordingly. Hence the natural frequencies are decreased for an increased angular velocity of a steadily whirling rod.

## *3.4 Existence and Uniqueness of Solutions*

Equations (3.1) and Equations (3.8) are termed two-point boundary value problems. Depending on the boundary conditions, these equations may have no solution, a unique solution or more than one solution. If solution does not exist, then the governing equations become inapplicable. On the other hand, if there are more than one solution, it will take some other means to determine which one is the physically correct solution. Conditions on existence and uniqueness of solution for both linear uniaxial and the proposed nonlinear models are derived as follows.

### *3.4.1 Linear Uniaxial Model*

**Theorem 3.1.** *Consider the following inhomogeneous Helmholtz differential equations,*

$$\frac{d^2u}{dx^2} + k^2u = -k^2x, \tag{3.11a}$$

$$u(0) = 0 \tag{3.11b}$$

*and*

$$\left[\frac{du}{dx}\right]_{x=L} = 0. \tag{3.11c}$$

*where $0 < x < L$ and $k \neq 0$. Following the methods of solving elementary differential equations, solution of Equation (3.11a) can be found to be*

$$u(x) = c_1\cos(kx) + c_2\sin(kx) - x.$$

*From the Boundary Conditions (3.11b,c), the arbitrary constants $c_1$ and $c_2$ can be determined from the matrix equation*

$$A\boldsymbol{y} = \boldsymbol{b}, \tag{3.12}$$

*where*

$$A = \begin{bmatrix} 1 & 0 \\ -k\sin(kL) & k\cos(kL) \end{bmatrix},$$

$$\boldsymbol{y} = \begin{bmatrix} c_1 \\ c_2 \end{bmatrix}$$

*and*

$$\boldsymbol{b} = \begin{bmatrix} 0 \\ 1 \end{bmatrix}.$$

*If the rank of matrix A equals to 2, then solution for Equations (3.11) exists and is unique.*

**Proof.**

(Existence) If the rank of matrix $A$ equals to 2, then **y** can be found from Equation (3.12) by multiplying **b** on the left with $A^{-1}$. Hence a solution exists.

(Uniqueness) Suppose $u_1(x)$ and $u_2(x)$ are the solutions of the Equations (3.11) and let

$$\zeta(x) = u_1(x) - u_2(x),$$

then

$$\frac{d^2\zeta}{dx^2} + k^2\zeta = 0, \tag{3.13a}$$

$$\zeta(0) = 0 \tag{3.13b}$$

and

$$\left[\frac{d\zeta}{dx}\right]_{x=L} = 0. \tag{3.13c}$$

where $0 < x < L$ and $k \neq 0$. Now

$$\frac{d}{dx}\left[\left(\frac{d\zeta}{dx}\right)^2 + k^2\zeta^2\right] = 2\left(\frac{d^2\zeta}{dx^2} + k^2\zeta\right)\frac{d\zeta}{dx} = 0$$

for $0 < x < L$ because of Equation (3.13a), it implies

$$\left(\frac{d\zeta}{dx}\right)^2 + k^2\zeta^2 = c^2, \tag{3.14}$$

where $c$ is a constant. Assuming $\zeta(x)$ has a Fourier representation, then

$$\zeta = b_0 + \sum_{i=1}^{\infty}\left(b_{2i-1}\cos\frac{2\pi ix}{L} + b_{2i}\sin\frac{2\pi ix}{L}\right) \tag{3.15}$$

and

$$\frac{d\zeta}{dx} = -\frac{2\pi}{L}\sum_{i=1}^{\infty} i\left(b_{2i-1}\sin\frac{2\pi ix}{L} - b_{2i}\cos\frac{2\pi ix}{L}\right), \tag{3.16}$$

where $b_0$ , $b_{2i-1}$ and $b_{2i}$ , $i = 1, 2, \ldots$, are constants. From Equation (3.15),

$$\zeta^2 = b_0^2 + 2b_0\sum_{i=1}^{\infty}\left(b_{2i-1}\cos\frac{2\pi ix}{L} + b_{2i}\sin\frac{2\pi ix}{L}\right)$$

$$+\sum_{i=1}^{\infty}\sum_{j=1}^{\infty}\left(b_{2i-1}b_{2j-1}\cos\frac{2\pi ix}{L}\cos\frac{2\pi jx}{L}\right)+\sum_{i=1}^{\infty}\sum_{j=1}^{\infty}\left(b_{2i-1}b_{2j}\cos\frac{2\pi ix}{L}\sin\frac{2\pi jx}{L}\right)$$

$$+\sum_{i=1}^{\infty}\sum_{j=1}^{\infty}\left(b_{2i}b_{2j-1}\sin\frac{2\pi ix}{L}\cos\frac{2\pi jx}{L}\right)+\sum_{i=1}^{\infty}\sum_{j=1}^{\infty}\left(b_{2i}b_{2j}\sin\frac{2\pi ix}{L}\sin\frac{2\pi jx}{L}\right). \quad (3.17)$$

Substituting Equation (3.16) into Equation (3.14),

$$\zeta^2=\frac{c^2}{k^2}-\left(\frac{2\pi}{kL}\right)^2\sum_{i=1}^{\infty}\sum_{j=1}^{\infty}\left(ijb_{2i-1}b_{2j-1}\sin\frac{2\pi ix}{L}\sin\frac{2\pi jx}{L}\right)$$

$$+\left(\frac{2\pi}{kL}\right)^2\sum_{i=1}^{\infty}\sum_{j=1}^{\infty}\left(ijb_{2i-1}b_{2j}\sin\frac{2\pi ix}{L}\cos\frac{2\pi jx}{L}\right)$$

$$+\left(\frac{2\pi}{kL}\right)^2\sum_{i=1}^{\infty}\sum_{j=1}^{\infty}\left(ijb_{2i}b_{2j-1}\cos\frac{2\pi ix}{L}\sin\frac{2\pi jx}{L}\right)$$

$$-\left(\frac{2\pi}{kL}\right)^2\sum_{i=1}^{\infty}\sum_{j=1}^{\infty}\left(ijb_{2i}b_{2j}\cos\frac{2\pi ix}{L}\cos\frac{2\pi jx}{L}\right). \quad (3.18)$$

Since Equation (3.17) and Equation (3.18) must be equivalent to each other, it implies

$$b_0=\frac{c}{k}$$

and

$$b_{2i-1}=b_{2i}=0$$

because $\cos\frac{2\pi ix}{L}$ and $\sin\frac{2\pi ix}{L}$ are linearly independent from $\cos\frac{2\pi ix}{L}\cos\frac{2\pi jx}{L}$, $\cos\frac{2\pi ix}{L}\sin\frac{2\pi jx}{L}$, $\sin\frac{2\pi ix}{L}\cos\frac{2\pi jx}{L}$ and $\sin\frac{2\pi ix}{L}\sin\frac{2\pi jx}{L}$ for $1 \le i, j < \infty$. Therefore,

$$\zeta(x)=b_0=\frac{c}{k},$$

for $0 < x < L$. By enforcing Equation (3.13) and Equation (3.14),

$$\zeta(x)=0$$

for $0 \le x \le L$. Hence the proof is completed. □

Solutions of Equations (3.1) do not exist when

$$\Omega=\frac{(2N-1)\pi}{2L}\sqrt{\frac{E}{\rho_0}},$$

where $N = 1, 2, 3, \ldots$, that is, when solutions of Equations (3.1) become singular. For

$$0 \le \Omega < \frac{\pi}{2L}\sqrt{\frac{E}{\rho_0}},$$

solutions of Equations (3.1) exist according to Subsection 3.1.1 and are unique according to Theorem 3.1. For

$$\frac{\pi}{2L}\sqrt{\frac{E}{\rho_0}} < \Omega < \frac{2\pi}{L}\sqrt{\frac{E}{\rho_0}},$$

solutions of Equations (3.1) are negative for some Lagrangian coordinate $x \in [0, L]$. Similar arguments can be applied to solutions when

$$\Omega > \frac{2\pi}{L}\sqrt{\frac{E}{\rho_0}}.$$

As a result, solution of Equations (3.1) does not exist for

$$\Omega \ge \frac{\pi}{2L}\sqrt{\frac{E}{\rho_0}}.$$

For the numerical experiment using the parameters in Section 3.3, solution of Equations (3.1) becomes invalid when

$$\Omega \ge \frac{\pi}{2L}\sqrt{\frac{E}{\rho_0}} \approx 7929 \text{ rad/s}.$$

Although Bhuta and Jones (1963a) did not work out this condition, they termed it the "static instability".

### *3.4.2 Proposed Non-Linear Model*

**Theorem 3.2.** *Let I be the closed interval $0 \le x \le L$ and u(x) be continuous with continuous first order derivatives in I. If u(x) satisfies Equations (3.8) and $0 \le d(x) \le d_0$ $\forall x \in I$, where d(x) is the diameter of the rotating rod and $d_0$ is the original diameter of the non-rotating rod, then u(x) is a solution of Equations (3.8). Nevertheless, u(x) is not the only function in I with such properties. In addition, if*

$$d(x) < \frac{2}{3} d_0$$

*for some or all $x \in I$ while the angular velocity $\Omega \neq 0$, there exists no physically correct u(x) that will satisfy Equations (3.8).*

**Proof.** From Poisson's relation,

$$\varepsilon(x) = -\frac{d - d_0}{d_0 \upsilon},$$

where $d = d(x)$. Substituting this into Equation (3.2) gives

$$d^2[d - d_0] = -\frac{4}{\pi E} d_0 \upsilon F,$$

where $0 \le d = d(x) \le d_0$. Now let

$$h_1(d) = d^2[d - d_0],$$

then

$$h_1'(d) = 3d^2 - 2dd_0$$

and

$$h_1''(d) = 6d - 2d_0.$$

When $h_1'(d) = 0$, $d = \frac{2}{3} d_0$. Hence $h_1\left(\frac{2}{3} d_0\right)$ is minimum because

$$h_1''\left(\frac{2}{3} d_0\right) = 2d_0 > 0.$$

Also let

$$h_2(d) = -\frac{4}{\pi E} d_0 \upsilon F,$$

then for each $x \in [0, L]$, one of the two intersections of $h_1(d)$ and $h_2(d)$ is the physically correct solution of Equations (3.8) at a specified $\Omega$ provided that $h_2(d) > h_1\left(\frac{2}{3} d_0\right)$, the other solution is physically meaningless, or there is only one physically correct solution if $h_2(d) = h_1\left(\frac{2}{3} d_0\right)$. When $\frac{2}{3} d_0 < d(x) < d_0$, $h_2(d) = -\frac{4}{\pi E} d_0 \upsilon F$ is decreasing as the centripetal force $F = F(x)$ is increasing. Consequently the intersections of $h_1(d)$ with $h_2(d)$ indicate that the diameter of the whirling rod is decreasing because $h_1'(d) = 3d^2 - 2dd_0 > 0$. Hence the intersections between $h_1(d)$ and $h_2(d)$ give the physically correct solution. When $0 < d(x) < \frac{2}{3} d_0$, $h_2(d) = -\frac{4}{\pi E} d_0 \upsilon F$ is decreasing as the centripetal force $F = F(x)$ is increasing. Consequently the intersections of $h_1(d)$ with $h_2(d)$ indicate that the diameter of the whirling rod is increasing because $h_1'(d) = 3d^2 - 2dd_0 < 0$. Hence

the intersections between $h_1(d)$ and $h_2(d)$ give the physically incorrect solution. Moreover, if $\Omega$ keeps increasing beyond a point such that

$$h_2(d) < h_1\left(\frac{2}{3}d_0\right)$$

for some or all $x \in [0, L]$, then $h_1(d)$ and $h_2(d)$ will not intersect each other for those $x \in [0, L]$. Hence no solution will be obtained. As a result, there is no physically correct solution for Equations (3.8) when

$$d(x) < \frac{2}{3}d_0$$

for some or all $x \in [0, L]$. □

It is at this point when $d = \frac{2}{3}d_0$, nonlinear solution becomes unstable. For the numerical experiment using the method proposed in Subsection 3.2.2 and parameters in Section 3.3, numerical solutions become unstable when $\frac{d(0)}{d_0} < 0.7$. This is slightly different from the condition $\frac{d(0)}{d_0} < \frac{2}{3}$ stated in Theorem 2. The reason for this is probably because of the truncation and round-off errors. When $d(0) = 0.7\ d_0$, the corresponding angular velocity $\Omega \approx 4094$ rad/s from the numerical results compared to 7929 rad/s addressed by Theorem 1.

The proof of uniqueness in Theorem 3.1 is a proof by contradiction. Such a proof by contradiction had been applied by Sagan (1989) to show uniqueness of solution on heat and wave equations. This chapter establishes a formulation of steady whirling rods that could be further extended to nonlinear formulation of dynamic whirling rods or beams with non-circular cross section. Proposed numerical method has been demonstrated to be a simple, efficient and accurate numerical method. According to Section 3.4, vibration problems formulated in Lagrangian coordinate need to be concerned about the existence and uniqueness of solution. On the contrary, vibration problems formulated in Eulerian coordinate might be free from such an issue.

# Chapter 4

## Dynamic Motion of Rotating Annuli[10]

When a thin disc or annulus is rotating about its centre, each differentially small circular strip of the disc or annulus is subject to the centripetal tensile force due to the mass of the material beyond that strip. If an evenly distributed normal oscillation stress is applied around the outer edge of the disc or annulus, it is under axisymmetric radial vibration. On the other hand, if an evenly distributed shear oscillation stress is applied around the outer edge of the disc or annulus, it is under axisymmetric circumferential vibration. Axisymmetric vibration means that vibration of the rotating disc or annulus is autonomous to the circumferential direction. Usually, if the governing equations of a rotating disc or annulus are linear, then the static motion, which is due to the rotation, and the dynamic motion, which is due to the oscillation, may be considered separately. This allows the analytical analysis of the linear vibration problem possible. Since only thin disc or annulus is considered, the transverse contraction of the plate thickness in the direction perpendicular to the disc or annulus due to in-plane displacements is presumed to be negligible.

### *4.1 Governing Equations of Motion*

Axisymmetric in-plane vibrations of annular plates at constant low angular velocity $\Omega$ were formulated by Bhuta and Jones (1963b) in both Eulerian and Lagrangian coordinates and by Biezeno and Grammel (1954) in Eulerian coordinates. Some previous work had applied free edge boundary condition of rotating discs in Eulerian coordinates (Bhuta and Jones (1963b)). But this free edge position in Eulerian coordinate is exactly the same as the free edge of the disc when it is not rotating. However, this is obviously not true, because when the disc is rotating, that free edge in Eulerian coordinates under radial and circumferential strain must be different from the free edge position of the non-rotating disc. Therefore, problems

[10] Part of the work in this chapter had been submitted as reference 2 mentioned on p.98 and is now under editorial evaluation by the editor.

formulated in Lagrangian coordinates are better modelled than those in Eulerian coordinates because of the proper implementation of the free edge boundary condition. In order to compare the results obtained from these two models, Biezeno and Grammel's model is transformed below into Lagrangian coordinates ($r$, $\theta$). A geometric view of such a rotating annulus is depicted in Figure 1.

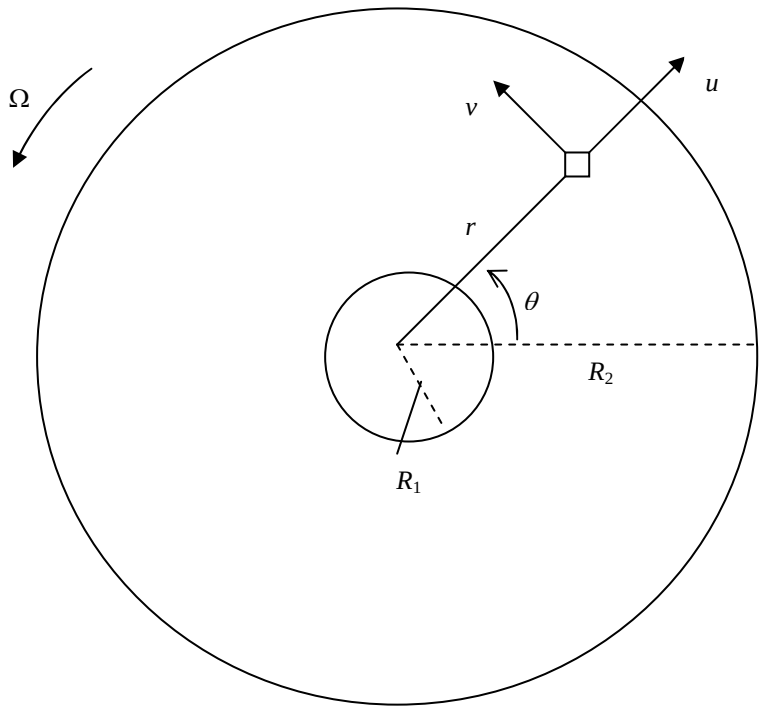


Figure 4.1. A view of an annular plate depicted in Lagrangian coordinates ($r$,$\theta$).

Figure 4.1 shows an annulus rotating at constant angular velocity Ω in Lagrangian coordinates ($r$, $\theta$) which has an inner radius $R_1$ and an outer radius $R_2$. The differentially small square element in the figure is under radial displacement $u$ and circumferential displacement $v$. Full derivations of both governing equations can be found in Appendix D of this thesis.

### *4.1.1 Bhuta and Jones' Model*

According to Bhuta and Jones (1963b), axisymmetric rotational motion of a thin parallel annulus in Lagrangian coordinate $r$ may be described by

$$\frac{\partial^2 u}{\partial r^2}+\frac{1}{r}\frac{\partial u}{\partial r}-\frac{u}{r^2}=(1-\upsilon^2)\frac{\rho_0}{E}\left[\frac{\partial^2 u}{\partial t^2}-2\Omega\frac{\partial v}{\partial t}-(r+u)\Omega^2\right], \tag{4.1a}$$

$$\frac{\partial^2 v}{\partial r^2}+\frac{1}{r}\frac{\partial v}{\partial r}-\frac{v}{r^2}=\frac{\rho_0}{G}\left[\frac{\partial^2 v}{\partial t^2}+2\Omega\frac{\partial u}{\partial t}-v\Omega^2\right]. \tag{4.1b}$$

Assuming a clamped boundary condition at the inner radius $r = R_1$, then

$$u(R_1) = 0 \tag{4.1c}$$

and

$$v(R_1) = 0. \tag{4.1d}$$

If excitation radial normal stress $P_r e^{j\omega t}$ and excitation torsional or circumferential shear stress $P_c e^{j\omega t}$ are applied at the outer radius $r = R_2$, then

$$\frac{E}{1-\upsilon^2}\left[\frac{\partial u}{\partial r}+\upsilon\frac{u}{r}\right]_{r=R_2} = P_r e^{j\omega t} \tag{4.1e}$$

and

$$G\left[\frac{\partial v}{\partial r}-\frac{v}{r}\right]_{r=R_2} = P_c e^{j\omega t}, \tag{4.1f}$$

where $\rho_0$ is the uniform material density of the annulus, $\upsilon$ is the Poisson's ratio, $E$ is the Young's modulus, $G = \frac{E}{2(1+\upsilon)}$ is the shear modulus, $\omega$ is the excitation frequency, $r$ is the Lagrangian radial distance from the axis of rotation, $t$ is the time variable, $P_r$ is the amplitude of the radial excitation normal stress and $P_c$ is the amplitude of the torsional or circumferential excitation shear stress. To the best knowledge of the author of this thesis, no previous work has applied such boundary conditions at the outer radius $R_2$ to determine the natural frequencies of rotating annuli. If the solutions of Equations (4.1) are written as

$$u(r,t) = u_0(r) + u_1(r)e^{j\omega t}$$

and

$$v(r,t) = v_0(r) + v_1(r)e^{j\omega t},$$

where $u_0$ is the static radial displacement due to rotation, $u_1$ is the dynamic radial displacement, $v_0$ is the static circumferential displacement and $v_1$ is the dynamic circumferential displacement, then Equations (4.1) can be split into two parts, the static and dynamic parts. Substituting the alleged forms for $u(r,t)$ and $v(r,t)$ into Equations (4.1) and retaining only the static motions, the static equations are given by

$$\frac{d^2u_0}{dr^2}+\frac{1}{r}\frac{du_0}{dr}-\frac{u_0}{r^2}=-(1-\upsilon^2)\frac{\rho_0}{E}(r+u_0)\Omega^2\,, \tag{4.2a}$$

$$\frac{d^2v_0}{dr^2}+\frac{1}{r}\frac{dv_0}{dr}-\frac{v_0}{r^2}=-\frac{\rho_0}{G}v_0\Omega^2\,, \tag{4.2b}$$

$$u_0(R_1)=0, \tag{4.2c}$$

$$v_0(R_1)=0, \tag{4.2d}$$

$$\left[\frac{du_0}{dr}+\upsilon\frac{u_0}{r}\right]_{r=R_2}=0 \tag{4.2e}$$

$$\left[\frac{dv_0}{dr}-\frac{v_0}{r}\right]_{r=R_2}=0. \tag{4.2f}$$

From the outer Boundary Conditions (4.2e,f), it can be seen that the dynamic oscillations have no effect on the steady rotating annulus. Substituting the alleged forms for $u(r,t)$ and $v(r,t)$ into Equations (4.1) and retaining only the dynamic motions, the dynamic equations are given by

$$\frac{d^2u_1}{dr^2}+\frac{1}{r}\frac{du_1}{dr}-\frac{u_1}{r^2}=-(1-\upsilon^2)\frac{\rho_0}{E}\left[\omega^2u_1+2j\omega\Omega v_1+u_1\Omega^2\right], \tag{4.3a}$$

$$\frac{d^2v_1}{dr^2}+\frac{1}{r}\frac{dv_1}{dr}-\frac{v_1}{r^2}=-\frac{\rho_0}{G}\left[\omega^2v_1-2j\omega\Omega u_1+v_1\Omega^2\right], \tag{4.3b}$$

$$u_1(R_1)=0, \tag{4.3c}$$

$$v_1(R_1)=0, \tag{4.3d}$$

$$\frac{E}{1-\upsilon^2}\left[\frac{du_1}{dr}+\upsilon\frac{u_1}{r}\right]_{r=R_2}=P_r \tag{4.3e}$$

$$G\left[\frac{dv_1}{dr}-\frac{v_1}{r}\right]_{r=R_2}=P_c. \tag{4.3f}$$

Notice that Equations (4.3) have been transformed from the time-domain into the frequency-domain problem where the term $e^{j\omega t}$ has been cancelled out throughout the equations. This allows the analysis of the dynamic motion of a monochromatic wave of frequency $\omega$ in a frozen time frame. From the outer Boundary Conditions (4.3e,f), the dynamic oscillations only associate with the dynamic motions of the vibrating annulus. Simple harmonic oscillations with frequency $\omega$ are applied to both radial and circumferential directions. This oscillation frequency $\omega$ corresponds to the resonance frequency when it coincides with one of the natural frequencies of a rotating annulus.

### *4.1.2 Biezeno and Grammel's Model*

According to Biezeno and Grammel (1954), axisymmetric rotating motion of a thin annular plate with varying thickness in Eulerian coordinates ($R$, $\Theta$) are governed by

$$\frac{\sigma_R}{y}\frac{dy}{dR}+\frac{\partial\sigma_R}{\partial R}+\frac{\sigma_R-\sigma_\Theta}{R}=f_R, \tag{4.4a}$$

$$\frac{\tau_{R\Theta}}{y}\frac{dy}{dR}+\frac{\partial\tau_{R\Theta}}{\partial R}+\frac{2\tau_{R\Theta}}{R}=f_\Theta, \tag{4.4b}$$

where $\sigma_R$ is the radial normal stress in Eulerian coordinates, $\sigma_\Theta$ is the circumferential normal stress in Eulerian coordinates, $\tau_{R\Theta}$ is the circumferential shear stress in Eulerian coordinates, $f_R$ is the radial body force per unit volume in Eulerian coordinates, $f_\Theta$ is the circumferential body force per unit volume in Eulerian coordinates and $y = y(R)$ is the thickness profile of the rotating annulus. Using small strain analysis described by Bhuta and Jones (1963b),

$$\left|\frac{\partial u}{\partial r}\right| << 1$$

and

$$\left|\frac{u}{r}\right| << 1,$$

together with the approximation

$$\frac{dy}{dR}\approx\left(1+\frac{du_0}{dr}\right)^{-1}\frac{dy}{dr}\approx\left(1+\frac{\partial u}{\partial r}\right)^{-1}\frac{dy}{dr}\approx\frac{dy}{dr},$$

where $R = r + u(r, t)$ and the approximation $\frac{dR}{dr}\approx\left(1+\frac{du_0}{dr}\right)\approx\left(1+\frac{\partial u}{\partial r}\right)\approx 1$ has been used, Equations (4.4) can be transformed into Lagrangian coordinates ($r$, $\theta$),

$$\frac{\sigma_r}{y}\frac{dy}{dr}+\frac{\partial\sigma_r}{\partial r}+\frac{\sigma_r-\sigma_\theta}{r}=f_r, \tag{4.5a}$$

$$\frac{\tau_{r\theta}}{y}\frac{dy}{dr}+\frac{\partial\tau_{r\theta}}{\partial r}+\frac{2\tau_{r\theta}}{r}=f_\theta, \tag{4.5b}$$

where $\sigma_r$ is the radial normal stress in Lagrangian coordinates, $\sigma_\theta$ is the circumferential normal stress in Lagrangian coordinates, $\tau_{r\theta}$ is the circumferential shear stress in Lagrangian coordinates, $f_r$ is the radial body force per unit volume in Lagrangian coordinates, $f_\theta$ is the circumferential body force per unit volume in Lagrangian

coordinates and $y = y(r)$ is the thickness profile of the rotating annulus. But From Gere and Timoshenko (1985),

$$\sigma_r = \frac{E}{1-\upsilon^2}\left[\frac{\partial u}{\partial r} + \upsilon\frac{u}{r}\right],$$

$$\sigma_\theta = \frac{E}{1-\upsilon^2}\left[\frac{u}{r} + \upsilon\frac{\partial u}{\partial r}\right],$$

$$\tau_{r\theta} = Gr\frac{\partial \vartheta}{\partial r},$$

and from Bhuta and Jones (1963b),

$$f_r = \rho\left[\frac{\partial^2 u}{\partial t^2} - 2\Omega r\frac{\partial \vartheta}{\partial t} - (r+u)\Omega^2\right],$$

$$f_\theta = \rho\left[\frac{\partial^2 \vartheta}{\partial t^2} + \frac{2\Omega}{r}\frac{\partial u}{\partial t} - \vartheta\Omega^2\right],$$

where $\vartheta$ is the angular displacement in Lagrangian coordinates, $\rho$ is the variable material density of the annulus when the annulus is rotating. Substituting these five expressions into Equations (4.5),

$$\frac{\partial^2 u}{\partial r^2} + \left(\frac{1}{y}\frac{dy}{dr} + \frac{1}{r}\right)\frac{\partial u}{\partial r} + \left(\frac{\upsilon}{ry}\frac{dy}{dr} - \frac{1}{r^2}\right)u = (1-\upsilon^2)\frac{\rho}{E}\left[\frac{\partial^2 u}{\partial t^2} - 2\Omega r\frac{\partial \vartheta}{\partial t} - (r+u)\Omega^2\right], \quad (4.6a)$$

$$\frac{\partial^2 \vartheta}{\partial r^2} + \left(\frac{1}{y}\frac{dy}{dr} + \frac{3}{r}\right)\frac{\partial \vartheta}{\partial r} = \frac{\rho}{G}\left[\frac{\partial^2 \vartheta}{\partial t^2} + \frac{2\Omega}{r}\frac{\partial u}{\partial t} - \vartheta\Omega^2\right]. \quad (4.6b)$$

Note that from plane geometry, the arc length of a circle is just the product of the radius of the circle and the angle subtended by the arc. Hence the relationship between the angular displacement $\vartheta(r, t)$ in Biezeno and Grammel's model and the circumferential displacement $v(r, t)$ in Bhuta and Jones' model is described by $v(r, t) = r\vartheta(r, t)$. Assuming a clamped boundary condition at $r = R_1$, then

$$u(R_1) = 0, \quad (4.6c)$$

and

$$\vartheta(R_1) = 0, \quad (4.6d)$$

If excitation radial normal stress $P_r e^{j\omega t}$ and excitation torsional or circumferential shear stress $P_c e^{j\omega t}$ are applied at the boundary $r = R_2$, then

$$\frac{E}{1-\upsilon^2}\left[\frac{\partial u}{\partial r} + \upsilon\frac{u}{r}\right]_{r=R_2} = P_r e^{j\omega t}, \quad (4.6e)$$

and

$$G\left[r\frac{\partial \vartheta}{\partial r}\right]_{r=R_2} = P_c e^{j\omega t}. \qquad (4.6f)$$

All the variables in Equations (4.6) are similarly defined as in Subsection 4.1.1. Again, such boundary conditions at the outer radius $R_2$ to find the natural frequencies of rotating annuli have not been previously applied by other researchers. In addition, material density $\rho$ in the original Biezeno and Grammel's model was assumed to be constant. For the case of parallel annulus, $y$ becomes a constant. Thus, Biezeno and Grammel's model reduces to Bhuta and Jones' model. For the current studies, Poisson's effect will be introduced into the steady rotation of the annulus. This model improves upon Equations (4.1) because the Poisson's effect, which accounts the variations of material density and thickness of annuli, has been included. From Poisson's ratio, the lateral strain $\varepsilon_z$ is given by

$$\varepsilon_z = \frac{y - y_0}{y_0},$$

where $y_0$ is the original constant thickness of the annulus. But from two-dimensional Hooke's law,

$$\varepsilon_z = -\frac{\upsilon}{E}(\sigma_r + \sigma_\theta) = -\frac{\upsilon}{1-\upsilon}(\varepsilon_r + \varepsilon_\theta).$$

where $\varepsilon_r$ is the radial normal strain in Lagrangian coordinates and $\varepsilon_\theta$ is the circumferential normal strain in Lagrangian coordinates. Combining the above two equations,

$$y = y(r) = y_0\left[1 - \frac{\upsilon}{1-\upsilon}(\varepsilon_r + \varepsilon_\theta)\right].$$

If small strain analysis is assumed, then $\varepsilon_r = \frac{\partial u}{\partial r}$ and $\varepsilon_\theta = \frac{u}{r}$ (Fung (1994)). By ignoring the dynamic effect, radial and circumferential normal strains become $\varepsilon_r = \frac{du_0}{dr}$ and $\varepsilon_\theta = \frac{u_0}{r}$ respectively. Substituting these two static strain-displacement relationships into the previous expression,

$$y = y(r) = y_0\left[1 - \frac{\upsilon}{1-\upsilon}\left(\frac{du_0}{dr} + \frac{u_0}{r}\right)\right].$$

By conservation of mass, the mass of each of the differentially small section with volume $yrd\theta dr$ in Lagrangian coordinates of a stationary annulus is equivalent to the

mass of the same differentially small section with volume $yRd\Theta dR$ in Eulerian coordinates while the annulus is steadily rotating. Hence

$$\int_0^{2\pi}\left[\int_{R_1}^{s+u(s)} y\rho R dR\right]d\Theta = \int_0^{2\pi}\left[\int_{R_1}^{s} y_0\rho_0 r dr\right]d\theta\,, \tag{4.7}$$

where $R_1 \le s \le R_2$. Integrating w.r.t. $\Theta$ on the left hand side and $\theta$ on the right hand side of Equation (4.7),

$$\int_{R_1}^{s+u(s)} y\rho R dR = \int_{R_1}^{s} y_0\rho_0 r dr\,.$$

Replacing $R$ by $r + u_0(r)$ by ignoring the dynamic effect and changing the order of integration in the above equation,

$$\int_{R_1}^{s}\left[y\rho(r+u_0)\frac{dR}{dr} - y_0\rho_0 r\right]dr = 0.$$

Since this integration is true $\forall s \in [R_1, R_2]$, the integrand of this integral must be zero. Therefore, after rearrangement, the variable density of a rotating annulus becomes

$$\rho = \rho(r) = \frac{y_0\rho_0 r}{y(r+u_0)}\left(1+\frac{du_0}{dr}\right)^{-1}.$$

Note that $\frac{dR}{dr} \approx \left(1+\frac{du_0}{dr}\right)$ has been used in the above expression. By small strain analysis, $\left|\frac{\partial u}{\partial r}\right| \approx \left|\frac{du_0}{dr}\right| << 1$ if dynamic effect is ignored. As a result,

$$\rho = \rho(r) = \frac{y_0\rho_0 r}{y(r+u_0)}.$$

If the solutions of the model are written as

$$u(r,t) = u_0(r) + u_1(r)e^{j\omega t}$$

and

$$\vartheta(r,t) = \vartheta_0(r) + \vartheta_1(r)e^{j\omega t}\,,$$

where $\vartheta_0$ is the static angular displacement and $\vartheta_1$ is the dynamic angular displacement, then Equations (4.6) can be split into two parts, the static and dynamic parts. Substituting the alleged forms for $u(r,t)$ and $\vartheta(r,t)$ into Equations (4.6) and retaining only the static motions, the static equations are given by

$$\frac{d^2u_0}{dr^2} + \left(\frac{1}{y}\frac{dy}{dr} + \frac{1}{r}\right)\frac{du_0}{dr} + \left(\frac{\upsilon}{ry}\frac{dy}{dr} - \frac{1}{r^2}\right)u_0 = -(1-\upsilon^2)\frac{\rho}{E}(r+u_0)\Omega^2\,, \tag{4.8a}$$

$$\frac{d^2\vartheta_0}{dr^2}+\left(\frac{1}{y}\frac{dy}{dr}+\frac{3}{r}\right)\frac{d\vartheta_0}{dr}=-\frac{\rho}{G}\,\vartheta_0\Omega^2\,, \tag{4.8b}$$

$$u_0(R_1)=0, \tag{4.8c}$$

$$\vartheta_0(R_1)=0, \tag{4.8d}$$

$$\left[\frac{du_0}{dr}+\upsilon\frac{u_0}{r}\right]_{r=R_2}=0, \tag{4.8e}$$

$$\left[\frac{d\vartheta_0}{dr}\right]_{r=R_2}=0. \tag{4.8f}$$

From the outer Boundary Conditions (4.2e,f), the dynamic oscillations have no effect on the steady rotating annulus. Substituting the alleged forms for $u(r,t)$ and $\vartheta(r,t)$ into Equations (4.6) and retaining only the dynamic motions, the dynamic equations are given by

$$\frac{d^2u_1}{dr^2}+\left(\frac{1}{y}\frac{dy}{dr}+\frac{1}{r}\right)\frac{du_1}{dr}+\left(\frac{\upsilon}{ry}\frac{dy}{dr}-\frac{1}{r^2}\right)u_1=-(1-\upsilon^2)\frac{\rho}{E}\left[\omega^2u_1+2j\omega\Omega r\vartheta_1+u_1\Omega^2\right], \tag{4.9a}$$

$$\frac{d^2\vartheta_1}{dr^2}+\left(\frac{1}{y}\frac{dy}{dr}+\frac{3}{r}\right)\frac{d\vartheta_1}{dr}=-\frac{\rho}{G}\left[\omega^2\vartheta_1-\frac{2j\omega\Omega}{r}u_1+\vartheta_1\Omega^2\right], \tag{4.9b}$$

$$u_1(R_1)=0, \tag{4.9c}$$

$$\vartheta_1(R_1)=0, \tag{4.9d}$$

$$\frac{E}{1-\upsilon^2}\left[\frac{du_1}{dr}+\upsilon\frac{u_1}{r}\right]_{r=R_2}=P_r, \tag{4.9e}$$

$$G\left[r\frac{d\vartheta_1}{dr}\right]_{r=R_2}=P_c. \tag{4.9 f}$$

Notice that Equations (4.9) have been transformed from the time-domain into the frequency-domain problem where the term $e^{j\omega t}$ has been cancelled out throughout the equations. This allows the analysis of the dynamic motion of a monochromatic wave of frequency $\omega$ in a frozen time frame. From the outer Boundary Conditions (4.9e,f), the dynamic oscillations only associate with the dynamic motions of the vibrating annulus. Simple harmonic oscillations with frequency $\omega$ are applied to both radial and circumferential directions. This oscillation frequency $\omega$ corresponds to the resonance frequency when it coincides with one of the natural frequencies of a rotating annulus.

## *4.2 Analytical Solution for Bhuta and Jones' Model*

Although Bhuta and Jones had attempted to solve Equations (4.1) analytically by splitting them to Equations (4.2) and Equations (4.3), their solutions nevertheless did not take any specific boundary conditions into account. Moreover, the closed form solutions for both Equations (4.2) and Equations (4.3) were somewhat different from what have been obtained below. This section is devoted to find the analytical solutions for Equations (4.2) and Equations (4.3) with specified boundary conditions. Since Bhuta and Jones' model is deduced under the assumption of small strain, the results obtained from these governing equations are limited to low angular velocity.

### *4.2.1 Exact Static Solution*

Since Equations (4.2) are inhomogeneous Bessel differential equations, by incorporating the homogeneous solution of Bessel differential equation from Spiegel (1971), the exact solution can be easily found to be

$$u_0(r) = m_1 J_1(\lambda r) + m_2 Y_1(\lambda r) - r$$

and

$$v_0(r) = 0,$$

where

$$m_1 = \frac{\begin{vmatrix} d_{a1} & a_{12} \\ d_{a2} & a_{22} \end{vmatrix}}{|A|},$$

$$m_2 = \frac{\begin{vmatrix} a_{11} & d_{a1} \\ a_{21} & d_{a2} \end{vmatrix}}{|A|},$$

$$|A| = \begin{vmatrix} a_{11} & a_{12} \\ a_{21} & a_{22} \end{vmatrix},$$

$$\lambda = \Omega \sqrt{(1-\upsilon^2)\frac{\rho_0}{E}},$$

$$a_{11} = J_1(\lambda R_1),$$

$$a_{12} = Y_1(\lambda R_1),$$

$$a_{21} = \frac{\lambda}{2}[\, J_0(\lambda R_2) - J_2(\lambda R_2)] + \frac{\upsilon}{R_2} J_1(\lambda R_2),$$

$$a_{22} = \frac{\lambda}{2}[\, Y_0(\lambda R_2) - Y_2(\lambda R_2)] + \frac{\upsilon}{R_2} Y_1(\lambda R_2),$$

$$d_{a1} = R_1 \,,$$

$$d_{a2} = 1 + \upsilon,$$

$J_n(.)$ is the Bessel function of the first kind of order $n$,

$Y_n(.)$ is the Bessel function of the second kind of order $n$.

The steady analytical solution indicates that there is no displacement occurs in the circumferential direction. This is obviously true because when the annulus is under static rotation, the centripetal force is the only force acting in the radial direction that produces no circumferential displacement in the tangential direction.

### *4.2.2 Approximate Dynamic Solution*

In view of Equations (4.3), it is a system of differential equations coupled with dynamic radial displacement $u_1$ and dynamic circumferential displacement $v_1$. Some previous researchers had decoupled the equations by assuming the Coriolis effect is minuscule. If the Coriolis terms $2j\omega\Omega u_1$ and $2j\omega\Omega v_1$ are ignored, Equations (4.3) can be decoupled to be homogeneous Bessel differential equations. As a result, solutions of the decoupled equations become the approximate solutions of Equations (4.3) with

$$\mathrm{Re}[u_1(r)] \approx m_3 J_1(\mu r) + m_4 Y_1(\mu r)$$

and

$$\mathrm{Im}[u_1(r)] \approx 0,$$

where

$$m_3 = \frac{\begin{vmatrix} d_{b1} & b_{12} \\ d_{b2} & b_{22} \end{vmatrix}}{|\, B \,|},$$

$$m_4 = \frac{\begin{vmatrix} b_{11} & d_{b1} \\ b_{21} & d_{b2} \end{vmatrix}}{|\, B \,|},$$

$$|B| = \begin{vmatrix} b_{11} & b_{12} \\ b_{21} & b_{22} \end{vmatrix},$$

$$\mu = \sqrt{(1-\upsilon^2)(\omega^2 + \Omega^2)\frac{\rho_0}{E}},$$

$$b_{11} = J_1(\mu R_1),$$

$$b_{12} = Y_1(\mu R_1),$$

$$b_{21} = \frac{\mu}{2}[\, J_0(\mu R_2) - J_2(\mu R_2)] + \frac{\upsilon}{R_2} J_1(\mu R_2),$$

$$b_{22} = \frac{\mu}{2}[\, Y_0(\mu R_2) - Y_2(\mu R_2)] + \frac{\upsilon}{R_2} Y_1(\mu R_2),$$

$$d_{b1} = 0,$$

$$d_{b2} = (1-\upsilon^2)\frac{P_r}{E}.$$

Furthermore,

$$\mathrm{Re}[v_1(r)] \approx m_5 J_1(\gamma r) + m_6 Y_1(\gamma r)$$

and

$$\mathrm{Im}[v_1(r)] \approx 0,$$

where

$$m_5 = \frac{\begin{vmatrix} d_{c1} & c_{12} \\ d_{c2} & c_{22} \end{vmatrix}}{|C|},$$

$$m_6 = \frac{\begin{vmatrix} c_{11} & d_{c1} \\ c_{21} & d_{c2} \end{vmatrix}}{|C|},$$

$$|C| = \begin{vmatrix} c_{11} & c_{12} \\ c_{21} & c_{22} \end{vmatrix},$$

$$\gamma = \sqrt{(\omega^2 + \Omega^2)\frac{\rho_0}{G}},$$

$$c_{11} = J_1(\gamma R_1),$$

$$c_{12} = Y_1(\gamma R_1),$$

$$c_{21} = \frac{\gamma}{2}[\, J_0(\gamma R_2) - J_2(\gamma R_2)] - \frac{1}{R_2} J_1(\gamma R_2),$$

$$c_{22} = \frac{\gamma}{2}[\, Y_0(\gamma R_2) - Y_2(\gamma R_2)] - \frac{1}{R_2} Y_1(\gamma R_2),$$

$$d_{c1} = 0,$$

$$d_{c2} = \frac{P_c}{G}.$$

When Equations (4.3) are decoupled, only the real parts of the dynamic solutions exist. The imaginary parts become non-existent and they are induced only if Coriolis effect is present. This approximate solution is supposed to have close agreement with the exact dynamic solution at low angular velocity discussed in the next subsection.

### *4.2.3 Exact Dynamic Solution*

Equations (4.3) are second order differential equations coupled with radial dynamic displacement $u_1(r)$ and circumferential dynamic displacement $v_1(r)$. Suppose $\chi$ denotes the second order differential operator

$$\frac{d^2}{dr^2} + \frac{1}{r}\frac{d}{dr} - \frac{1}{r^2},$$

then from Equation (4.3a),

$$v_1(r) = -\frac{1}{2j\omega\Omega k_1}[\chi(u_1) + k_1(\omega^2 + \Omega^2)u_1], \tag{4.10}$$

where

$$k_1 = (1 - \upsilon^2)\frac{\rho_0}{E}.$$

Substituting Equation (4.10) into Equation (4.3b),

$$\chi^2(u_1) + (k_1 + k_2)(\omega^2 + \Omega^2)\chi(u_1) + k_1 k_2 (\omega^2 - \Omega^2)^2 u_1 = 0,$$

where $\chi^2$ is the fourth order differential operator

$$\left(\frac{d^2}{dr^2} + \frac{1}{r}\frac{d}{dr} - \frac{1}{r^2}\right)^2$$

and

$$k_2 = \frac{\rho_0}{G}.$$

By factorizing the above fourth order differential equation into an equivalent differential equation with second order differential operators,

$$[\chi + \kappa_1^2][\chi + \kappa_2^2](u_1) = 0,$$

where

$$\kappa_1^2 = \frac{1}{2}\left[(k_1 + k_2)(\omega^2 + \Omega^2) - \sqrt{(k_1 + k_2)^2(\omega^2 + \Omega^2)^2 - 4k_1k_2(\omega^2 - \Omega^2)^2}\right],$$

and

$$\kappa_2^2 = \frac{1}{2}\left[(k_1 + k_2)(\omega^2 + \Omega^2) + \sqrt{(k_1 + k_2)^2(\omega^2 + \Omega^2)^2 - 4k_1k_2(\omega^2 - \Omega^2)^2}\right].$$

Notice that the second order differential operators $\chi + \kappa_1^2$ or $\chi + \kappa_2^2$ has the exact same form for a second order differential operator applied on a Bessel differential equation. The reason that the notations $\kappa_1^2$ and $\kappa_2^2$ are employed will become evident once they are proven to be non-negative. Suppose $\omega \neq 0$ and $\Omega \neq 0$, then

$$(k_1 + k_2)^2(\omega^2 + \Omega^2)^2 - 4\,k_1\,k_2\,(\omega^2 - \Omega^2)^2 > (k_1 + k_2)^2(\omega^2 - \Omega^2)^2 - 4\,k_1\,k_2\,(\omega^2 - \Omega^2)^2$$
$$= (k_1 - k_2)^2(\omega^2 - \Omega^2)^2 \geq 0.$$

These indicate that the square root quantities in the expressions of $\kappa_1^2$ and $\kappa_2^2$ are real and positive. Since $k_1 > 0$ and $k_2 > 0$,

$$\frac{(k_1 + k_2)^2(\omega^2 + \Omega^2)^2 - 4k_1k_2(\omega^2 - \Omega^2)^2}{(k_1 + k_2)^2(\omega^2 + \Omega^2)^2} = 1 - \frac{4k_1k_2(\omega^2 - \Omega^2)^2}{(k_1 + k_2)^2(\omega^2 + \Omega^2)^2} \leq 1$$

or

$$(k_1 + k_2)^2(\omega^2 + \Omega^2)^2 \geq (k_1 + k_2)^2(\omega^2 + \Omega^2)^2 - 4\,k_1\,k_2\,(\omega^2 - \Omega^2)^2.$$

Hence $\kappa_1^2 \geq 0$ and $\kappa_2^2 > 0$. Thus

$$u_1(r) = K_1\,J_1(\kappa_1 r) + K_2\,Y_1(\kappa_1 r) + K_3\,J_1(\kappa_2 r) + K_4\,Y_1(\kappa_2 r), \tag{4.11a}$$

where $K_1$ , $K_2$ , $K_3$ and $K_4$ are arbitrary complex constants which can be determined from Equations (4.3c,d,e,f). Using Equation (4.10) and Solution (4.11a), Equations (4.3c,d,e,f) become respectively

$$K_1\,J_1(\kappa_1 R_1) + K_2\,Y_1(\kappa_1 R_1) + K_3\,J_1(\kappa_2 R_1) + K_4\,Y_1(\kappa_2 R_1) = 0, \tag{4.11b}$$

$$[\kappa_1^2 - k_1(\omega^2 + \Omega^2)][K_1\,J_1(\kappa_1 R_1) + K_2\,Y_1(\kappa_1 R_1)]$$
$$+ [\kappa_2^2 - k_1(\omega^2 + \Omega^2)][K_3\,J_1(\kappa_2 R_1) + K_4\,Y_1(\kappa_2 R_1)] = 0, \tag{4.11c}$$

$$K_1\left[\kappa_1 J_0(\kappa_1 R_2) + \left(\frac{\upsilon - 1}{R_2}\right)J_1(\kappa_1 R_2)\right] + K_2\left[\kappa_1 Y_0(\kappa_1 R_2) + \left(\frac{\upsilon - 1}{R_2}\right)Y_1(\kappa_1 R_2)\right]$$
$$+ K_3\left[\kappa_2 J_0(\kappa_2 R_2) + \left(\frac{\upsilon - 1}{R_2}\right)J_1(\kappa_2 R_2)\right] + K_4\left[\kappa_2 Y_0(\kappa_2 R_2) + \left(\frac{\upsilon - 1}{R_2}\right)Y_1(\kappa_2 R_2)\right]$$
$$= \frac{1 - \upsilon^2}{E}P_r, \tag{4.11d}$$

$$[\kappa_1^2 - k_1(\omega^2 + \Omega^2)] \times$$

$$\left\{K_1\left[\kappa_1 J_0(\kappa_1 R_2) - \frac{2}{R_2} J_1(\kappa_1 R_2)\right] + K_2\left[\kappa_1 Y_0(\kappa_1 R_2) - \frac{2}{R_2} Y_1(\kappa_1 R_2)\right]\right\}$$

$$+ [\kappa_2^2 - k_1(\omega^2 + \Omega^2)] \times$$

$$\left\{K_3\left[\kappa_2 J_0(\kappa_2 R_2) - \frac{2}{R_2} J_1(\kappa_2 R_2)\right] + K_4\left[\kappa_2 Y_0(\kappa_2 R_2) - \frac{2}{R_2} Y_1(\kappa_2 R_2)\right]\right\}$$

$$= 2j\omega\Omega k_1 \frac{P_c}{G}. \tag{4.11e}$$

By the same token, from Equation (4.3b),

$$u_1(r) = \frac{1}{2j\omega\Omega k_2}[\chi(v_1) + k_2(\omega^2 + \Omega^2)v_1]. \tag{4.12}$$

Substituting Equation (4.12) into Equation (4.3a),

$$\chi^2(v_1) + (k_1 + k_2)(\omega^2 + \Omega^2)\chi(v_1) + k_1 k_2 (\omega^2 - \Omega^2)^2 v_1 = 0.$$

As a result,

$$[\chi + \kappa_1^2][\chi + \kappa_2^2](v_1) = 0,$$

Thus

$$v_1(r) = K_5 J_1(\kappa_1 r) + K_6 Y_1(\kappa_1 r) + K_7 J_1(\kappa_2 r) + K_8 Y_1(\kappa_2 r), \tag{4.13a}$$

where $K_5$, $K_6$, $K_7$ and $K_8$ are arbitrary complex constants which can be determined from Equations (4.3c,d,e,f). Using Equation (4.12) and Solution (4.13a), Equations (4.3c,d,e,f) become respectively

$$[\kappa_1^2 - k_2(\omega^2 + \Omega^2)][K_5 J_1(\kappa_1 R_1) + K_6 Y_1(\kappa_1 R_1)]$$

$$+ [\kappa_2^2 - k_2(\omega^2 + \Omega^2)][K_7 J_1(\kappa_2 R_1) + K_8 Y_1(\kappa_2 R_1)] = 0, \tag{4.13b}$$

$$K_5 J_1(\kappa_1 R_1) + K_6 Y_1(\kappa_1 R_1) + K_7 J_1(\kappa_2 R_1) + K_8 Y_1(\kappa_2 R_1) = 0, \tag{4.13c}$$

$$[\kappa_1^2 - k_2(\omega^2 + \Omega^2)] \times$$

$$\left\{K_5\left[\kappa_1 J_0(\kappa_1 R_2) + \left(\frac{\upsilon - 1}{R_2}\right) J_1(\kappa_1 R_2)\right] + K_6\left[\kappa_1 Y_0(\kappa_1 R_2) + \left(\frac{\upsilon - 1}{R_2}\right) Y_1(\kappa_1 R_2)\right]\right\}$$

$$+ [\kappa_2^2 - k_2(\omega^2 + \Omega^2)] \times$$

$$\left\{K_7\left[\kappa_2 J_0(\kappa_2 R_2) + \left(\frac{\upsilon - 1}{R_2}\right) J_1(\kappa_2 R_2)\right] + K_8\left[\kappa_2 Y_0(\kappa_2 R_2) + \left(\frac{\upsilon - 1}{R_2}\right) Y_1(\kappa_2 R_2)\right]\right\}$$

$$= -2j\omega\Omega k_2 \frac{1 - \upsilon^2}{E} P_r, \tag{4.13d}$$

$$K_5\left[\kappa_1 J_0(\kappa_1 R_2)-\frac{2}{R_2}J_1(\kappa_1 R_2)\right]+K_6\left[\kappa_1 Y_0(\kappa_1 R_2)-\frac{2}{R_2}Y_1(\kappa_1 R_2)\right]$$

$$+K_7\left[\kappa_2 J_0(\kappa_2 R_2)-\frac{2}{R_2}J_1(\kappa_2 R_2)\right]+K_8\left[\kappa_2 Y_0(\kappa_2 R_2)-\frac{2}{R_2}Y_1(\kappa_2 R_2)\right]$$

$$=\frac{P_c}{G}. \qquad (4.13e)$$

From the above solutions, if in Solutions (4.11),

$$K_1=-\frac{\kappa_1^2-k_2(\omega^2+\Omega^2)}{2j\omega\Omega k_2}K_5,$$

$$K_2=-\frac{\kappa_1^2-k_2(\omega^2+\Omega^2)}{2j\omega\Omega k_2}K_6,$$

$$K_3=-\frac{\kappa_2^2-k_2(\omega^2+\Omega^2)}{2j\omega\Omega k_2}K_7$$

and

$$K_4=-\frac{\kappa_2^2-k_2(\omega^2+\Omega^2)}{2j\omega\Omega k_2}K_8,$$

Solutions (4.11) are equivalent to Solutions (4.13). This can be shown to be true by direct substitution of the above identities into Solutions (4.11). On the other side of the coin, when in Solutions (4.13),

$$K_5=\frac{\kappa_1^2-k_1(\omega^2+\Omega^2)}{2j\omega\Omega k_1}K_1,$$

$$K_6=\frac{\kappa_1^2-k_1(\omega^2+\Omega^2)}{2j\omega\Omega k_1}K_2,$$

$$K_7=\frac{\kappa_2^2-k_1(\omega^2+\Omega^2)}{2j\omega\Omega k_1}K_3$$

and

$$K_8=\frac{\kappa_2^2-k_1(\omega^2+\Omega^2)}{2j\omega\Omega k_1}K_4,$$

Solutions (4.13) are equivalent to Solutions (4.11). Again, this can be shown to be true by direct substitution of the above identities into Solutions (4.13). Hence the solutions obtained for both $u_1(r)$ and $v_1(r)$ from either Solutions (4.11) or Solutions (4.13) are essentially the same. Compared to the approximate solution in Subsection 4.2.2, the exact solution has non-zero imaginary parts. Moreover, both $u_1(r)$ and $v_1(r)$ are

complex functions of four linearly independent Bessel functions of first and second kind. In the approximate solution, both $u_1(r)$ and $v_1(r)$ are real functions of two linearly independent Bessel functions of first and second kind. Although Coriolis effect is included in this exact solution, results are only valid at low angular velocity because of small strain analysis.

### *4.3 Proposed Numerical Solution*

Since it is very difficult, although not impossible, to obtain an analytical solution for the Biezeno and Grammel's model (Equations (4.8) and (4.9)), numerical solutions are sought here. The same numerical method will be applied to solve the Bhuta and Jones' model (Equations (4.2) and (4.3)). This proposed numerical method has briefly been mentioned in Subsection 1.3.3. The difference between this method and the collocation type of methods is this proposed numerical method chooses the prescribed functions $\{f_i(r)\}_{i=0}^{\infty}$ that are valid representation of the unknown solution. This simply means the prescribed functions are chosen in such a way that the unknown solution can be approximated closely by a finite number of terms in $\{f_i(r)\}_{i=0}^{\infty}$. Assuming $\{f_i(r)\}_{i=0}^{\infty}$ is an infinite sequence with linear combinations of the functions representing unknown real variables $u_0(r)$ and $v_0(r)$, then

$$u_0(r) = \sum_{i=0}^{\infty} a_i f_i(r)$$

and

$$v_0(r) = \sum_{i=0}^{\infty} b_i f_i(r),$$

where $r \in [R_1, R_2]$, $a_i$'s and $b_i$'s are unknown real constants to be determined. For the current study, $\{f_i(r)\}_{i=0}^{\infty}$ is chosen to be $\left\{\left(\frac{r-R_1}{c}\right)^i\right\}_{i=0}^{\infty}$, where $c$ is a predefined constant. Now consider the following static equations

$$\Psi_{\Xi}^{1}\ (u_0(r)) = g_1(r),\ r \in \Xi, \tag{4.14a}$$

$$\Psi_{\Xi}^{2}\ (v_0(r)) = g_2(r),\ r \in \Xi, \tag{4.14b}$$

$$\Psi_{\partial\Xi}^{1}(u_0(r)) = g_3(r),\ r \in \partial\Xi, \tag{4.14c}$$

$$\Psi_{\partial\Xi}^{2}\ (u_0(r)) = g_4(r),\ r \in \partial\Xi, \tag{4.14d}$$

$$\Psi^3_{\partial\Xi}(v_0(r)) = g_5(r),\ r \in \partial\Xi, \tag{4.14e}$$

$$\Psi^4_{\partial\Xi}(v_0(r)) = g_6(r),\ r \in \partial\Xi, \tag{4.14f}$$

where $\Psi^1_{\Xi}$ and $\Psi^2_{\Xi}$ are second order differential operators on interior of domain $r$, $\Psi^1_{\partial\Xi}$, $\Psi^2_{\partial\Xi}$, $\Psi^3_{\partial\Xi}$ and $\Psi^4_{\partial\Xi}$ are differential operators at the boundary of domain $r$, $\Xi$ represents the interior of domain $r$, $\partial\Xi$ represents the boundary of domain $r$, $u_0(r)$ and $v_0(r)$ are unknown real functions of variable $r$ and $g_1(r)$, $g_2(r)$, $g_3(r)$, $g_4(r)$, $g_5(r)$ and $g_6(r)$ are known real functions of variable $r$. In order to implement a numerical solution in a computer, $u_0(r)$ and $v_0(r)$ can only be approximated by a finite number of terms in the sequence $\{f_i(r)\}_{i=0}^{\infty}$. Therefore,

$$u_0(r) \approx \sum_{i=0}^{n} a_i f_i(r)$$

and

$$v_0(r) \approx \sum_{i=0}^{n} b_i f_i(r),$$

where $n$ is a finite non-negative integer, are approximate solutions of Equations (4.14). By using the assumed forms for $u_0(x)$ and $v_0(x)$ together with choosing $r_k \in \Xi$, $k = 1, 2, \ldots n-1$, $r_0$ , $r_n \in \partial\Xi$, Equations (4.14) can be approximated by

$$\Psi^1_{\Xi}\left(\sum_{i=0}^{n} a_i f_i(r_k)\right) = g_1(r_k),\ r_k \in \Xi,\ k = 1, 2, \ldots n-1, \tag{4.15a}$$

$$\Psi^2_{\Xi}\left(\sum_{i=0}^{n} b_i f_i(r_k)\right) = g_2(r_k),\ r_k \in \Xi,\ k = 1, 2, \ldots n-1, \tag{4.15b}$$

$$\Psi^1_{\partial\Xi}\left(\sum_{i=0}^{n} a_i f_i(r_0)\right) = g_3(r_0),\ r_0 \in \partial\Xi, \tag{4.15c}$$

$$\Psi^2_{\partial\Xi}\left(\sum_{i=0}^{n} a_i f_i(r_n)\right) = g_4(r_n),\ r_n \in \partial\Xi, \tag{4.15d}$$

$$\Psi^3_{\partial\Xi}\left(\sum_{i=0}^{n} b_i f_i(r_0)\right) = g_5(r_0),\ r_0 \in \partial\Xi, \tag{4.15e}$$

$$\Psi^4_{\partial\Xi}\left(\sum_{i=0}^{n} b_i f_i(r_n)\right) = g_6(r_n),\ r_n \in \partial\Xi, \tag{4.15f}$$

Equations (4.15) are a system of $2n + 2$ nonlinear algebraic equations with $2n + 2$ unknowns $a_0$ , $a_1$ , …, $a_n$ and $b_0$ , $b_1$ , …, $b_n$ which can now be solved by Newton's

method. Equations (4.15) can be used to solve Equations (4.2) when $u_0(x)$ and $v_0(x)$ are replaced by $\sum_{i=0}^{n} a_i f_i(x)$ and $\sum_{i=0}^{n} b_i f_i(r)$ respectively. Defining

$$e_{0k} = \begin{cases} \Psi^1_{\partial\Xi}\left(\sum_{i=0}^{n} a_i f_i(r_0)\right) - g_3(r_0), k = 0, \\ \Psi^1_{\Xi}\left(\sum_{i=0}^{n} a_i f_i(r_k)\right) - g_1(r_k), k = 1,2,\ldots n-1, \\ \Psi^2_{\partial\Xi}\left(\sum_{i=0}^{n} a_i f_i(r_n)\right) - g_4(r_n), k = n, \end{cases}$$

$$e_{0(n+k+1)} = \begin{cases} \Psi^3_{\partial\Xi}\left(\sum_{i=0}^{n} b_i f_i(r_0)\right) - g_5(r_0), k = 0, \\ \Psi^2_{\Xi}\left(\sum_{i=0}^{n} b_i f_i(r_k)\right) - g_2(r_k), k = 1,2,\ldots n-1, \\ \Psi^4_{\partial\Xi}\left(\sum_{i=0}^{n} b_i f_i(r_n)\right) - g_6(r_n), k = n, \end{cases}$$

then the stopping criterion for the Newton's iteration is when the error tolerance $\sum_{k=0}^{2n+1} e_{0k}^2$ << 1. For the particular problem in Equations (4.2), it is required that $u_0(r)$ and $v_0(r) \in C^2(R_1, R_2]$, where $C^2(R_1, R_2]$ is a class of functions that are twice continuously differentiable $\forall r \in (R_1, R_2)$ and continuously differentiable at $r = R_2$. For the problem in Equations (4.8), replace $v_0(r)$ by $\vartheta_0(r)$ in the calculations mentioned above. Next, consider the following coupled dynamic equations

$$\Phi^{1t}_{\Xi}(u_1(r)\, e^{j\omega t}, v_1(r)\, e^{j\omega t}) = h_1(r)\, e^{j\omega t}, r \in \Xi, \quad (4.16a)$$

$$\Phi^{2t}_{\Xi}(u_1(r)\, e^{j\omega t}, v_1(r)\, e^{j\omega t}) = h_2(r)\, e^{j\omega t}, r \in \Xi, \quad (4.16b)$$

$$\Phi^{1}_{\partial\Xi}(u_1(r)\, e^{j\omega t}) = h_3(r)\, e^{j\omega t}, r \in \partial\Xi, \quad (4.16c)$$

$$\Phi^{2}_{\partial\Xi}(u_1(r)\, e^{j\omega t}) = h_4(r)\, e^{j\omega t}, r \in \partial\Xi, \quad (4.16d)$$

$$\Phi^{3}_{\partial\Xi}(v_1(r)\, e^{j\omega t}) = h_5(r)\, e^{j\omega t}, r \in \partial\Xi, \quad (4.16e)$$

$$\Phi^{4}_{\partial\Xi}(v_1(r)\, e^{j\omega t}) = h_6(r)\, e^{j\omega t}, r \in \partial\Xi, \quad (4.16f)$$

where $\Phi^{1t}_{\Xi}$ and $\Phi^{2t}_{\Xi}$ are time-domain second order differential operators on interior of domain $r$ and time $t$, $\Phi^{1}_{\partial\Xi}$, $\Phi^{2}_{\partial\Xi}$, $\Phi^{3}_{\partial\Xi}$ and $\Phi^{4}_{\partial\Xi}$ are differential operators at the boundary of domain $r$, $u_1(r)$ and $v_1(r)$ are unknown complex functions of variable $r$ and $h_1(r)$, $h_2(r)$, $h_3(r)$, $h_4(r)$, $h_5(r)$ and $h_6(r)$ are known complex functions of variable $r$. If a finite

number of terms in the sequence $\{f_i(r)\}_{i=0}^{\infty}$ approximately represent the unknown complex variables $u_1(r)$ and $v_1(r)$, then

$$u_1(r) \approx \sum_{i=0}^{n} \alpha_i f_i(r) + j \sum_{i=0}^{n} \beta_i f_i(r)$$

and

$$v_1(r) \approx \sum_{i=0}^{n} \xi_i f_i(r) + j \sum_{i=0}^{n} \eta_i f_i(r),$$

where $j = \sqrt{-1}$ is the complex constant, $\alpha_i$'s, $\beta_i$'s, $\xi_i$'s and $\eta_i$'s are unknown real constants to be determined. By using the assumed forms for $u_1(r)$ and $v_1(r)$ together with choosing $r_k \in \Xi$, $k = 1, 2, \ldots n-1$, $r_0$ , $r_n \in \partial\Xi$, Equations (4.16) can be approximated by

$$\Phi_{\Xi}^{1\omega}\left(\sum_{i=0}^{n} \alpha_i f_i(r_k) + j\sum_{i=0}^{n} \beta_i f_i(r_k), \sum_{i=0}^{n} \xi_i f_i(r_k) + j\sum_{i=0}^{n} \eta_i f_i(r_k)\right) = h_1(r_k),$$

$$r_k \in \Xi, k = 1, 2, \ldots n-1, \quad (4.17a)$$

$$\Phi_{\Xi}^{2\omega}\left(\sum_{i=0}^{n} \alpha_i f_i(r_k) + j\sum_{i=0}^{n} \beta_i f_i(r_k), \sum_{i=0}^{n} \xi_i f_i(r_k) + j\sum_{i=0}^{n} \eta_i f_i(r_k)\right) = h_2(r_k),$$

$$r_k \in \Xi, k = 1, 2, \ldots n-1, \quad (4.17b)$$

$$\Phi_{\partial\Xi}^{1}\left(\sum_{i=0}^{n} \alpha_i f_i(r_0) + j\sum_{i=0}^{n} \beta_i f_i(r_0)\right) = h_3(r_0),\ r_0 \in \partial\Xi, \quad (4.17c)$$

$$\Phi_{\partial\Xi}^{2}\left(\sum_{i=0}^{n} \alpha_i f_i(r_n) + j\sum_{i=0}^{n} \beta_i f_i(r_n)\right) = h_4(r_n),\ r_n \in \partial\Xi, \quad (4.17d)$$

$$\Phi_{\partial\Xi}^{3}\left(\sum_{i=0}^{n} \xi_i f_i(r_0) + j\sum_{i=0}^{n} \eta_i f_i(r_0)\right) = h_5(r_0),\ r_0 \in \partial\Xi, \quad (4.17e)$$

$$\Phi_{\partial\Xi}^{4}\left(\sum_{i=0}^{n} \xi_i f_i(r_n) + j\sum_{i=0}^{n} \eta_i f_i(r_n)\right) = h_6(r_n),\ r_n \in \partial\Xi, \quad (4.17f)$$

where $\Phi_{\Xi}^{1\omega}$ and $\Phi_{\Xi}^{2\omega}$ are the frequency-domain equivalent of the time-domain operators $\Phi_{\Xi}^{1t}$ and $\Phi_{\Xi}^{2t}$ respectively. Equations (4.17) are a system of $4n + 4$ nonlinear algebraic equations with $4n + 4$ unknowns $\alpha_0$ , $\alpha_1$ , …, $\alpha_n$ , $\beta_0$ , $\beta_1$ , …, $\beta_n$ , $\xi_0$ , $\xi_1$ , …, $\xi_n$ and $\eta_0$ , $\eta_1$ , …, $\eta_n$ which can now be solved by Newton's method. Note that the number of unknowns in the dynamic equations doubled those in the static equations because the dynamic equations have real and imaginary parts. Equations (4.17) is applicable to solve Equations (4.3) when $u_1(r)$ and $v_1(r)$ are respectively replaced by

$$\sum_{i=0}^{n} \alpha_i f_i(r) + j \sum_{i=0}^{n} \beta_i f_i(r)$$

and

$$\sum_{i=0}^{n} \xi_i f_i(r) + j \sum_{i=0}^{n} \eta_i f_i(r) .$$

Defining

$$e_{1k} = \begin{cases} \mathrm{Re}[\Phi^{1}_{\partial\Xi}(.) - h_3(r_0)], k = 0, \\ \mathrm{Re}[\Phi^{1\omega}_{\Xi}(.) - h_1(r_k)], k = 1,2,\ldots n-1, \\ \mathrm{Re}[\Phi^{2}_{\partial\Xi}(.) - h_4(r_n)], k = n, \end{cases}$$

$$e_{1(n+k+1)} = \begin{cases} \mathrm{Im}[\Phi^{1}_{\partial\Xi}(.) - h_3(r_0)], k = 0, \\ \mathrm{Im}[\Phi^{1\omega}_{\Xi}(.) - h_1(r_k)], k = 1,2,\ldots n-1, \\ \mathrm{Im}[\Phi^{2}_{\partial\Xi}(.) - h_4(r_n)], k = n, \end{cases}$$

$$e_{1(2n+k+2)} = \begin{cases} \mathrm{Re}[\Phi^{3}_{\partial\Xi}(.) - h_5(r_0)], k = 0, \\ \mathrm{Re}[\Phi^{2\omega}_{\Xi}(.) - h_2(r_k)], k = 1,2,\ldots n-1, \\ \mathrm{Re}[\Phi^{4}_{\partial\Xi}(.) - h_6(r_n)], k = n, \end{cases}$$

$$e_{1(3n+k+3)} = \begin{cases} \mathrm{Im}[\Phi^{3}_{\partial\Xi}(.) - h_5(r_0)], k = 0, \\ \mathrm{Im}[\Phi^{2\omega}_{\Xi}(.) - h_2(r_k)], k = 1,2,\ldots n-1, \\ \mathrm{Im}[\Phi^{4}_{\partial\Xi}(.) - h_6(r_n)], k = n, \end{cases}$$

where the dots inside the parentheses indicate the same expressions being operated on by the corresponding operators in Equations (4.17), then the stopping criterion for the Newton's iteration is when the error tolerance $\sum_{k=0}^{4n+3} e_{1k}^2 << 1$. For the particular problem in Equations (4.3), it is required that $u_1(r)$ and $v_1(r) \in C^2(R_1, R_2]$. For the problem in Equations (4.9), replace $v_1(r)$ by $\vartheta_1(r)$ in the above calculations.

### *4.4 Results and Comparisons*

Numerical experiments are performed on an annulus made of steel with arbitrarily chosen parameters. Relevant parameters are density of material $\rho_0$ = 7850 kg/m$^3$, shear modulus $G$ = 77.5 GPa, Young's modulus $E$ = 200 GPa, Poisson's ratio $\upsilon$ = 0.29, inner radius of annulus $R_1$ = 0.02 m, outer radius of annulus $R_2$ = 0.06 m, original thickness of annulus $y_0$ = 0.0015 m and angular velocity $\Omega = 200\pi$ rad/s. Except Figures 4.2 and Figures 4.4 for static motions, excitation forcing frequency $\omega = 20\pi$ rad/s, radial normal

and circumferential shear stress amplitudes are respectively $P_r$ = 100 kPa and $P_c$ = 100 kPa in all the other dynamic figures. Size of the series $n$ in Equations (4.15) and Equations (4.17) is chosen to be twenty as the error tolerance is approximately $O(10^{-20})$ in the stopping criterion of the Newton's method. For $n$ = 30, there are no significant difference on the results compared to $n$ = 20. If $n$ > 30, the error tolerance of $O(10^{-20})$ is not achievable due to significant round off errors.

### *4.4.1 In-Plane Displacements*

Figures 4.2 display the static displacements and Figures 4.3 display the dynamic displacements of the rotating annular plate.

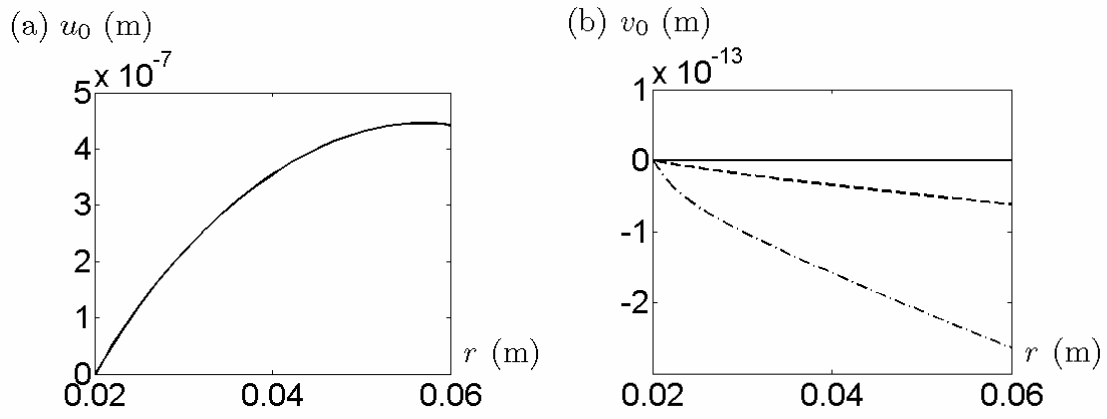


Figures 4.2. Comparison of the static (a) radial (b) circumferential displacement of a rotating annular plate. Solid line – is the exact solution of Bhuta and Jones' model of Equations (4.2). Dashed line –– is the numerical solution of Bhuta and Jones' model of Equations (4.2). Dash-dot line –. is the numerical solution of Biezeno and Grammel's model of Equations (4.8). $\rho_0$ = 7850 kg/m$^3$, $G$ = 77.5 GPa, $E$ = 200 GPa, $\upsilon$ = 0.29, $R_1$ = 0.02 m, $R_2$ = 0.06 m and $\Omega = 200\pi$ rad/s.

In order to compare the results obtained from Bhuta & Jones' model with Biezeno and Grammel's model, the static angular displacements are multiplied to the radial distance to give the static circumferential displacements by using the relationships $v_0(r) = r\vartheta_0(r)$. It may appear that there are discrepancies indicated by Figure 4.1(b), however, numerical results on $v_0(r)$ are of the order $O(10^{-13})$, which are almost equal to the exact solution $v_0(r) = 0$. Hence the numerical solution on $v_0(r)$ basically agrees with the exact solution at low angular velocity $\Omega$.

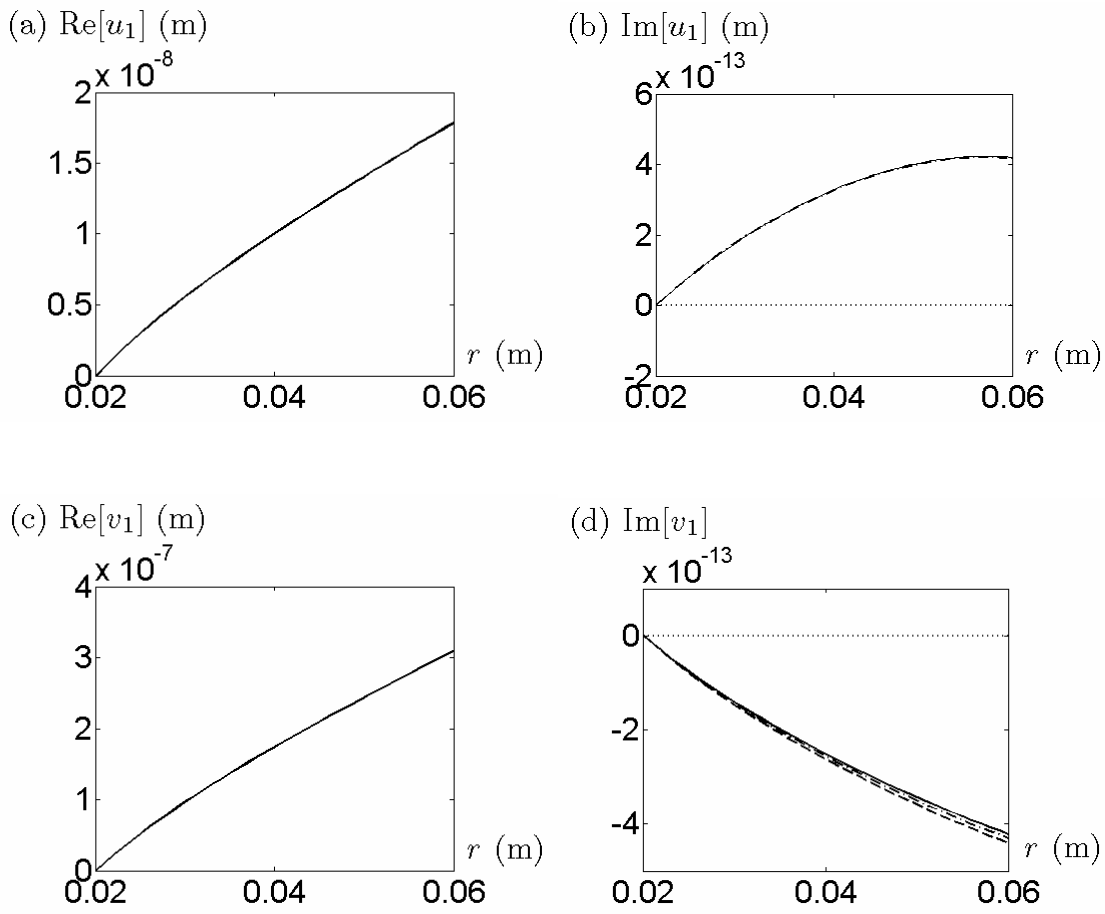


Figures 4.3. Comparison of the dynamic (a) real radial (b) imaginary radial (c) real circumferential (d) imaginary circumferential displacement of a rotating annular plate. Solid line – is the exact solution of Bhuta and Jones' model of Equations (4.3). Dashed line –– is the numerical solution of Bhuta and Jones' model of Equations (4.3). Dash-dot line –. is the numerical solution of Biezeno and Grammel's model of Equations (4.9). Dotted line ···· is the approximate solution of decoupled Equations (4.3) without Coriolis effect. $\rho_0$ = 7850 kg/m$^3$, $G$ = 77.5 GPa, $E$ = 200 GPa, $\upsilon$ = 0.29, $R_1$ = 0.02 m, $R_2$ = 0.06 m, $\Omega = 200\pi$ rad/s, $\omega = 20\pi$ rad/s, $P_r$ = 100 kPa and $P_c$ = 100 kPa.

In order to compare the results obtained from Bhuta & Jones' model with Biezeno and Grammel's model, the dynamic angular displacements are multiplied to the radial distance to give the dynamic circumferential displacements by using the relationships $v_1(r) = r\vartheta_1(r)$. The discrepancies appeared on Im[$u_1(r)$] and Im[$v_1(r)$] in Figure 4.3(b) and Figure 4.3(d) respectively are of the order $O(10^{-13})$, which indicates the Coriolis effect is minute on the imaginary parts of the exact solutions at low angular velocity $\Omega$.

### *4.4.2. Material Density and Thickness Profiles*

Although there are no analytical or experimental data to compare with, material density profile $\rho(r)$ and deformed thickness profile $y(r)$ of the initially parallel annular plate while in non-vibrating rotation for the Biezeno and Grammel's model are plotted in Figure 4.4, where $\rho(r)$ and $y(r)$ are the expressions as defined in Subsection 4.1.2.

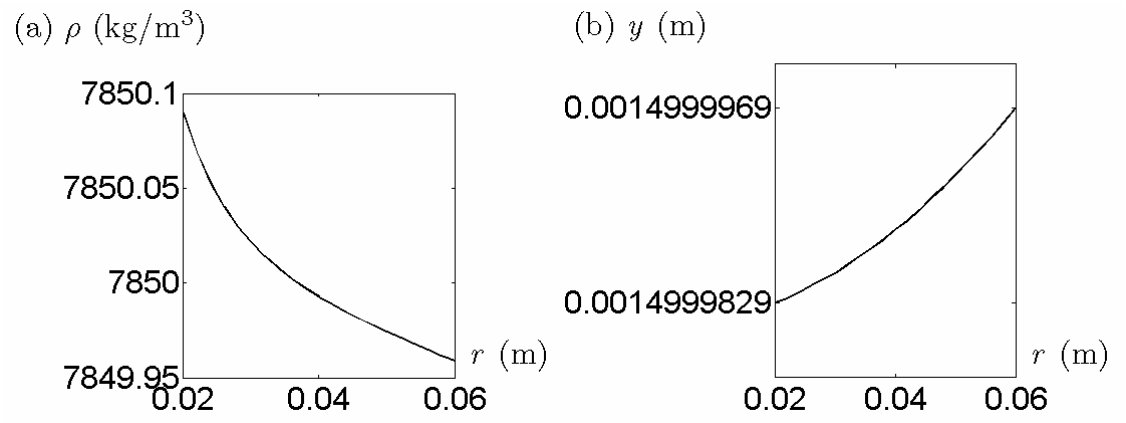


Figures 4.4. Static (a) density and (b) thickness profile of rotating annulus for the Biezeno and Grammel's model. $R_1$ = 0.02 m, $R_2$ = 0.06 m, $y_0$ = 0.0015 m, $\rho_0$ = 7850 kg/m$^3$, $G$ = 77.5 GPa, $E$ = 200 GPa, $\upsilon$ = 0.29 and $\Omega = 200\pi$ rad/s.

The plots show that while thickness is increasing, density is decreasing towards the free edge of the rotating annulus. This seems to be unfavourable as the density distribution of the annulus in static rotation should have values lower than the original density $\rho_0$ and should be increasing towards the free edge while in rotation. The above unexpected result is probably due to the static rotation being applied with small strain assumption and the effects on these variables due to dynamic vibration and large deformation are being neglected. Such an awkward situation is subject to further investigation in the future.

### *4.4.3. In-Plane Natural Frequencies*

If Coriolis forces are ignored, radial and circumferential natural frequencies of annulus are values of $\omega$ such that non-trivial solutions of decoupled Equations (4.3) are obtained with no oscillation stresses applied at the free edge of the annulus. Exact solutions or

numerical approach are required when Coriolis forces are involved. In order to find the radial and circumferential natural frequencies of vibration, a simple harmonic radial oscillation normal stress $P_r e^{j\omega t}$ and a simple harmonic circumferential oscillation shear stress $P_c e^{j\omega t}$ are applied at the free edge of the annulus. The condition for searching a radial or a circumferential natural frequency is to locate a local maximum of $| u_1(r) |$ or $| v_1(r) |$ respectively over an excitation frequency spectrum $\omega$ at the free edge of the annulus. For the Biezeno and Grammel's model, circumferential natural frequency is found by locating a local maximum of $| r\vartheta_1(r) |$ instead. Results on radial natural frequencies are compared in Table 4.1 and Table 4.2. Results on circumferential natural frequencies are compared in Table 4.3 and Table 4.4.

Table 4.1. First five radial natural frequencies of the non-rotating annulus with uniform thickness.

| | $N = 1$ | $N = 2$ | $N = 3$ | $N = 4$ | $N = 5$ |
|---|---|---|---|---|---|
| $\omega_{rN}^{0}$ (rad/s) | 218608 | 629955 | 1041261 | 1453995 | 1867344 |
| $\phi_{rN}^{0}$ (rad/s) | 218608 | 629955 | 1041261 | 1453995 | 1867344 |
| $\zeta_{rN}^{0}$ (rad/s) | 218608 | 629955 | 1041261 | 1453995 | 1867345 |
| $\varphi_{rN}^{0}$ (rad/s) | 218608 | 629955 | 1041261 | 1453995 | 1867345 |

Table 4.2. First five radial natural frequencies of the rotating annulus at $\Omega = 200\pi$ rad/s.

| | $N = 1$ | $N = 2$ | $N = 3$ | $N = 4$ | $N = 5$ |
|---|---|---|---|---|---|
| $\omega_{rN}^{200\pi}$ (rad/s) | 218607 | 629955 | 1041261 | 1453995 | 1867343 |
| $\phi_{rN}^{200\pi}$ (rad/s) | 218611 | 629957 | 1041262 | 1453996 | 1867344 |
| $\zeta_{rN}^{200\pi}$ (rad/s) | 218611 | 629957 | 1041262 | 1453996 | 1867345 |
| $\varphi_{rN}^{200\pi}$ (rad/s) | 218610 | 629957 | 1041262 | 1453996 | 1867345 |

Table 4.3. First five circumferential natural frequencies of the non-rotating annulus with uniform thickness.

| | $N = 1$ | $N = 2$ | $N = 3$ | $N = 4$ | $N = 5$ |
|---|---|---|---|---|---|
| $\omega_{cN}^{0}$ (rad/s) | 56949 | 360896 | 611725 | 860068 | 1107682 |
| $\phi_{cN}^{0}$ (rad/s) | 56949 | 360896 | 611725 | 860068 | 1107682 |
| $\zeta_{cN}^{0}$ (rad/s) | 56949 | 360896 | 611725 | 860068 | 1107683 |
| $\varphi_{cN}^{0}$ (rad/s) | 56949 | 360896 | 611725 | 860068 | 1107690 |

Table 4.4. First five circumferential natural frequencies of the rotating annulus at $\Omega = 200\pi$ rad/s.

| | $N = 1$ | $N = 2$ | $N = 3$ | $N = 4$ | $N = 5$ |
|---|---|---|---|---|---|
| $\omega_{cN}^{200\pi}$ (rad/s) | 56946 | 360895 | 611724 | 860067 | 1107682 |
| $\phi_{cN}^{200\pi}$ (rad/s) | 56945 | 360894 | 611724 | 860067 | 1107681 |
| $\zeta_{cN}^{200\pi}$ (rad/s) | 56945 | 360894 | 611724 | 860067 | 1107682 |
| $\varphi_{cN}^{200\pi}$ (rad/s) | 56945 | 360894 | 611724 | 860067 | 1107689 |

$\omega_{rN}^{0}$, $\omega_{rN}^{200\pi}$, $\omega_{cN}^{0}$ and $\omega_{cN}^{200\pi}$ represent natural frequencies of an annulus with no Coriolis forces predicted by the approximate solution in Subsection 4.2.2. $\phi_{rN}^{0}$, $\phi_{rN}^{200\pi}$, $\phi_{cN}^{0}$ and $\phi_{cN}^{200\pi}$ represent natural frequencies of an annulus with Coriolis forces predicted by the exact analytical solution in Subsection 4.2.3. $\zeta_{rN}^{0}$, $\zeta_{rN}^{200\pi}$, $\zeta_{cN}^{0}$ and $\zeta_{cN}^{200\pi}$ represent natural frequencies of an annulus with Coriolis forces predicted by Bhuta and Jones' model using proposed numerical method in Section 4.3. $\varphi_{rN}^{0}$, $\varphi_{rN}^{200\pi}$, $\varphi_{cN}^{0}$ and $\varphi_{cN}^{200\pi}$ represent natural frequencies of an annulus with Coriolis forces predicted by Biezeno and Grammel's model using proposed numerical method in Section 4.3. Superscripts indicate the angular velocity of the annulus in rad/s. Subscripts *rN* are the *N*th radial modes and *cN* are the *N*th circumferential modes. All natural frequencies in the above tables are rounded to the nearest integer. At angular velocity $\Omega = 0$ rad/s, either approximate solution in Subsection 4.2.2 or the exact solution in Subsection 4.2.3 can be employed. This is because when $\Omega = 0$ rad/s, the approximate solutions obtained in Subsection 4.2.2 become the exact solutions. If exact solution in Subsection 4.2.3 is employed, solution is acquired by setting $\Omega$ to be a small positive quantity not equal to zero. The reason for this is because the exact solution has a division by $\Omega$, solution will be undefined if $\Omega = 0$ rad/s. All four results on natural frequencies give roughly the same predictions at the same angular velocity $\Omega$.

### *4.4.4. In-Plane Mode Shapes*

Exact and numerical results on Bhuta and Jones' model will be produced for the mode shapes. Figures 4.5 show the radial mode shapes. Figures 4.6 show the circumferential mode shapes. Modes shapes are depicted according to the natural frequencies outlined in Table 4.2 for radial modes and Table 4.4 for circumferential modes.

(a) Re[$u_1$] (m)

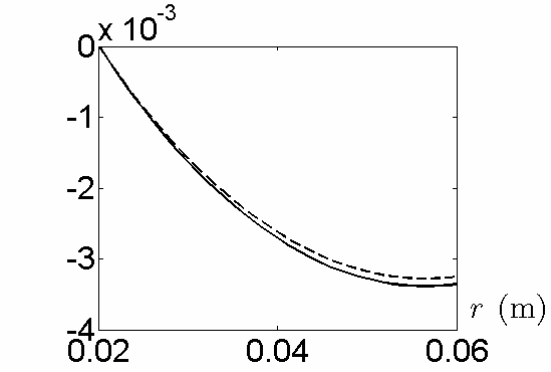


(b) Im[$u_1$] (m)

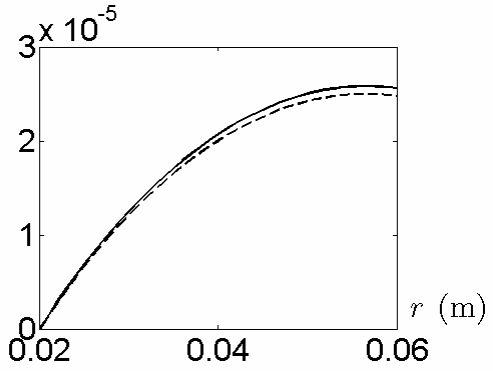


(c) Re[$u_1$] (m)

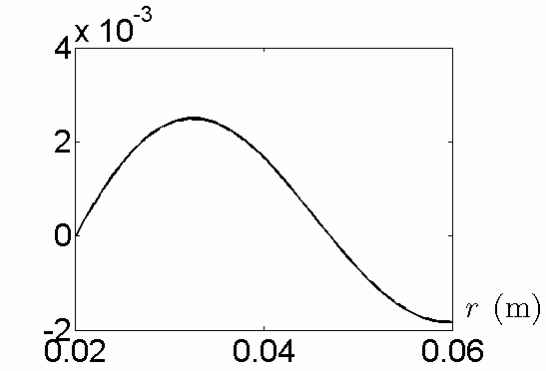


(d) Im[$u_1$] (m)

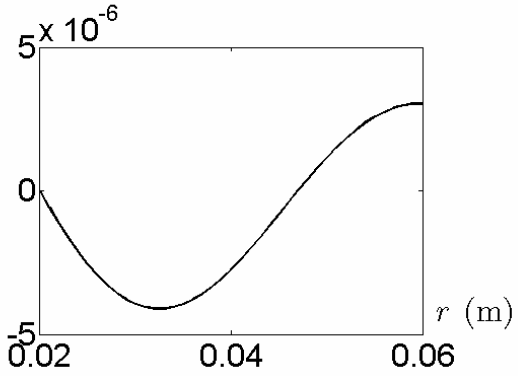


(e) Re[$u_1$] (m)

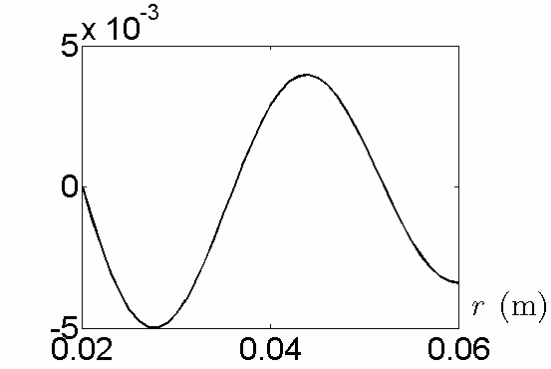


(f) Im[$u_1$] (m)

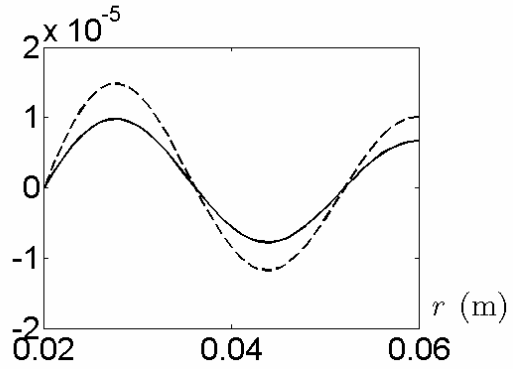

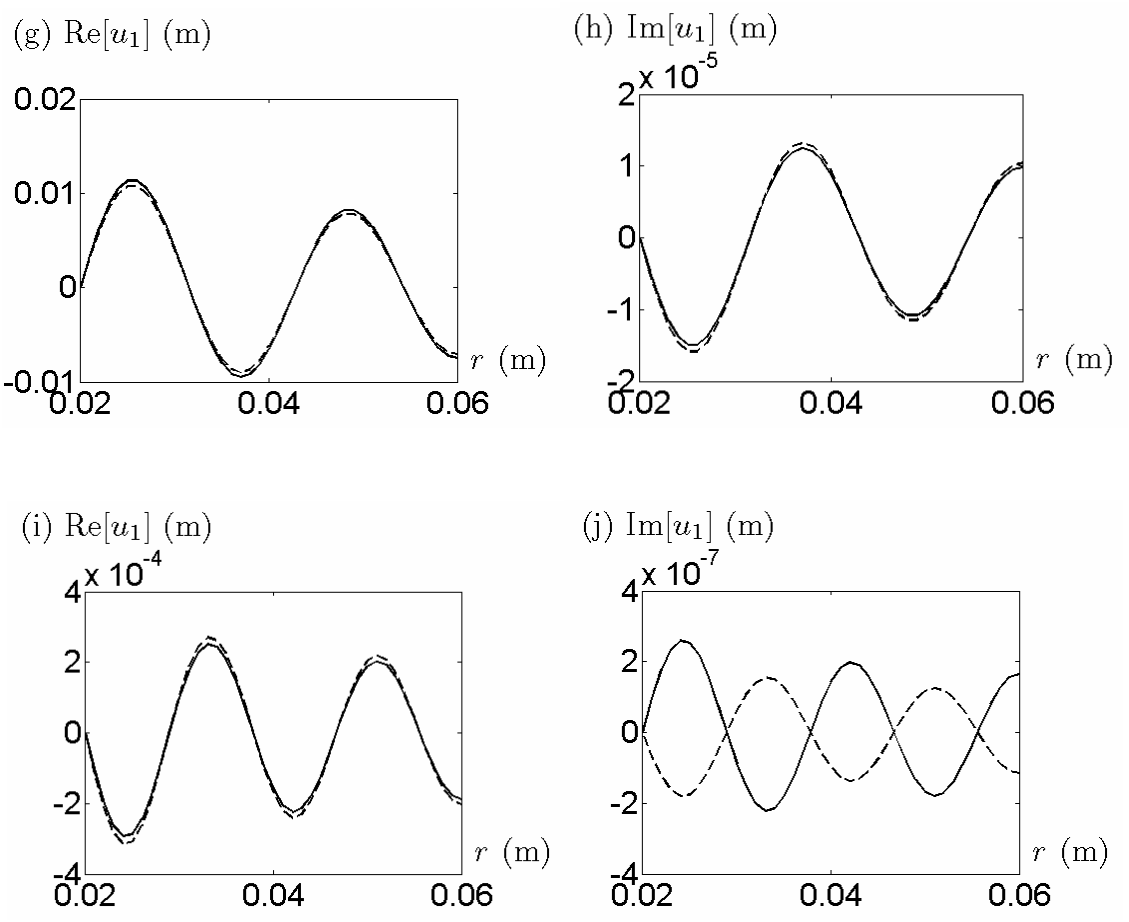


Figures 4.5. (a) 1st real (b) 1st imaginary (c) 2nd real (d) 2nd imaginary (e) 3rd real (f) 3rd imaginary (g) 4th real (h) 4th imaginary (i) 5th real (j) 5th imaginary radial mode shape of the annulus. Solid line – is the exact solution of Bhuta and Jones' model of Equations (4.3). Dashed line –– is the numerical solution of Bhuta and Jones' model of Equations (4.3). $R_1$ = 0.02 m, $R_2$ = 0.06 m, $y_0$ = 0.0015 m, $\rho_0$ = 7850 kg/m$^3$, $G$ = 77.5 GPa, $E$ = 200 GPa, $\upsilon$ = 0.29, $\Omega = 200\pi$ rad/s, $P_r$ = 100 kPa and $P_c$ = 100 kPa. For (a) & (b) $\omega$ = 218611 rad/s, (c) & (d) $\omega$ = 629957 rad/s, (e) & (f) $\omega$ = 1041262 rad/s, (g) & (h) $\omega$ = 1453996 rad/s, (i) & (j) $\omega$ = 1867345 rad/s.

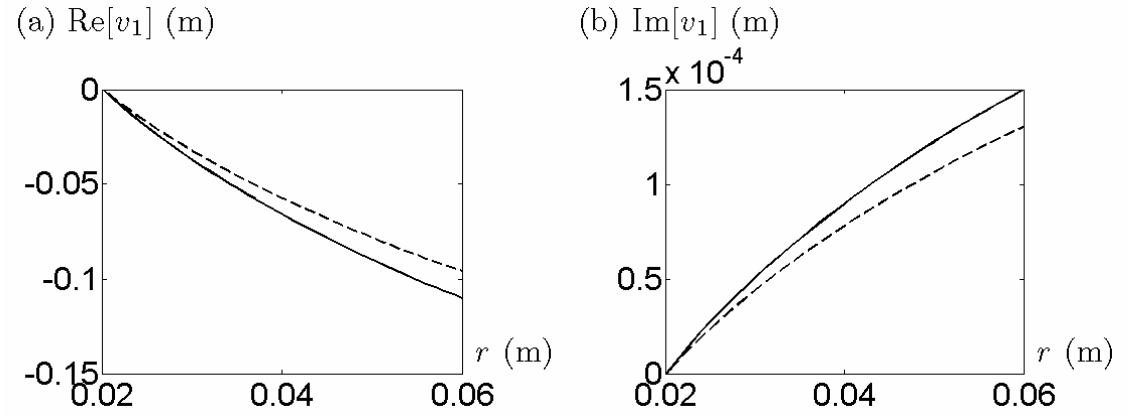

(c) Re[$v_1$] (m)

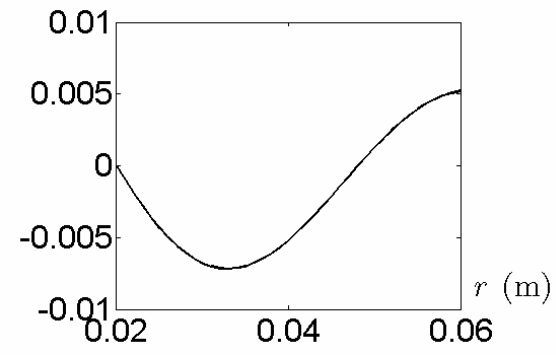


(d) Im[$v_1$] (m)

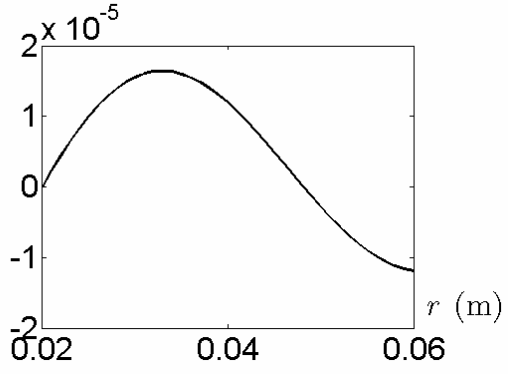


(e) Re[$v_1$] (m)

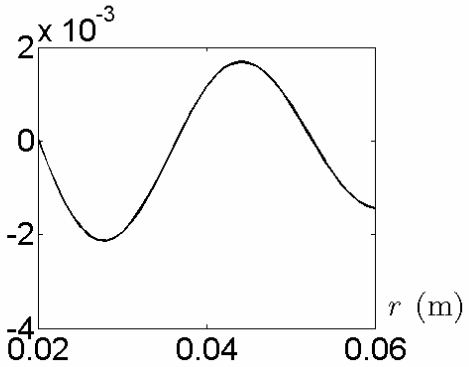


(f) Im[$v_1$] (m)

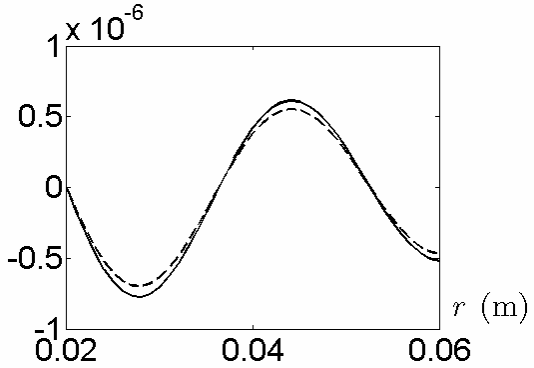


(g) Re[$v_1$] (m)

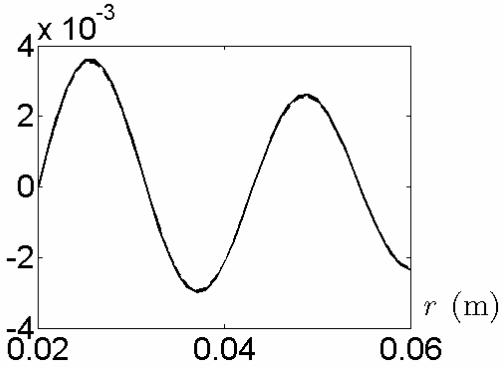


(h) Im[$v_1$] (m)

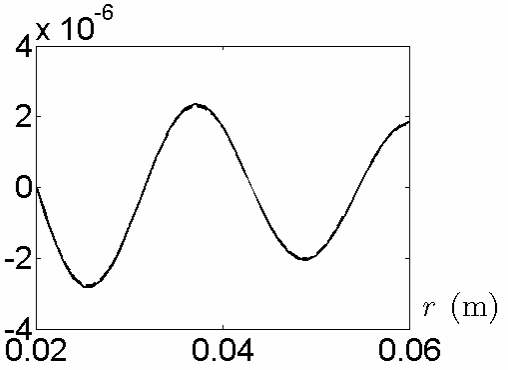

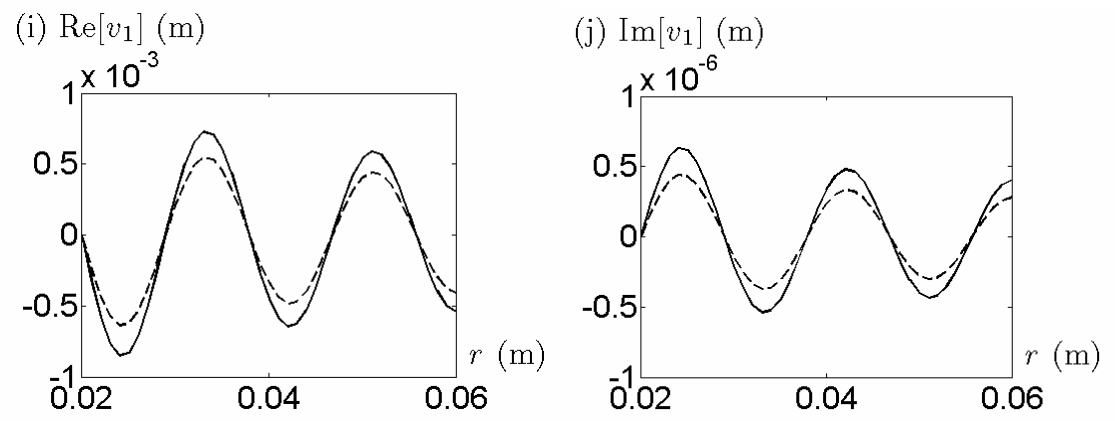


Figures 4.6. (a) 1st real (b) 1st imaginary (c) 2nd real (d) 2nd imaginary (e) 3rd real (f) 3rd imaginary (g) 4th real (h) 4th imaginary (i) 5th real (j) 5th imaginary circumferential mode shape of the annulus. Solid line – is the exact solution of Bhuta and Jones' model of Equations (4.3). Dashed line –– is the numerical solution of Bhuta and Jones' model of Equations (4.3). $R_1$ = 0.02 m, $R_2$ = 0.06 m, $y_0$ = 0.0015 m, $\rho_0$ = 7850 kg/m$^3$, $G$ = 77.5 GPa, $E$ = 200 GPa, $\upsilon$ = 0.29, $\Omega = 200\pi$ rad/s, $P_r$ = 100 kPa and $P_c$ = 100 kPa. For (a) & (b) $\omega$ = 56945 rad/s, (c) & (d) $\omega$ = 360894 rad/s, (e) & (f) $\omega$ = 611724 rad/s, (g) & (h) $\omega$ = 860067 rad/s, (i) & (j) $\omega$ = 1107682 rad/s.

In the above figures for mode shape, the imaginary parts are at most $O(10^{-2})$ times of the corresponding real parts. This implies $|u_1(r)|$ and $|v_1(r)|$ are more or less identical to $|\mathrm{Re}[u_1(r)]|$ and $|\mathrm{Re}[v_1(r)]|$ respectively. Results acquired from the Biezeno and Grammel's model and the approximate solution on Bhuta and Jones' model predict similar mode shapes but with different amplitudes and phase angles in the neighbourhood of the natural frequencies. Hence they are not displayed although compared. Both radial and circumferential mode shapes exhibit near sinusoidal behaviour in the vicinity of the natural modes of vibrations. In addition, radial mode shapes occurs at about $\frac{2N-1}{4}$ of a wavelength with $N$ = 1, 2, …, 5 and circumferential mode shapes occurs at about $\frac{4N-3}{8}$ of a wavelength with $N$ = 1, 2, …, 5. Reminding that $N$ denotes the numeric order of the mode shapes. If the natural frequencies are multiplied to their corresponding wavelengths, results are approximately equal to the radial or circumferential wave propagation speed.

# Chapter 5

# Discussion

## *5.1 Critique on Mathematical Models*

Mathematical models that describe the motions of whirling rods and rotating annuli in previous and present work will be discussed. Recommendations on further improvement of the models will also be offered.

### *5.1.1 Whirling Rods*

In the previous derivations (Bhuta and Jones 1963a) of governing equations of whirling rods, longitudinal displacements were allowed to vary while material density and cross-sectional area of rods were kept constant. This condition violates the law of conservation of mass and is only accurate for small strain analyses. The proposed nonlinear model for steady rotation in this thesis for whirling rods allows variations in longitudinal displacement, material density and cross-sectional area of whirling rods that establishes a basic study on nonlinear vibration of rods. The classical approach to extract the natural frequencies from this proposed nonlinear model is to view a whirling rod as a stationary rod being subjected to the centripetal force distribution caused by the rotation. Thus, the Coriolis effect is excluded from the whirling motion when determining the natural frequencies.

However for a rod engaged in a dynamic whirling motion, longitudinal vibration will induce a transverse vibration and vice versa. Such vibrations occur because transverse and longitudinal displacements are coupled through the Coriolis effect. While some previous work (Bhuta and Jones 1963a) had recognised such a circumstance, none had successfully derived and solved a model for whirling rods coupled with longitudinal and transverse displacements. The governing equations of whirling rods with Coriolis effect that employ nonlinear strain-displacement relationship are nonlinear time-dependent problems. Solutions for such nonlinear

equations are analytically formidable and hence numerical approaches are recommended. To the best knowledge of the author of this thesis, no solution, either analytically or numerically, has been offered for nonlinear time-dependent coupled differential equations for whirling rods.

### *5.1.2 Rotating Discs or Annuli*

Similar to the derivation of equations on whirling rods, equations that govern the in-plane motions of rotating discs or annuli have not taken the Poisson's effect into account (Bhuta and Jones 1963b, Biezeno and Grammel 1954). Nonetheless, governing equations coupled between radial and circumferential displacements due to Coriolis forces has been derived (Bhuta and Jones 1963b, Biezeno and Grammel 1954). Again, previous derivations did not allow for variations of material density and plate thickness of rotating discs. Although Biezeno and Grammel (1954) had considered an annulus with plate thickness variation, this variation remains constant with time under any external tension or compression stresses.

For the current studies, Poisson's effect is put into the static governing equations of the Biezeno and Grammel's model. However, such a manoeuvre becomes invalid when the dynamic displacements become too large. As a result, this manoeuvre is only valid for small strain analysis. Large amplitude dynamic vibrations will occur when the frequencies of oscillations are at or near the natural modes of the discs or annuli. The reason that Poisson's effect due to dynamic motion is not incorporated into the present studies is that the resulting governing equations are nonlinear time-dependent coupled differential equations. These nonlinear equations do not permit the solutions to assume small oscillations of vibration being superimposed on the steady state of the annulus while it is in rotation. Referring to all the solution methods available, even a numerical approach becomes an apprehensive task. While this time-dependent nonlinear problem is an improved version of the current formulation, it will be saved as a further challenge for future investigations.

The current studies delve into axisymmetric vibrations of rotating annuli. Axisymmetric vibrations of rotating annuli are one-dimensional problems without circumferential variations. That is, they are independent of $\Theta$ and $\theta$ in Eulerian and

Lagrangian coordinates respectively. In general, the equations of motion for asymmetric vibrations of annuli that include differential change in circumferential direction will govern the asymmetric rotating motion. These problems are two-dimensional vibration problems that involve radial and circumferential normal stresses as well as radial and circumferential shear stresses.

## *5.2 Critique on Boundary Conditions*

The current studies on whirling rods used clamped-free boundary conditions. For a rotating annulus, the inner radius boundary is clamped and simple harmonic oscillations are applied at the outer edge. These boundary conditions are specifically chosen for the current studies with no loss of generality if other types of boundary condition such as simply-supported and no shearing force boundary conditions are applied. The approaches to acquire the natural vibration modes of whirling rods and rotating annuli are principally different. For whirling rods, natural modes are obtained according to the steady motion of the deformed geometry of a rod by excluding the Coriolis effect. On the other hand for rotating annuli, natural modes are obtained according to the dynamic motion with applied forces imposed at an outer edge by including the Coriolis effect with small strain hypothesis.

### *5.2.1 Whirling Rods*

With respect to the Lagrangian coordinate, the displacement $u(0)$ is fixed at the clamped end of a whirling rod. The cross-sectional area $A_0$ in the linear uniaxial model is a constant while the cross-sectional area $A(x)$ is permitted to constrict under tensile force in the proposed nonlinear model. The axial tensile stress $\sigma(0)$ and axial tensile strain $\varepsilon(0)$ are largest at $x = 0$. Since there is no external tensile force or any internal centripetal force due to the rod segment acting on the free end of a whirling rod, the axial tensile stress $\sigma(L)$ and axial tensile strain $\varepsilon(L)$ vanish. The classical receptance approach to find a natural frequency is determined by applying an axial excitation force at the free end of a rod with a frequency corresponds to the resonance frequency. Because of the steady motion, Coriolis effect due to whirling motion does not play a role in determining the natural modes of vibration.

### *5.2.2 Rotating Annuli*

With respect to the Lagrangian coordinate, the in-plane displacements $u(R_1)$ and $v(R_1)$ are fixed at the clamped inner radius $R_1$ of a rotating annulus. The thickness of the annular plate $y_0$ does not change in Bhuta and Jones' model and the thickness of the annular plate $y(r)$ is permitted to constrict under tensile strain in the Biezeno and Grammel's model. For the amplitude of stress and strain, radial normal stress $\sigma_r(R_1)$ and radial normal strain $\varepsilon_r(R_1)$ are largest. At the outer radius $R_2$ of an annular plate, there are radial and circumferential external tensile forces but no internal centripetal force due to any annulus segment beyond the outer edge of a rotating annulus acting on the plate thickness $y(R_2)$. Hence regarding to the amplitude of stress and strain, radial normal stress $\sigma_r(R_2)$ corresponds to the externally applied radial stresses, and circumferential shear stress $\tau_{r\theta}(R_2)$ corresponds to the externally applied circumferential stresses. Moreover, it is known from static equilibrium that $\tau_{r\theta}(r) = \tau_{\theta r}(r)$, where circumferential shear stress $\tau_{r\theta}(r)$ is a stress acting in the $\theta$ direction on the plane perpendicular to the $r$ direction and radial shear stress $\tau_{\theta r}(r)$ is a stress acting in the $r$ direction on the plane perpendicular to the $\theta$ direction. Natural frequencies are located by the resonance phenomenon. That is, the frequency of the excitation oscillation applied at the free edge is the resonance frequency when it coincides with any one of the natural modes of the rotating annulus.

## *5.3 Critique on Cross-Sectional Area of Rods and Thickness of Annuli*

In this section, whirling rods with non-circular cross-section and the thicknesses of rotating annuli will be commented.

### *5.3.1 Cross-Sectional Area of Rods*

The cross-sectional area of a whirling rod in the uniaxial model is assumed to be constant everywhere along the rod at all time. Throughout the derivation of the proposed nonlinear model for a rod in Lagrangian coordinate $x$, the cross-sectional area is assumed to be circular. Nevertheless, the Poisson's ratio is applicable to non-circular cross-section rods. Recall that Poisson's ratio is the ratio between the lateral

strain and the longitudinal strain for uniaxial stress. If each cross-sectional area of a rod under consideration is described by the product of two quantities, namely $l_0(x)$ and $w_0(x)$, then

$$\varepsilon_L(x) = \frac{l(x) - l_0(x)}{l_0(x)} = -\upsilon\varepsilon(x)$$

and

$$\varepsilon_L(x) = \frac{w(x) - w_0(x)}{w_0(x)} = -\upsilon\varepsilon(x),$$

where $l(x)$ and $w(x)$ are the new deformed quantities from the original undeformed quantities $l_0(x)$ and $w_0(x)$ respectively. After rearranging the above two equations,

$$l(x) = l_0(x)\,[1 - \upsilon\varepsilon(x)]$$

and

$$w(x) = w_0(x)\,[1 - \upsilon\varepsilon(x)].$$

As a result,

$$l(x)\,w(x) = l_0(x)\,w_0(x)\,[1 - \upsilon\varepsilon(x)]^2.$$

Defining the new deformed cross-sectional area $A(x) = l(x)\,w(x)$ and the original undeformed cross-sectional area $A_0(x) = l_0(x)\,w_0(x)$ at location $x$, then from the previous equation,

$$A(x) = A_0(x)\,[1 - \upsilon\varepsilon(x)]^2.$$

If this expression is embraced in deriving the proposed nonlinear model, Equation (3.7) shall be replaced by

$$EA_0(x)[1 - \upsilon\varepsilon(x)]^2\varepsilon(x) = \int_x^L \rho_0 A_0(x)(x+u)\Omega^2 dx\,.$$

Hence the only difference in deriving the proposed nonlinear governing equation for whirling rods with non-circular cross-section is to engage the original undeformed cross-sectional area profile $A_0(x)$ on both sides of Equation (3.8a).

### *5.3.2 Thickness of Annuli*

In the Bhuta and Jones' model, a parallel disc is assumed and is taken to remain the same everywhere in the annular plate at all time. In Biezeno and Grammel's model, the original thickness of an annulus is allowed to vary with radial distance but not with time. Nonetheless, both models are appropriate for axisymmetric vibration only

with in-plane displacements autonomous of the tangential direction. Moreover, transverse strain $\varepsilon_z$ due to Poisson's effect is negligible if the plate is considered to be thin. From Chapter 4, thickness of a plate is given by

$$y = y_0\left[1-\frac{\upsilon}{1-\upsilon}\left(\varepsilon_r+\varepsilon_\theta\right)\right].$$

After rearrangement,

$$y - y_0 = -y_0\frac{\upsilon}{1-\upsilon}(\varepsilon_r + \varepsilon_\theta).$$

From this expression, it can be perceived that if $O(y_0) \sim O(\varepsilon_r + \varepsilon_\theta)$, then $O(y - y_0) << O(\varepsilon_r + \varepsilon_\theta)$. This implies if the original thickness $y_0$ of an annulus is miniscule, the change of thickness $y - y_0$ may be neglected. On the other hand, if $O(y_0) \sim O(1)$, then $O(y - y_0) \sim O(\varepsilon_r + \varepsilon_\theta)$. This implies if the original thickness $y_0$ of an annulus is much larger than $\varepsilon_r + \varepsilon_\theta$, the change of thickness $y - y_0$ is at least comparable to $\varepsilon_r + \varepsilon_\theta$ which cannot be neglected. This simply means a thin rotating annulus could assume undeformed thickness at all time.

## *5.4 Critique on Analytical Solutions*

Solutions in both Chapter 3 and Chapter 4 have been obtained in Lagrangian coordinates. At this point, it would be interesting to ask if the solutions obtained in Eulerian coordinates are much different from those in Lagrangian coordinates. In this section, only analytical solutions will be discussed by contrasting the solutions obtained in both Eulerian and Lagrangian coordinates.

### *5.4.1 Whirling Rods*

Consider an isotropic non-vibrating whirling rod in Eulerian coordinate $z$ rotating at constant angular velocity $\Omega$, constant material density $\rho_0$ and constant cross-sectional area $A_0$. The governing equation according to Bhuta and Jones (1963a) is

$$E\frac{d^2u}{dz^2} = -\rho_0\,\Omega^2 z. \tag{5.1a}$$

For a clamped rod with no axial displacement at $z = 0$,

$$u(0) = 0. \tag{5.1b}$$

Since axial stress $\sigma(z) = \dfrac{F(z)}{A_0} = E\varepsilon(z)$, $F(z) = EA_0\varepsilon(z)$. Applying the linear strain-displacement relationship $\varepsilon(z) = \dfrac{du}{dz}$ in Eulerian coordinate together with the fact that $F(z) = 0$ at the free end,

$$EA_0\left[\frac{du}{dz}\right]_{z=L} = 0. \tag{5.1c}$$

The above Eulerian formulation is equivalent to Lagrangian formulation of Equations (3.1). Apparently when a rod is everywhere under a tensile force, the free end should be at a location $z > L$. However, the free end boundary condition Equation (5.1c) is applied at $z = L$ in Eulerian coordinate. This is only approximately true when the problem is undergoing a small strain analysis. Bhuta and Jones (1963a) had constructed the analytical solution for Equations (5.1) and it is repeated below.

Integrating Equation (5.1a) twice w.r.t. $z$ gives

$$u(z) = -\frac{\rho_0}{6E}\Omega^2 z^3 + c_1 z + c_2,$$

where $c_1$ and $c_2$ are arbitrary constants. Applying Equation (5.1b),

$$c_2 = 0.$$

Applying Equation (5.1c),

$$c_1 = \frac{\rho_0}{2E}\Omega^2 L^2.$$

Hence

$$u(z) = -\frac{\rho_0}{6E}\Omega^2 z^3 + \frac{\rho_0}{2E}\Omega^2 L^2 z.$$

By direct inspection of this Eulerian solution, $u(z)$ exists for $z \geq 0$ and any values of $\Omega \geq 0$. Comparing to the analytical solution of Equations (3.1) repeated below,

$$u(x) = \frac{\sin(kx)}{k\cos(kL)} - x,$$

where $k = \sqrt{\dfrac{\rho_0}{E}}\,\Omega$, which does not exist beyond certain angular velocity $\Omega$ according to the discussions in Section 3.4.

*5.4.2 Rotating Annuli*

Consider an isotropic rotating annulus in Eulerian coordinate $R$ rotating at constant angular velocity $\Omega$, constant material density $\rho_0$ and uniform thickness (i.e. a parallel annulus). The governing equation according to Bhuta and Jones (1963b) is

$$\frac{d^2u_0}{dR^2}+\frac{1}{R}\frac{du_0}{dR}-\frac{u_0}{R^2}=-\frac{1-\upsilon^2}{E}\rho_0\,\Omega^2R, \tag{5.2a}$$

For a clamped annulus at the inner radius $R = R_1$, no radial displacement occurs. Hence

$$u_0(R_1) = 0 \tag{5.2b}$$

Since no radial stress $\sigma_R = \frac{E}{1-\upsilon^2}\left(\frac{du_0}{dR}+\upsilon\frac{u_0}{R}\right)$ occurs at the outer radius $R = R_2$,

$$\left[\frac{du_0}{dR}+\upsilon\frac{u_0}{R}\right]_{R=R_2} = 0, \tag{5.2c}$$

The above Eulerian formulation is equivalent to Lagrangian formulation of Equations (4.2). Apparently when an annulus is under an axisymmetric radial tensile force, the free edge should be at a location $R > R_2$. However, the free edge boundary condition Equation (5.2c) is applied at $R = R_2$ in Eulerian coordinate. This is only approximately true when the problem is undergoing a small strain analysis. Juvinall (Section 7.3, 1967) reported the analytical solution for Equation (5.2a) with no specified boundary conditions. However, his formulation was originally deduced for a rotating cylinder by assuming no transverse displacement in the direction perpendicular to the cross-sectional area of the cylinder. Juvinall's solution is repeated below for convenience.

Equation (5.2a) may be written as

$$\frac{d}{dR}\left(\frac{du_0}{dR}+\frac{u_0}{R}\right)=-\frac{1-\upsilon^2}{E}\rho_0\,\Omega^2R.$$

Integrating the above equation once w.r.t. $R$,

$$\frac{du_0}{dR}+\frac{u_0}{R}=-\frac{1-\upsilon^2}{2E}\rho_0\,\Omega^2R^2+2m_1,$$

where $m_1$ is an arbitrary constant. Multiplying the above equation throughout by $R$,

$$R\frac{du_0}{dR}+u_0=-\frac{1-\upsilon^2}{2E}\rho_0\,\Omega^2R^3+2m_1R$$

or

$$\frac{d}{dR}(Ru_0) = -\frac{1-\upsilon^2}{2E}\rho_0 \Omega^2 R^3 + 2m_1 R.$$

Integrating the above equation w.r.t. $R$ again,

$$Ru_0 = -\frac{1-\upsilon^2}{8E}\rho_0 \Omega^2 R^4 + m_1 R^2 + m_2.$$

where $m_2$ is an arbitrary constant. Dividing the above equation throughout by $R$,

$$u_0(R) = m_1 R + \frac{m_2}{R} - \lambda R^3.$$

After applying Equations (5.2b,c),

$$m_1 = \frac{\begin{vmatrix} d_{a1} & a_{12} \\ d_{a2} & a_{22} \end{vmatrix}}{|A_E|},$$

$$m_2 = \frac{\begin{vmatrix} a_{11} & d_{a1} \\ a_{21} & d_{a2} \end{vmatrix}}{|A_E|},$$

$$|A_E| = \begin{vmatrix} a_{11} & a_{12} \\ a_{21} & a_{22} \end{vmatrix},$$

$$\lambda = \frac{1-\upsilon^2}{8E}\rho_0 \Omega^2,$$

$$a_{11} = R_1,$$

$$a_{12} = \frac{1}{R_1},$$

$$a_{21} = 1 + \upsilon,$$

$$a_{22} = \frac{\upsilon - 1}{R_2^2},$$

$$d_{a1} = \frac{\lambda}{8} R_1^3,$$

$$d_{a2} = (3 + \upsilon)\frac{\lambda}{8} R_2^2.$$

But

$$|A_E| = \begin{vmatrix} a_{11} & a_{12} \\ a_{21} & a_{22} \end{vmatrix} = \frac{\left(R_1^2 - R_2^2\right)\upsilon - \left(R_1^2 + R_2^2\right)}{R_1 R_2^2} < 0,$$

which implies $u_0(R)$ exists for $R_2 > R_1 > 0$ and any values of $\Omega \geq 0$. Comparing to the analytical solution of Equations (4.2) repeated below,

$$u_0(r) = m_1 J_1(\lambda r) + m_2 Y_1(\lambda r) - r,$$

where

$$m_1 = \frac{\begin{vmatrix} d_{a1} & a_{12} \\ d_{a2} & a_{22} \end{vmatrix}}{|A_L|},$$

$$m_2 = \frac{\begin{vmatrix} a_{11} & d_{a1} \\ a_{21} & d_{a2} \end{vmatrix}}{|A_L|},$$

$$|A_L| = \begin{vmatrix} a_{11} & a_{12} \\ a_{21} & a_{22} \end{vmatrix},$$

$$\lambda = \Omega \sqrt{(1-\upsilon^2)\frac{\rho_0}{E}},$$

$$a_{11} = J_1(\lambda R_1),$$

$$a_{12} = Y_1(\lambda R_1),$$

$$a_{21} = \frac{\lambda}{2}[\, J_0(\lambda R_2) - J_2(\lambda R_2)] + \frac{\upsilon}{R_2} J_1(\lambda R_2),$$

$$a_{22} = \frac{\lambda}{2}[\, Y_0(\lambda R_2) - Y_2(\lambda R_2)] + \frac{\upsilon}{R_2} Y_1(\lambda R_2),$$

$$d_{a1} = R_1\,,$$

$$d_{a2} = 1 + \upsilon,$$

which does not exist at certain values of $\Omega$. By searching the values of $\Omega$ using the parameters given in Section 4.4 such that $|A_L| = 0$, it is found that $\Omega_1 \approx 218608$ rad/s, $\Omega_2 \approx 629955$ rad/s, $\Omega_3 \approx 1041261$ rad/s, $\Omega_4 \approx 1453995$ rad/s, $\Omega_5 \approx 1867344$ rad/s, … etc. are singularities of the analytical solution for Equations (4.2). For all test cases when $\Omega > \Omega_1$, solutions $u_0(r)$ of Equations (4.2) become negative. This suggests the possibility that solutions of Equations (4.2) only exist for $\Omega < \Omega_1$. By analogy to the whirling rods, the condition for the non-existence of solution could be referred to as "static instability" for steady rotating annuli.

Since there is a "static instability", it is legitimate to ask if there is a "dynamic instability". The answer to this question is yes because the "dynamic instability" is just the resonance caused by the dynamic oscillation of an annulus. Referring to

Equations (4.11b,c,d,e) which determine the unknown coefficients $K_1$, $K_2$, $K_3$ and $K_4$, the coefficient matrix $A$ for these four equations is

$$A = \begin{bmatrix} a_{11} & a_{12} & a_{13} & a_{14} \\ a_{21} & a_{22} & a_{23} & a_{24} \\ a_{31} & a_{32} & a_{33} & a_{34} \\ a_{41} & a_{42} & a_{43} & a_{44} \end{bmatrix},$$

where

$$a_{11} = J_1(\kappa_1 R_1),$$

$$a_{12} = Y_1(\kappa_1 R_1),$$

$$a_{13} = J_1(\kappa_2 R_1),$$

$$a_{14} = Y_1(\kappa_2 R_1),$$

$$a_{21} = [\kappa_1^2 - k_1(\omega^2 + \Omega^2)]\, J_1(\kappa_1 R_1),$$

$$a_{22} = [\kappa_1^2 - k_1(\omega^2 + \Omega^2)]\, Y_1(\kappa_1 R_1),$$

$$a_{23} = [\kappa_2^2 - k_1(\omega^2 + \Omega^2)]\, J_1(\kappa_2 R_1),$$

$$a_{24} = [\kappa_2^2 - k_1(\omega^2 + \Omega^2)]\, Y_1(\kappa_2 R_1),$$

$$a_{31} = \kappa_1 J_0(\kappa_1 R_2) + \left(\frac{\upsilon - 1}{R_2}\right) J_1(\kappa_1 R_2),$$

$$a_{32} = \kappa_1 Y_0(\kappa_1 R_2) + \left(\frac{\upsilon - 1}{R_2}\right) Y_1(\kappa_1 R_2),$$

$$a_{33} = \kappa_2 J_0(\kappa_2 R_2) + \left(\frac{\upsilon - 1}{R_2}\right) J_1(\kappa_2 R_2)$$

$$a_{34} = \kappa_2 Y_0(\kappa_2 R_2) + \left(\frac{\upsilon - 1}{R_2}\right) Y_1(\kappa_2 R_2)$$

$$a_{41} = [\kappa_1^2 - k_1(\omega^2 + \Omega^2)] \left[\kappa_1 J_0(\kappa_1 R_2) - \frac{2}{R_2} J_1(\kappa_1 R_2)\right],$$

$$a_{42} = [\kappa_1^2 - k_1(\omega^2 + \Omega^2)] \left[\kappa_1 Y_0(\kappa_1 R_2) - \frac{2}{R_2} Y_1(\kappa_1 R_2)\right],$$

$$a_{43} = [\kappa_2^2 - k_1(\omega^2 + \Omega^2)] \left[\kappa_2 J_0(\kappa_2 R_2) - \frac{2}{R_2} J_1(\kappa_2 R_2)\right],$$

$$a_{44} = [\kappa_2^2 - k_1(\omega^2 + \Omega^2)] \left[\kappa_2 Y_0(\kappa_2 R_2) - \frac{2}{R_2} Y_1(\kappa_2 R_2)\right],$$

"Dynamic instability" or resonance occurs when $|A| = 0$, this happens if $\omega_1 \approx 218608$ rad/s, $\omega_2 \approx 629955$ rad/s, $\omega_3 \approx 1041261$ rad/s, $\omega_4 \approx 1453995$ rad/s, $\omega_5 \approx 1867344$ rad/s, … etc. for radial modes and $\omega_1 \approx 56949$ rad/s, $\omega_2 \approx 360896$ rad/s, $\omega_3 \approx 611725$ rad/s, $\omega_4 \approx 860068$ rad/s, $\omega_5 \approx 1107682$ rad/s, … etc. for circumferential modes at $\Omega = 0$ rad/s. By comparing these values obtained in Table 4.1 to Table 4.4, they are just the natural frequencies of the non-rotating annulus with the given parameters in Section 4.4 when $\Omega = 0$ rad/s. Similar conclusions can be drawn for the case when $\Omega = 200\pi$ rad/s. The exact same results will be obtained if Equations (4.13b,c,d,e) are employed instead. Note that the above approach is just an alternative approach in locating the natural frequencies compared to the frequency response approach described in Subsection 4.4.3.

### *5.5 Critique on Proposed Numerical Method*

The running time for the numerical solution of the current steady or equilibrium one-dimensional problems is only a fraction of a second on a Pentium III computing machine. However, the order of matrix to be solved by the Newton's iteration is $O(n^i)$, where $n$ is the number of terms chosen in the series representation of the unknown solutions in the proposed numerical method and $i = 1$, 2 or 3 is the dimension of the vibration problem. As the dimension of the problem goes up, computational cost and computer storage go up exponentially in the order of $O(n^i)$. Say for instance a three-dimensional problem is tackled with one hundred grid points selected in each of the three spatial coordinates, the order of the matrix in the Newton's iterations for each time step becomes one million. Such a task is only achievable by supercomputers with probably massively parallel computations.

The method that is employed to solve the matrix in the Newton's iteration is Gauss elimination with partial pivoting. Due to the limited precision of the computing machine, $n$ is chosen to be thirty or less in the current studies. For $n$ greater than thirty, numerical round off error starts to set in significantly. Hence, in order to acquire a more accurate solution, a higher precision machine such as quadruple rather than double precision is recommended. The error tolerance for stopping criteria of the Newton's iterations is in the order of $O(10^{-20})$ at low angular velocities that are not too

close to the natural frequencies. When the oscillation frequencies of the applied external stresses get higher, numerical accuracies become harder to attain. For the numerical computations on the third or higher natural modes of vibration in the rotating annuli problems, error tolerance can only be reached in the vicinity of $O(10^{-4})$, which signifies that numerical computations is less likely to be as accurate as the exact analytical solution due to significant round off error.

## *5.6 Critique on Results of Mathematical Models*

The mathematical linear models formulated for whirling rods and rotating annuli are based on small strain limitation. Results are alleged not to be valid at large strain or in the neighbourhood of a natural frequency. By including the Poisson's effect in the proposed nonlinear model for rods and Biezeno and Grammel's static model for annuli, the cross-sectional area of rods and thickness of annuli become variables. This section will discuss the reliability of the small strain analysis at large strain and near resonance frequencies as well as the deformed shape profile for rods and annuli.

### *5.6.1 Whirling Rods Strain*

Embracing the parameters in the numerical experiment given in Chapter 3, at low angular velocity $\Omega = 200\pi$ rad/s,

$$\varepsilon(x) \sim O(10^{-3}),$$

which shows that at normal engineering strain, small strain analysis is valid. At high angular velocity $\Omega = 1000\pi$ rad/s,

$$\varepsilon(x) \sim O(10^{-1}),$$

which shows at large engineering strain, the difference of strains between the linear uniaxial and the proposed nonlinear models is about 19% at $x = 0$. Such a strain is beyond engineering material strain. Hence the small strain analysis at this angular velocity is invalid.

From the proposed nonlinear model, the cross-sectional area of the deformed rod while rotating can be calculated. Figure 5.1 shows that such a rod exhibits a trumpet like shape.

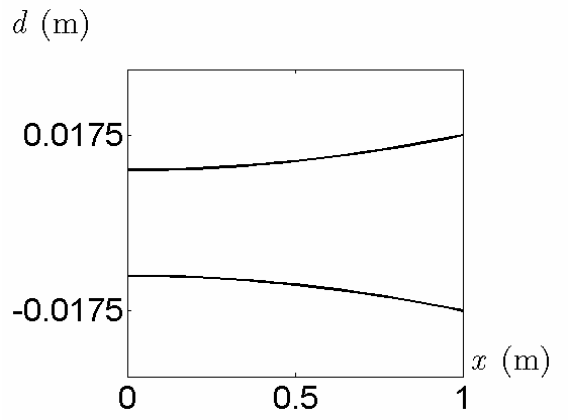


Figure 5.1. Geometric configuration of the whirling rod rotating at angular velocity $\Omega = 200\pi$ rad/s.

The figure shows that the whirling rod at $x = 0$ is constricted most and the constriction is decreasing towards the free end of the rod.

### *5.6.2 Rotating Annuli Strains*

Suppose numerical results are obtained for the Bhuta and Jones model with inner radius $R_1 = 0.02$ m and outer radius $R_2 = 0.06$ m of an annulus. At angular velocity $\Omega = 200\pi$ rad/s, maximum static radial normal strain

$$\varepsilon_{r0}\,(r = 0.02) = 2.79\times10^{-5}$$

and maximum static circumferential normal strain

$$\varepsilon_{\theta 0}\,(r = 0.043) = 8.93\times10^{-6}\,.$$

At angular velocity $\Omega = 4000\pi$ rad/s, maximum static radial normal strain

$$\varepsilon_{r0}\,(r = 0.02) = 1.12\times10^{-2}$$

and maximum static circumferential normal strain

$$\varepsilon_{\theta 0}\,(r = 0.059) = 3.02\times10^{-3}\,.$$

Although there are no results obtained from nonlinear equations using nonlinear strain-displacement relationship, the above static strains on the Bhuta and Jones' model indicate that small strain analysis is likely to be invalid beyond $\Omega = 4000\pi$ rad/s (120000 rpm).

From the linear strain-displacement relationships by Fung (1994) at constant time, dynamic radial normal strain

$$\varepsilon_{r1} = \frac{du_1}{dr},$$

dynamic circumferential normal strain

$$\varepsilon_{\theta 1} = \frac{u_1}{r}$$

and dynamic circumferential shear strain

$$\gamma_{r\theta 1} = \frac{dv_1}{dr} - \frac{v_1}{r}.$$

Since the dynamic components have real and imaginary parts, the maximum amplitudes of the dynamic components are just the square root of the sum of squares of the corresponding real and imaginary parts. From the numerical experiments performed on the Bhuta and Jones' model, absolute magnitudes of radial normal, circumferential normal and circumferential shear strains are listed in the following tables at resonance frequencies. Table 5.1 and Table 5.2 show the strain magnitudes at radial and circumferential resonance frequencies respectively.

Table 5.1. Order of absolute magnitudes of radial normal $|\varepsilon_{r1}|$, circumferential normal $|\varepsilon_{\theta 1}|$ and circumferential shear $|\gamma_{r\theta 1}|$ strains at the first five radial resonance frequencies $\omega$.

| Radial mode | $\omega$ (rad/s) | $\lvert\varepsilon_{r1}\rvert$ | $\lvert\varepsilon_{\theta 1}\rvert$ | $\lvert\gamma_{r\theta 1}\rvert$ |
|---|---|---|---|---|
| 1st | 218611 | $O(10^{-1})$ | $O(10^{-2})$ | $O(10^{-4})$ |
| 2nd | 629957 | $O(10^{-1})$ | $O(10^{-2})$ | $O(10^{-3})$ |
| 3rd | 1041262 | $O(10^{-1})$ | $O(10^{-1})$ | $O(10^{-3})$ |
| 4th | 1453996 | $O(10^{-1})$ | $O(10^{-1})$ | $O(10^{-3})$ |
| 5th | 1867345 | $O(10^{-2})$ | $O(10^{-3})$ | $O(10^{-5})$ |

Table 5.2. Order of absolute magnitudes of radial normal $|\varepsilon_{r1}|$, circumferential normal $|\varepsilon_{\theta 1}|$ and circumferential shear $|\gamma_{r\theta 1}|$ strains at the first five circumferential resonance frequencies $\omega$.

| Circumferential mode | $\omega$ (rad/s) | $\lvert\varepsilon_{r1}\rvert$ | $\lvert\varepsilon_{\theta 1}\rvert$ | $\lvert\gamma_{r\theta 1}\rvert$ |
|---|---|---|---|---|
| 1st | 56945 | $O(10^{-3})$ | $O(10^{-3})$ | $O(10^{0})$ |
| 2nd | 360894 | $O(10^{-3})$ | $O(10^{-4})$ | $O(10^{0})$ |
| 3rd | 611724 | $O(10^{-4})$ | $O(10^{-4})$ | $O(10^{-1})$ |
| 4th | 860067 | $O(10^{-3})$ | $O(10^{-4})$ | $O(10^{0})$ |
| 5th | 1107682 | $O(10^{-5})$ | $O(10^{-6})$ | $O(10^{-2})$ |

Although there are no results obtained from nonlinear equations using nonlinear strain-displacement relationship, the above dynamic strains on the Bhuta and Jones' model reveal that small strain analysis is invalid at the first five radial and circumferential natural modes of vibration.

From the static Biezeno and Grammel's model, the thickness profile of the deformed annulus while rotating can be calculated. Figure 5.2 shows that such an annulus exhibits a concave lens shape.

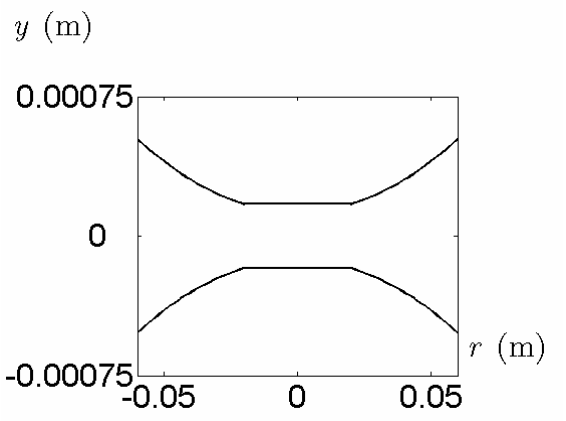


Figure 5.2. Geometric configuration of the rotating annulus rotating at angular velocity $\Omega = 200\pi$ rad/s.

The hole of the annulus is located at $-0.02 < r < 0.02$. The figure shows that the rotating annulus at $|r| = 0.02$ is constricted most and the constriction is decreasing towards the free edge of the annulus.

### *5.6.3 Natural Frequencies*

The controversy over whether natural frequencies of vibrations are rising or falling while angular velocity is increasing has been debated for over 40 years. According to the results obtained in this thesis, axial natural frequencies drop for steadily rotating rods while natural frequencies do not show any specific pattern for dynamically rotating annuli with Coriolis effect. Thus, it is logical to conclude that when an object is under tensile force due to rotation, its natural frequencies are different with and without the Coriolis effect. This implies Coriolis effect plays a role in altering the natural modes of vibration.

## *5.7 Implications for Machine Design*

One of the major reasons to have theoretical and numerical studies on vibration problems is to offer a less expensive alternative than experimental study. Theoretical and numerical solutions obtained in this thesis may be used to generate desirable results before any whirling or rotating components of a machine are designed and manufactured. However, solutions offered in Lagrangian coordinates are subjected to an upper limit of some angular velocity of rotation. Beyond that rotational speed, no existing analytical or numerical solutions are adequate. When the oscillation frequencies due to external forces coincide with the natural frequencies of vibration, resonance occurs. Hence a fast and cheap calculation on the natural frequencies of the components given certain material parameters is essential in order to avoid a catastrophic failure before the manufacturing of a machine. From the numerical experiments of whirling rods and rotating annuli, natural frequencies of a component can be driven up with a greater Young's modulus and/or a smaller material density. This implies a lighter and/or stiffer material should be selected for a more sustainable material before reaching the fundamental frequency of a whirling or rotating component. Table 5.3 shows the mechanical properties of four selected materials.

Table 5.3. Mechanical properties of four selected materials.

| Material | $E$, Young's modulus (GPa) | Tensile Strength (GPa) | $\rho$, Density (kg/m$^3$) | $E/\rho \times 10^{-9}$ (m$^2$rad$^2$/s$^2$) |
|---|---|---|---|---|
| Multi wall nanotube | 1200 | 150 | 2600 | 0.4615 |
| Steel | 208 | 0.4 | 7800 | 0.0267 |
| Wood | 16 | 0.008 | 600 | 0.0267 |
| Epoxy | 3.5 | 0.005 | 1250 | 0.0028 |

From the above table, the ratio $E/\rho$ is highest for multi wall carbon nanotube which also has a much higher tensile strength than steel. Recent developments on carbon composite material in the areas of application such as sports rackets and aerospace structures are evident for the above implication.

# Chapter 6

# Concluding Remarks

## *6.1 Static Whirling Rods*

Results for the axial displacements for steadily rotating rods show that the non-linear strain-displacement relationship should be taken into account at high angular velocity. However, even when made of high-yield steel, which has a yield stress of about 1200 MPa, the corresponding rotational speed according to the linear uniaxial model is 558 rad/s, which is well below the limit 7929 rad/s for the existence and uniqueness of solution described in Subsection 3.4.1. The corresponding rotational speed according to the nonlinear model is 551 rad/s, which is well below the limit 4094 rad/s for the existence and uniqueness of solution described in Subsection 3.4.2. This indicates that existing materials will fail well before the linear or non-linear solutions become invalid. Furthermore, beyond the rotational speed at yield stress, Hooke's law ceases to be valid. Hence, for the prediction of axial displacements of steel rods with angular velocities below 558 rad/s, the linear uniaxial model will be adequate. Since the linear uniaxial model does not take the variation of cross-sectional area and density of material into account, it is difficult to determine which method predicts the axial natural frequencies is more accurate. Recall that the receptance approach takes the variation of area and material density into account for nonlinear deformation. Based on the results obtained in this thesis, axial natural frequencies are lowered when the rod is in static rotation compared to its non-rotating stationary state. Rotating rods are in horn shape according to the numerical results. Density of rotating rod decreases towards the free end of the rod. Solutions for the linear uniaxial model with angular velocities rotating up to the yield point of high-strength steel exist and are unique. Solutions for the nonlinear model with angular velocities rotating up to the yield point of high-strength steel exist but are non-unique. This is because one of the solutions is physically correct, the other solution is physically implausible with reasoning mentioned in Subsection 3.4.2. If numerical iterations converge to physically meaningless solutions, a different $n$ must be

attempted until a physically correct solution is found. Recall that $n$ is the size of a complete series in Equations (3.10).

### *6.2 Dynamic Rotating Annuli*

In Figure 4.2a, the static radial displacement has a negative slope close to the free edge of the annulus. The reason for that is because circumferential strain contracts the radial displacement more than the radial strain extends the radial displacement. According to the Bhuta and Jones' model, the physical outcome of the dynamic vibration remains the same if the roles of excitation frequency $\omega$ and angular velocity $\Omega$ are interchanged. Formulated problems in Section 4.1 are termed two-point boundary value problems. When the proposed numerical method in Section 4.3 is applied to solve two-point boundary value problems, a solution does not exist if some of the displacements turn out to be negative. Solutions of these two-point boundary value problems are not unique when numerical results are different with different $n$, although displacements are positive. Recall that $n$ is the size of the truncated complete series. For Bhuta and Jones' model, numerical solutions conform to the exact solutions for different test cases except those mode shapes at higher modes of resonances. Nevertheless, Biezeno and Grammel's model will give non-uniqueness property for various values of $n$ at certain boundary conditions. Such non-uniqueness property arises if for instance the inner radius of the annulus is changed to $R_1 = 0.01$ m in the numerical experiment of Section 4.4. This phenomenon can be explained by the nonlinear nature of the static equations of Biezeno and Grammel's model. The closed form conditions for existence and uniqueness of solution of a particular two-point boundary value problem is not attempted here because it is out of the scope of this thesis. From the figures in Section 4.4.1, the induced displacement $\mathrm{Im}[v_1(r)]$ due to Coriolis effect is minute compared to $\mathrm{Re}[u_1(r)]$ and the induced displacement $\mathrm{Im}[u_1(r)]$ due to Coriolis effect is minute compared to $\mathrm{Re}[v_1(r)]$. The differences between the exact and the approximate solution for both $\mathrm{Im}[u_1(r)]$ and $\mathrm{Im}[v_1(r)]$ are in the order of $O(10^{-13})$, which indicates that Coriolis effect is insignificant for rotating annulus at low angular velocities. By taking into account the deformed thickness and the varying material density of an annular plate while it is in rotation in the Biezeno and Grammel's model, results do not significantly change the in-plane displacements at low angular velocities and the first

four natural modes of vibrations. Nonetheless, these variations are derived under the assumption that dynamic motion of the annulus does not significantly alter the Poisson's effect on the plate. Hence the expressions derived are limited to steady rotation only. Non-linear dynamic formulation will be required when Poisson's effect is being considered under a large amplitude dynamic oscillation. Radial natural frequencies increase if Coriolis forces are included. On the other hand, radial natural frequencies drop if Coriolis forces are not taken into consideration while the plates are in rotation. Furthermore, whether Coriolis forces are included or not, circumferential natural frequencies drop. Numerical accuracies on mode shapes drop when the excitation frequency $\omega$ tends to be large. The mathematical models in Section 4.1 are only valid up to the yield points. For the particular numerical experiment in Section 4.4, radial yield stress of the steady rotational motion for high-strength steel is at about 1.2 GPa. The corresponding angular velocity is $\Omega \approx 9613$ rad/s for Bhuta and Jones' model, and $\Omega \approx 8802$ rad/s for Biezeno and Grammel's model. To produce a circumferential yield stress of 1.2 GPa, angular velocity $\Omega \approx 17813$ rad/s for Bhuta and Jones' model, and $\Omega \approx 16303$ rad/s for Biezeno and Grammel's model. These estimations are only valid for linear stain-displacement relationship. For high angular velocity or large amplitude vibration displacements, nonlinear stain-displacement relationship should be employed for the estimation of angular velocity at yield stress.

### *6.3 Contributions in the Making*

- Theoretical derivation of the non-linear governing equations of motion of steadily whirling rods. (*Subsection 3.2.1*)

- Existence and uniqueness of solution for the steady linear uniaxial model and the proposed steady nonlinear model of whirling rods. (*Section 3.4*)

- Transformation of the Biezeno and Grammel's model from the Eulerian coordinates to Lagrangian coordinates and the inclusion of the Poisson's effect on material density and thickness of an annulus. (*Subsection 4.1.2*)

- Exact and approximate analytical solutions for the Bhuta and Jones' model of dynamic rotating discs with specified boundary conditions. (*Section 4.2*)

- The frequency response approach to solve for the in-plane natural frequencies of rotating annulus that can be generalized to objects of arbitrary shapes with excitation force applying at any location of the objects. (*Subsection 4.4.3*)

- Proposed numerical method that solves the nonlinear integral-differential and coupled differential governing equations. (*Subsection 3.2.2* and *Section 4.3*)

- Inclusion of varying cross-sectional area into non-prismatic rods and the proof of the assumption that thin discs or annuli have negligible change of thickness under tension or compression. (*Section 5.3*)

### *6.4 Suggested Future Work*

Whirling rods with dynamic motion by including the Coriolis effect could be scrutinized. Compare to the steady motion of whirling rod with axial displacement only, dynamic motion will couple the transverse and axial displacement of vibration. Non-linear strain-displacement relationships may be implemented for large strain deformation or large amplitude vibration of rotating annuli problems. The resulting equations are nonlinear and time-dependent. The proposed numerical method could be extended to study the multi-dimensional problems such as asymmetric rotating discs or annuli, cylinders and elastic shells problems, where 2-D or 3-D Hooke's laws should be applied to establish governing equations with dependence in radial, circumferential and transverse directions.

# References


Abbas, B., 1979, "Simple Finite Elements for Dynamic Analysis of Thick Pre-Twisted Blades", *Aeronautical Journal*, **83**, pp. 450 – 453.

Adams, G.G., 1987, "Critical Speeds for a Flexible Spinning Disk", *International Journal of Mechanical Sciences*," **29**, pp. 525 – 531.

Akoz, A.Y., Omurtag, M.H. and Dogruoglu, A.N., 1991, "The Mixed Finite Element Formulation for Three Dimensional Bars", *International Journal of Solids and Structures*, **28**, pp. 225 – 234.

Anderson, G.L., 1975, "On the Extensional and Flexural Vibrations of Rotating Bars", *International Journal of Non-Linear Mechanics*, **10**, pp. 223 – 236.

Bapat, C.N., 1995, "Vibration of Rods with Uniformly Tapered Sections", *Journal of Sound and Vibrations*, **185**, pp. 185 – 189.

Bathe, K.J. and Dvorkin, E.N., 1985, "A Four-Node Plate Bending Element Based on Mindlin/Reissner Plate Theory and a Mixed Interpolation", *International Journal of Numerical Method Engineering*, **21**, pp.367 – 383.

Berdichevskii, V.L., 1981, "On the Energy of an Elastic Rod," *Journal of Applied Mathematics and Mechanics*, **45**, pp. 518 – 529.

Berger, H.M., 1955, "A New Approach to the Analysis of Large Deflections of Plates", *Journal of Applied Mechanics*, **20 – 22**, pp. 465 – 472.

Bertholf, L.D., 1967, "Numerical Solution for Two-dimensional Elastic Wave Propagation in Finite Bars", *Journal of Applied Mechanics*, **34**, pp. 725 – 734.

Bhat, R.B. , 1986, "Transverse Vibrations of a Rotating Uniform Cantilever Beam with Tip Mass As Predicted by Using Beam Characteristic Orthogonal Polynomials in the Rayleigh-Ritz Method", *Journal of Sound and Vibration*, **105**, pp. 199 – 210.

Bhuta, P.G. and Jones, J.P., 1963a, "On Axial Vibrations of a Whirling Bar", *The Journal of the Acoustical Society of America*, **35**, pp. 217 – 221.

Bhuta, P.G. and Jones, J.P., 1963b, "Symmetric Planar Vibrations of a Rotating Disk", *The Journal of the Acoustical Society of America*, **35**, pp. 982 – 989.

Bickford, W.B. and Reddy, E.S., 1985, "On the In-plane Vibrations of Rotating Rings", *Journal of Sound and Vibration*, **101**, pp. 13 – 22.

Biezeno, C.B. and Grammel, R., 1954, "*Engineering Dynamics, Volume 3 Steam Turbines (Translated from the original German (1939, 1953) by E.F. Winter and H.A. Havemann)*", Blackie and Son Ltd, pp. 34.

Bishop, R.E.D. and Johnson, D.C., 1960, "*The Mechanics of Vibration*", Cambridge University Press.

Brunelle, E.J., 1971, "Stress Redistribution and Instability of Rotating Beams and Disks", *American Institute of Aeronautics and Astronautics Journal*, **9**, pp. 758 – 759.

Burdess, J.S., Wren, T. and Fawcett, J.N., 1987, "Plane Stress Vibrations in Rotating Discs", *Proceedings of the Institution of Mechanical Engineers*, **201(C1)**, pp. 37 – 44.

Carnegie, W., 1959, "Vibrations of Rotating Cantilever Blading : Theoretical Approaches to the Frequency Problem Based on Energy Methods", *Journal of Mechanical Engineering Sciences*, **1**, pp.235 – 240.

Carnegie, W., 1967, "The Application of Variational Method to Derive the Equations of Motion of Vibrating Cantilever Blading Under Rotation", *Bulletin of Mechanical Engineering Education*, **6**, pp. 29.

Carrier, G.F., 1945, "On the Vibrations of the Rotating Ring", *Quarterly of Applied Mathematics*, **3**, pp. 235 – 245.

Chantasiriwan, S., 2004a, "Investigation of the Use of Radial Basis Functions in Local Collocation Method for Solving Diffusion Problems", *International Communications in Heat and Mass Transfer*, **31**, pp. 1095 – 1104.

Chantasiriwan, S., 2004b, "Cartesian Grid Methods Using Radial Basis Functions for Solving Poisson, Helmholtz and Diffusion-Convection Equations", *Engineering Analysis with Boundary Elements*, **28**, pp. 1417 – 1425.

Chen, J.S. and Jhu, J.L., 1996, "On the In-Plane Vibration and Stability of a Spinning Annular Disk", *Journal of Sound and Vibration*, **195**, pp. 585 – 593.

Chen, R.S., 1997, "Evaluation of Natural Vibration Frequency of a Compression Bar with Varying Cross-Section by Using the Shooting Method", *Journal of Sound and Vibration*, **201**, pp. 520 – 527.

Cherukuri, H.P. and Shawki, T.G., 1996, "A Finite-Difference Scheme for Elastic Wave Propagation in a Circular Disk", *The Journal of the Acoustical Society of America*, **100**, pp. 2139 – 2155.

Chree, C., 1889, "On Longitudinal Vibrations", *Quarterly Journal of Pure and Applied Mathematics*, **23**, pp. 317 – 342.

Chung, J., Oh, J.-E. and Yoo, H.H., 2000, "Non-Linear Vibration of a Flexible Spinning Disc with Angular Acceleration", *Journal of Sound and Vibration*, **231**, pp. 375 – 391.

Dawson, B., 1968, "Coupled Bending-Bending Vibrations of Pre-Twisted Cantilever Blading Treated by the Rayleigh-Ritz Energy Method", *Journal of Mechanical Engineering Science*, **10**, pp. 381 – 388.

Dentsoras, A.J. and Dimarogonas, A.D., 1983, "Resonance Controlled Fatigue Crack Propagation in a Beam Under Longitudinal Vibrations", *International Journal of Fracture*, **23**, pp. 15 – 22.

Doby, R, 1969, "On the Elastic Stability of Coriolis-coupled Oscillations of a Rotating Disc", *Journal of The Franklin Institute*, **288**, pp. 203 – 212.

Eisenberger, M., 1991, "Exact Longitudinal Vibration Frequencies of a Variable Cross-Section Rod", *Applied Acoustics*, **34**, pp. 123 – 130.

Eversman, W. and Dodson, R.O., 1969, "Free Vibration of a Centrally Clamped Spinning Circular Disk", *American Institute of Aeronautics and Astronautics Journal*, **7**, pp. 2010 – 2012.

Farag, N.H. and Pan, J., 2003, "Modal Characteristics of In-Plane Vibration of Circular Plates Clamped at the Outer Edge", *The Journal of the Acoustical Society of America*, **113**, pp. 1935 – 1946.

Farag, N.H. and Pan, J., 1998, "Free and Forced In-Plane Vibration of Rectangular Plates", *The Journal of the Acoustical Society of America*, **103**, pp. 408 – 413.

Farag, N.H. and Pan, J., 1999, "Modal Characteristics of In-Plane Vibration of Rectangular Plates", *The Journal of the Acoustical Society of America*, **105**, pp. 3295 – 3310.

Fung, Y.C., 1994, "*A First Course in Continuum Mechanics (Third Edition)*", Prentice Hall.

Gazis, D.C. and Mindlin, R.D., 1960, "Extensional Vibrations and Waves in a Circular Disk and a Semi-Infinite Plate", *Journal of Applied Mechanics*, **27**, pp. 541 – 547.

Gere, J.M., and Timoshenko, S.P., 1985, "*Mechanics of Materials (Second SI Edition)*", PWS Engineering, Wadsworth International.

Green A.E. and Laws, N., 1966, "A General Theory of Rods", *Proceedings of the Royal Society of London, Series A*, **293**, pp. 145 – 155.

Green, A.E., Naghdi, P.M. and Wenner, M.L., 1974a, "On the Theory of Rods. I. Derivations from the Three Dimensional Equations", *Proceedings of the Royal Society of London, Series A*, **337**, pp. 451 – 483.

Green, A.E., Naghdi, P.M. and Wenner, M.L., 1974b, "On the Theory of Rods. II. Developments by Direct Approach", *Proceedings of the Royal Society of London, Series A*, **337**, pp. 485 – 507.

Heo, J.W. and Chung, J., 2004, "Vibration Analysis of a Flexible Rotating Disk with Angular Misalignment," *Journal of Sound and Vibration*, **274**, pp. 821 – 841.

Hestermann, D.C., Entwistle, R.D., and Stone, B.J., 1996, "Axial and Torsional Receptances for Tapered Circular Shafts", *Modal Analysis: The International journal of Analytical and Experimental Modal Analysis,* **11**, pp. 178 – 193.

Hodges, D.H., 1977, "On the Extensional Vibrations of Rotating Bars", *International Journal of Nonlinear Mechanics*, **12**, pp. 293 – 296.

Hodges, D.H., 1983, Comments on "On the Axial Vibrations of Rotating Bars", *Journal of Sound and Vibrations*, **87**, pp. 513 – 515.

Hodges, D.H. and Bless, R.R., 1994, "Axial Instability of Rotating Rods Revisited", *International Journal of Non-Linear Mechanics*, **29**, pp. 879 – 887.

Huang, C.L.D. and Al-Khattat, I.M., 1977, "Finite Amplitude Vibrations of a Circular Plate", *International Journal of Non-Linear Mechanics*, **12**, pp. 297 – 305.

Hutchinson, J.R., 1972, "Axisymmetric Vibration of a Free Finite Length Rod", *The Journal of the Acoustical Society of America*, **51**, pp. 233 – 240.

Hutton, S.G., Chonan, S. and Lehmann, B.F., 1987, "Dynamic Response of a Guided Circular Saw", *Journal of Sound and Vibration*, **112**, pp. 527 – 539.

Inman, D.J., 2001, "*Engineering Vibration (Second Edition)*", Prentice Hall.

Irie, T., Yamada, G. and Muramoto, Y., 1984, "Natural Frequencies of In-Plane Vibration of Annular Plates", *Journal of Sound and Vibration*, **97**, pp. 171 – 175.

Irons, J. and Kennedy, W., 1989, "Non-Linear Vibration of Centrally Clamped Thin Discs", *International Journal of Non-Linear Mechanics*, **24**, pp. 345 – 352.

Juvinall, R.C., 1967. "*Engineering Considerations of Stress, Strain and Strength*", McGraw-Hill.

Kinkaid, N.M., O'Reilly, O.M. and Turcotte, J.S., 2001, "On the Steady Motions of a Rotating Elastic Rod", *Journal of Applied Mechanics*, **68**, pp. 766 – 771.

Kirkhope, J., 1977, "In-Plane Vibration of a Thick Circular Ring", *Journal of Sound and Vibration*, **50**, pp. 219 – 227.

Krishnaswamy, S. and Batra, R.C., 1998, "On External Vibration Modes of Elastic Rods of Finite Length Which Include the Effect of Lateral Deformation", *Journal of Sound and Vibration*, **215**, pp. 577 – 586.

Kumar, B.M. and Sujith, R.I., 1997, "Exact Solution for the Longitudinal Vibration of Non-Uniform Rods", *Journal of Sound and Vibration*, **207**, pp. 721 – 729.

Lakin, W.D., 1974, "On the Differential Equation of a Rapidly Rotating Slender Rod", *Quarterly of Applied Mathematics*, **32**, pp. 11 – 27.

Lakin, W.D. and Nachman, A., 1978, "Unstable Vibrations and Buckling of Rotating Flexible Rods", *Quarterly of Applied Mathematics*, **35**, pp. 479 – 493.

Lakin, W.D. and Nachman, A., 1979, "Vibration and Buckling of Rotating Flexible Rods at Transitional Parameter Values", *Journal of Engineering Mathematics*, **13**, pp. 339 – 346.

Lamb, H. and Southwell, R.V., 1921, "The Vibrations of a Spinning Disk", *Proceedings of the Royal Society*, **99**, pp. 272 – 280.

Langley, R.S., 1989, "Application of the Dynamic Stiffness Method to the Free and Forced Vibration of Aircraft Panels", *Journal of Sound and Vibration*, **135**, pp. 319 – 331.

Lee, H.P. and Ng, T.Y., 1995, "Vibration and Critical Speeds of a Spinning Annular Disk of Varying Thickness", *Journal of Sound and Vibration*, **187**, pp. 39 – 50.

Lessen, M. and Gangal, M.D., 1970, "Effect of Coriolis Acceleration on the Vibrations of Rotating Disks", *Applied Scientific Research*, **22**, pp. 338 – 344.

Leung, R.C.N. and Pinnington, R.J., 1987, "Vibration of a Rotating Disc Subjected to an In-Plane force at Its Rim or at Its Centre", *Journal of Sound and Vibration*, **114**, pp. 281 – 295.

Lin, S.-Y., 1995, "Coupled Vibration and Natural Frequency Analysis of Isotropic Cylinders or Disks of Finite Dimensions", *Journal of Sound and Vibration*, **185**, pp. 193 – 199.

Lo, H. and Renbarger, J.L., 1951, "Bending Vibrations of a Rotating Beam", *First U.S. Congress of Applied Mechanics*, pp. 75 – 79.

Lo, H., 1952, "A Non-Linear Problem in the Bending Vibration of a Rotating Beam", *Journal of Applied Mechanics*, pp. 461 – 464.

Love, A.E.H., 1944, "*A Treatise on the Mathematical Theory of Elasticity*", Dover, New York, pp. 289.

Luo, A.C.J., 2000, "An Approximate Theory for Geometrically Nonlinear Thin Plates", *International Journal of Solids and Structures*, **37**, pp. 7655 – 7670.

Luo, A.C.J. and Mote Jr., C.D., 2003, "Asymmetric Responses of Rotating Thin Disks Experiencing Large Deflections", *Computers and Mathematics with Applications*, **45**, pp. 217 – 228.

Matins, J.A.C. and Oden, J.T., 1983, "A Numerical Analysis of a Class of Problems in Elastodynamics with Friction", *Computer Methods in Applied Mechanics and Engineering*, **40**, pp. 327 – 360.

Mindlin, R.D. and Medick, M.A., 1959, "Extensional Vibrations of Elastic Plates", *Journal of Applied Mechanics*, **26**, pp. 561 – 569.

Mizusawa, T., 1993, "Vibration of Rectangular Mindlin Plates with Tappered Thickness by the Spline Strip Method", *Computers and Structures*, **46**, pp. 451 – 463.

Naghdi, P.M. and Rubin, M.B., 1984, "Constrained Theories of Rods", *Journal of Elasticity*, **14**, pp. 343 – 361.

Naghdi, P.M. and Rubin, M.B., 1989, "On the Significance of Normal Cross-Sectional Extension in Beam Theory with Application to Contact Problems", *International Journal of Solids and Structures*, **25**, pp. 249 – 265.

Niordson, F., 1997, "Optimal Disks in Vibration", *International Journal of Solids and Structures*, **34**, pp. 2957 – 2968.

Oh, S. -Y., Song, O. and Librescu, L., 2003, "Effects of Pretwist and Presetting on Coupled Bending Vibrations of Rotating Thin-Walled Composite Beams", *International Journal of Solids and Structures*, **40**, pp. 1203 – 1224.

O'Reilly, O.M. and Turcotte, J.S., 1997a, "On the Free Vibration of a Whirling Rod", *Proceedings of DETC'97: 1997 ASME Design Engineering Technical Conferences*, Paper Number DETC97VIB4072.

O'Reilly, O.M. and Turcotte, J.S., 1997b, "Elastic Rods with Moderate Rotation", *Journal of Elasticity*, **48**, pp. 193 – 216.

Papadopoulos, C.A. and Dimarogonas, A.D., 1987, "Coupled Longitudinal and Bending Vibrations of a Rotating Shaft with an Open Crack", *Journal of Sound and Vibration*, **117**, pp. 81 – 93.

Phylactopoulos, A.and Adams, G.G., 1999a, "Transverse Vibration of a Rectangularly Orthotropic Spinning Disk, Part 1: Formulation and Free Vibration", *Journal of Vibration and Acoustics*, **121**, pp. 273 – 279.

Phylactopoulos, A. and Adams G.G., 1999b, "Transverse Vibration of a Rectangularly Orthotropic Spinning Disk, Part 2: Forced Vibration and Critical Speeds", *Journal of Vibration and Acoustics*, **121**, pp. 280 – 285.

Pnueli, D., 1972, "Natural Bending Frequency Comparable to Rotational Frequency in Rotating Cantilever Beam", *Journal of Applied Mechanics*, **39**, pp. 602 – 604.

Pochnammer, L., 1876, *Journal fur. Mathematik (Crelle)*, Bd. **81**, pp. 324.

Ramaiah, G.K., 1981, "Natural Frequencies of Spinning Annular Plates", *Journal of Sound and Vibration*, **74**, pp. 303 – 310.

Rao, J.S. and Carnegie, W., 1970, "Non-linear Vibrations of Rotating Cantilever Beams", *Aeronautical Journal*, **74**, pp. 161 – 165.

Rao, J.S. and Carnegie, W., 1972, "Non-linear Vibrations of Rotating Cantilever Blades Treated by the Ritz Averaging Process", *Aeronautical Journal*, **76**, pp. 566 – 569.

Rao, J.S. and Carnegie, W., 1973, "A Numerical Procedure for the Determination of the Frequencies and Mode Shapes of Lateral Vibration of Blades Allowing for the Effects of Pre-Twist and Rotation", *International Journal of Mechanical Engineering Education*, **1**, pp.37 – 47.

Rubinstein, N. and Stadter, J.T., 1972 "Bounds to Bending Frequencies of a Rotating Beam", *Journal of The Franklin Institute*, **294**, pp. 217 – 229.

Sagan, H., 1989, "*Boundary and Eigenvalue Problems in Mathematical Physics*", Dover Publications, Inc., New York, pp. 329 – 331.

Sankin, Yu.N. and Yuganova, N.A., 2001, "Longitudinal Vibrations of Elastic Rods of Stepwise-Variable Cross-Section Colliding with a Rigid Obstacle", *Journal of Applied Mathematics and Mechanics*, **65**, pp. 427 – 433.

Schilhansl, M.J., 1958, "Bending Frequency of a Rotating Cantilever Beam", *Journal of Applied Mechanics*, **25**, pp. 25 – 30.

Shen, I.Y. and Song, Y., 1996, "Stability and Vibration of a Rotating Circular Plate Subjected to Stationary In-Plane Edge Loads", *Journal of Applied Mechanics*, **63**, pp. 121 – 127.

Shield, R.T. and Im, S., 1986, "Small Strain Deformations of Elastic Beams and Rods Including Large Deflections", *Journal of Applied Mathematics and Physics (ZAMP)*, **37**, pp. 491 – 513.

Spiegel, M.R., 1971, "*Schaum's Outline Series: Advanced Mathematics*", McGraw-Hill Book Company.

Srinivasan, V. and Ramamurti, V., 1980, "Dynamic Response of an Annular Disk to a Moving Concentrated In-Plane Edge Load", *Journal of Sound and Vibration*, **72**, pp. 251 – 262.

Subrahmanyam, K.B., Kulkarni, S.V. and Rao, J.S., 1981, "Coupled Bending-Bending Vibrations of Pre-Twisted Cantilever Blading Allowing for Shear Deflection and Rotary Inertia by the Ressner Method", *International Journal of Mechanical Science*, **23**, pp.517 – 530.

Tobias, S.A., 1957, "Free Undamped Non-Linear Vibrations of Imperfect Circular Disks", *Proceedings of the Institute of Mechanical Engineers*, **171**, pp. 691 – 701.

Venkatesan, C. and Nagaraj, V.T., 1981, "On the Axial Vibrations of Rotating Bars", *Journal of Sound and Vibration*, **74**, pp. 143 – 147.

Wah, T., 1963, "Vibration of Circular Plates at Large Amplitudes", Journal of the Engineering Mechanics Division, *Proceedings of the American Society of Civil Engineers*, **89**, pp. 1 – 15.

Wahed, I.F.A. and Bishop, R.E.D., 1976, “On the Equations Governing the Free and Forced Vibrations of a General Non-Conservative System”, *Journal Mechanical Engineering Science*, **18**, pp. 6 – 10.

# Publications

1. W.S. Shum and R.D. Entwistle, “In-plane natural frequencies of asymmetric rotating annuli”, *Journal of Computational Physics* (In preparation).

2. W.S. Shum and R.D. Entwistle, “Analytical studies of in-plane natural frequencies of axisymmetric rotating annuli”, *The Journal of the Acoustical Society of America* (submitted and under editorial evaluation by the editor).

3. W.S. Shum and R.D. Entwistle, “Longitudinal vibrations frequencies of steadily whirling rods”, *The Journal of the Acoustical Society of America*, **119**, 909–916 (2006).

4. W.S. Shum and R.D. Entwistle, “On axial natural frequencies of whirling rods”, *Proceedings of the 4$^{th}$ Australasian Congress on Applied Mechanics*, Melbourne, Australia, February 16-18, 2005, 219-224.

# Appendix A

## Poisson's Ratio, Stress-Strain Relationship and Hooke's Law

### *A.1 Poisson's Ratio*

Imagine a prismatic rod being stretched by a tensile force $F$ applied normally throughout the whole cross-section at both ends of the rod with original undeformed length $L$ and uniform cross-sectional area $A_0 = \frac{\pi d_0^2}{4}$, where $d_0$ is the original diameter of the rod. A schematic diagram of a rod under stretching force is plotted in Figure A.1.

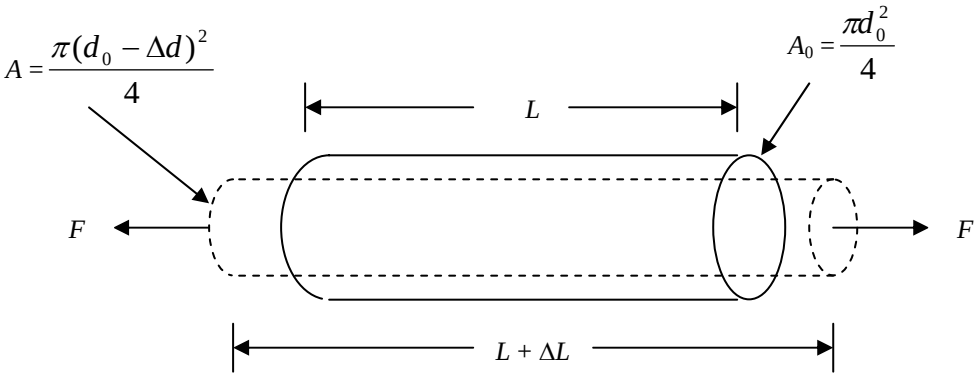


Figure A.1. A schematic diagram of a rod with original length $L$ and original constant cross-sectional area $A_0$ with diameter $d_0$ under stretching force $F$. $\Delta L$ is the change of length of the rod and $\Delta d$ is the change of diameter of the rod.

For a rod made of steel while it is stretched axially, the length of the rod elongates by $\Delta L$ and the diameter of the rod contracts by $\Delta d$. When a normal stress $\sigma = \frac{F}{A}$ is applied at both ends of a rod, it will experience an axial strain $\varepsilon = \frac{\Delta L}{L}$ and is accompanied by a lateral strain $\varepsilon_L = -\frac{\Delta d}{d}$. If the rod is isotropic, i.e. material has the same elastic

properties in all directions, then in the linear elastic region of the stress-strain relationship for steel, the Poisson's ratio $\upsilon$ is defined as $\upsilon = -\frac{\varepsilon_L}{\varepsilon}$. If the rod is stretched, i.e. $\varepsilon > 0$, its lateral length will be reduced, i.e. $\varepsilon_L < 0$. On the other hand, if the rod is contracted, i.e. $\varepsilon < 0$, its lateral length will be expanded, i.e. $\varepsilon_L > 0$. Therefore, $\upsilon$ is a positive quantity for material steel.

### *A.2 Stress-Strain Relationship*

Objects that are made of steel follow a stress-strain relationship with a typical plot shown in Figure A.2.

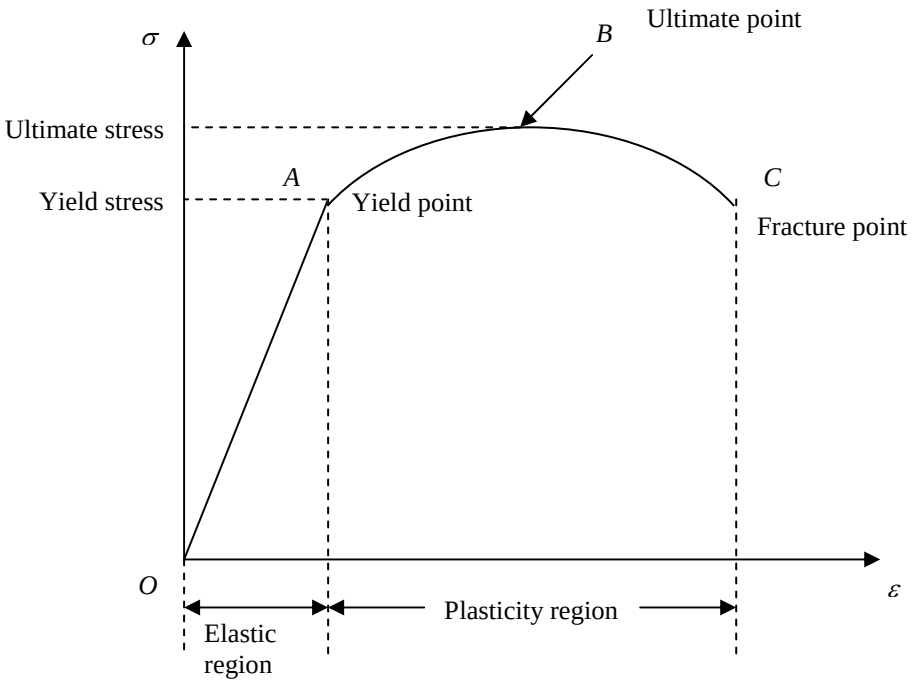


Figure A.2. Schematic plot of a stress-strain relationship of an elastic material made of steel.

$\sigma$ is the normal stress, $\varepsilon$ is the normal axial strain. Material yields at point *A* and is called the yield point with corresponding yield stress. Material has the maximum stress at point *B* and is called the ultimate point with corresponding ultimate stress and material fails at point *C* and is called the fracture point with corresponding fracture stress. Line *OA* is the elastic region. An elastic region is a region in which the material restores its original shape after a load is removed from it. Curve *ABC* is the non-linear curve in the plasticity region. A plasticity region is a region in which the material alters

its shape permanently after being deformed by a force. Note that Figure A.2 is a simplified plot of a stress-strain relationship for illustration purpose. Some other materials might involve other regions other than linear and plasticity regions such as strain hardening and necking regions. Strain hardening is a region where material undergoes atomic and crystalline structural change that result in increased resistance of the material to further deformation. Necking is a region where reduction in cross-sectional area is clearly visible than the other part of a rod. Figure A3 shows the necking region, the visible reduction of area region, of a rod under tension.

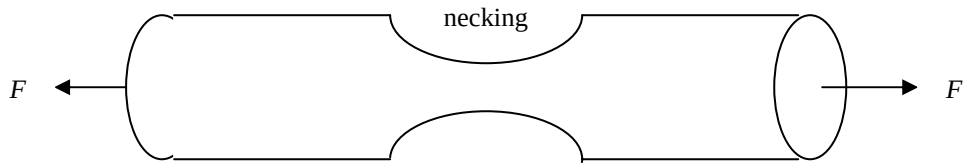


A.3. Necking of a rod in tension with force *F* applied at both ends over the whole cross-section.

## *A.3 Hooke's Law*

The physical rule that governs this stress-strain relationship in the linear elastic region is the Hooke's law. A reference on Hooke's law can be found in any standard textbook, such as Gere and Timoshenko (1985), and is repeated below for convenience.

### *A.3.1 1-D Hooke's Law*

Linear elastic materials, under an axial load below the yield stress are governed by

$$\sigma = E\varepsilon,$$

where constant $E$ is known as modulus of elasticity or Young's modulus. This elastic region is a linear relation between the stress $\sigma$ and strain $\varepsilon$ if the Young's modulus $E$ is a constant.

*A.3.2 2-D Hooke's law*

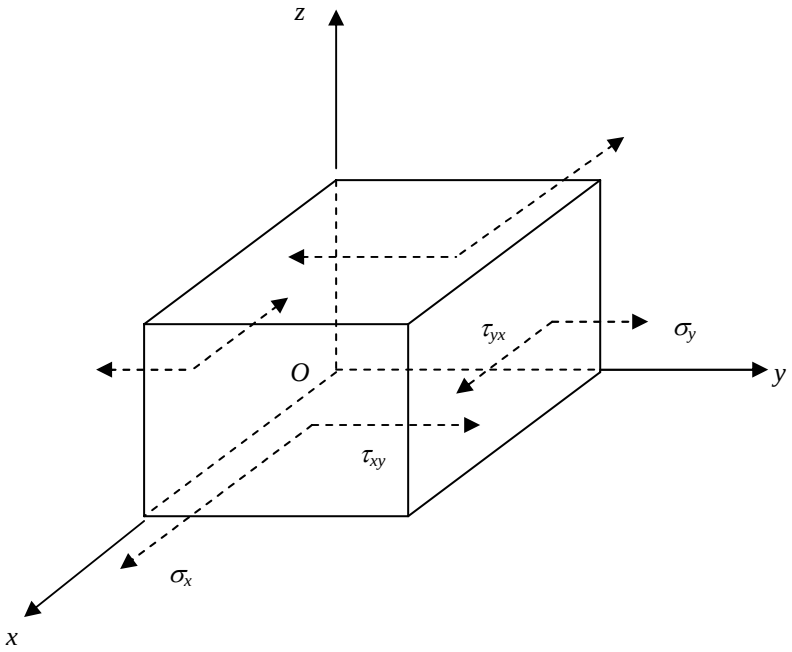


Figure A.4. An infinitesimally small material element located in the Cartesian coordinates ($x$,$y$,$z$) centered at the origin $O$. $\sigma_x$ and $\sigma_y$ are the normal stresses in the directions of $x$ and $y$ respectively. $\tau_{xy}$ is the shear stress on the surface perpendicular to the $x$-axis and in the direction of $y$.

When dealing with thin discs, Hooke's law for plane stress is required. Consider a differentially small cube material element in Figure A.4 being cut out of a disc with its thickness in the $z$-direction corresponds to the thickness of the disc. By using the Hooke's law for 1-D and the Poisson's ratio, Hooke's law for plane stress or 2-D in Cartesian coordinates ($x$, $y$, $z$) may be expressed as

$$\varepsilon_x = \frac{1}{E}(\sigma_x - \upsilon\sigma_y), \tag{A.1a}$$

$$\varepsilon_y = \frac{1}{E}(\sigma_y - \upsilon\sigma_x), \tag{A.1b}$$

$$\varepsilon_z = -\frac{\upsilon}{E}(\sigma_x + \sigma_y), \tag{A.1c}$$

$$\gamma_{xy} = \frac{\tau_{xy}}{G}. \tag{A.1d}$$

After rearranging Equations (A.1a,b and d),

$$\sigma_x = \frac{E}{1-\upsilon^2}(\varepsilon_x + \upsilon\varepsilon_y),$$

$$\sigma_y = \frac{E}{1-\upsilon^2}(\varepsilon_y + \upsilon\varepsilon_x),$$

$$\tau_{xy} = G\gamma_{xy},$$

where $\sigma_x$ and $\sigma_y$ are normal stresses along the $x$ and $y$ axes respectively, $\varepsilon_x$, $\varepsilon_y$ and $\varepsilon_z$ are normal strains along the $x$, $y$ and $z$ axes respectively, $G = \frac{E}{2(1+\upsilon)}$ is called the shear modulus of elasticity or modulus of rigidity, $\tau_{xy}$ is the shear stress acting parallel to the $y$-axis on the surface perpendicular to the $x$-axis and $\gamma_{xy}$ is the shear strain which is also the change of angle in radians between the planes perpendicular to $x$ and $y$ axes. Due to the static equilibrium of the element, normal or shear stresses along the same coordinate axis are equal in magnitude but opposite in direction on the positive and negative faces of the element. Also, the moment summed about the $z$-axis is zero, i.e. $\tau_{xy}(\Delta y\Delta z)\Delta x = \tau_{yx}(\Delta x\Delta z)\Delta y$, where $\Delta x$, $\Delta y$ and $\Delta z$ are the infinitesimal lengths of the cube along the $x$, $y$ and $z$ axes respectively. Hence, $\tau_{xy} = \tau_{yx}$. Positive values of stresses and strains indicate that the element is in tension. Negative values of stresses and strains indicate that the element is in compression. To illustrate the meaning of shear stress $\tau_{xy}$ and shear strain $\gamma_{xy}$, consider an observer viewing above the infinitesimally small material element in Figure A.4. The view will be similar to the diagram in Figure A.5 with the $z$-axis directed out of the page.

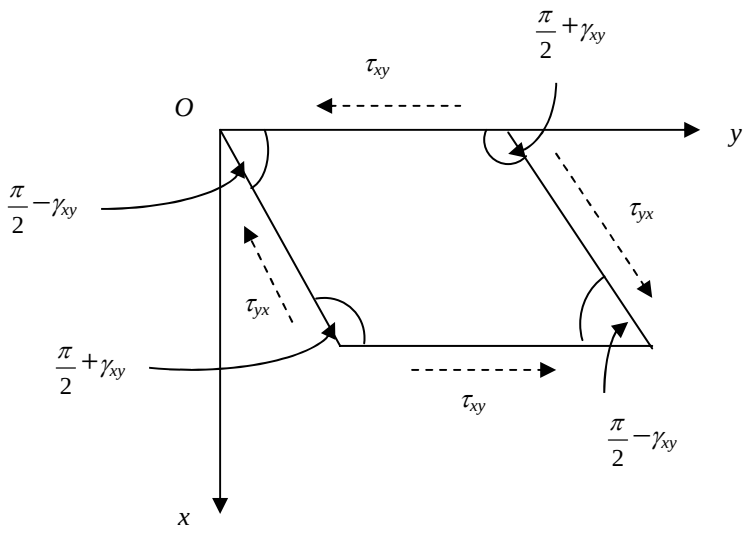


Figure A.5. A view above the cubical element drawn in Figure A.4. The shape of the surface perpendicular to the $z$-axis has changed from square to rhombus.

The original square shape is altered to rhombus shape by the shear stress $\tau_{xy}$ to produce a change of angle $\gamma_{xy}$, which is also known as the shear strain.

If the system is in cylindrical coordinates ($r, \theta, z$), then Hooke's law in 2-D may be described by

$$\varepsilon_r = \frac{1}{E}(\sigma_r - \upsilon\sigma_\theta), \tag{A.2a}$$

$$\varepsilon_\theta = \frac{1}{E}(\sigma_\theta - \upsilon\sigma_r), \tag{A.2b}$$

$$\varepsilon_z = -\frac{\upsilon}{E}(\sigma_r + \sigma_\theta), \tag{A.2c}$$

$$\gamma_{r\theta} = \frac{\tau_{r\theta}}{G}. \tag{A.2d}$$

After rearranging Equations (A.2a,b and d),

$$\sigma_r = \frac{E}{1-\upsilon^2}(\varepsilon_r + \upsilon\varepsilon_\theta),$$

$$\sigma_\theta = \frac{E}{1-\upsilon^2}(\varepsilon_\theta + \upsilon\varepsilon_r),$$

$$\tau_{r\theta} = G\gamma_{r\theta},$$

where $\sigma_r$ and $\sigma_\theta$ are normal stresses in $r$ and $\theta$ directions respectively, $\varepsilon_r$ and $\varepsilon_\theta$ are normal strains in $r$ and $\theta$ directions respectively, $\tau_{r\theta}$ is the shear stress acting in $\theta$ direction and on the plane perpendicular to the $r$-axis and $\gamma_{r\theta}$ is the shear strain which is also the change of angle in radian between the planes perpendicular to $r$ and $\theta$ axes. Equations (A.2) will be applied to in-plane vibrations of circular discs or annuli because it is more convenient to model the stresses and strains in the radial and circumferential directions.

### *A.3.3 3-D Hooke's law*

Although Hooke's law in 3-D is not being used in the context of this thesis, the full set of equations are listed below for reference.

$$\varepsilon_x = \frac{\sigma_x}{E} - \frac{\upsilon}{E}(\sigma_y + \sigma_z),$$

$$\varepsilon_y = \frac{\sigma_y}{E} - \frac{\upsilon}{E}(\sigma_z + \sigma_x),$$

$$\varepsilon_z = \frac{\sigma_z}{E} - \frac{\upsilon}{E}(\sigma_x + \sigma_y),$$

$$\gamma_{xy} = \frac{\tau_{xy}}{G},\ \gamma_{xz} = \frac{\tau_{xz}}{G},\ \gamma_{yz} = \frac{\tau_{yz}}{G}.$$

After rearrangement, the above equations become

$$\sigma_x = \frac{E}{(1+\upsilon)(1-2\upsilon)}[(1-\upsilon)\varepsilon_x + \upsilon(\varepsilon_y + \varepsilon_z)],$$

$$\sigma_y = \frac{E}{(1+\upsilon)(1-2\upsilon)}[(1-\upsilon)\varepsilon_y + \upsilon(\varepsilon_z + \varepsilon_x)],$$

$$\sigma_z = \frac{E}{(1+\upsilon)(1-2\upsilon)}[(1-\upsilon)\varepsilon_z + \upsilon(\varepsilon_x + \varepsilon_y)],$$

$$\tau_{xy} = G\gamma_{xy},\ \tau_{xz} = G\gamma_{xz},\ \tau_{yz} = G\gamma_{yz},$$

where $\sigma_z$ is the normal stress parallel to the *z*-axis, $\tau_{xz}$ is the shear stress acts in the *z* direction on the *yz* plane and $\tau_{yz}$ is shear stress acts in the *z* direction on the *xz* plane. All other components are similarly defined as in the 2-D case. From static equilibrium, it is required that $\tau_{xy} = \tau_{yx}$, $\tau_{xz} = \tau_{zx}$ and $\tau_{yz} = \tau_{zy}$.

# Appendix B

## Derivation and Analytical Solution of the Linear Uniaxial Model for Steady Whirling Rods

### *B.1 Governing Equation of Motion*

Consider a whirling non-vibrating rod in Eulerian coordinate $z$ rotating at constant angular velocity $\Omega$ with material density $\rho(z)$ and cross-sectional area $A(z)$ in Figure B.1.

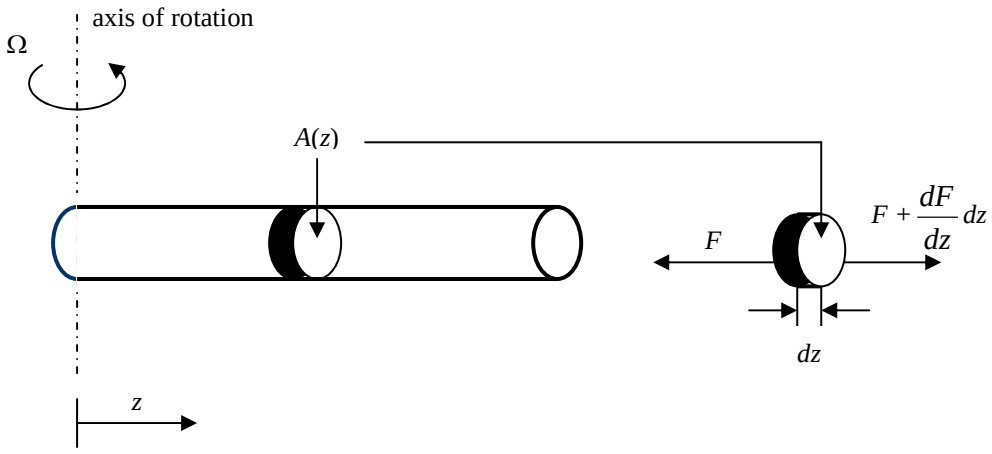


Figure B.1. Geometric configuration of a rod rotating about the axis of rotation at an angular velocity Ω. $A(z)$ is the cross-sectional area of the rod and $\rho(z)$ is the material density.

According to the free body diagram of the infinitesimal element being cut out of the rotating rod, $\frac{dF}{dz} = -\rho(z)A(z)\Omega^2 z$. But from Hooke's law, $F = EA(z)\varepsilon_z$, where $\varepsilon_z$ is the axial strain in Eulerian coordinate. As a result,

$$\frac{d}{dz}\left(EA(z)\varepsilon_z\right) = -\rho(z)A(z)\Omega^2 z. \tag{B.1}$$

For an isotropic and prismatic rod, Equation (B.1) becomes

$$\frac{E}{\rho_0}\frac{d\varepsilon_z}{dz} = -\Omega^2 z, \tag{B.2}$$

where $\rho_0$ is the constant density of the non-whirling undeformed rod. By using the relationship $z = x + u(x)$, where $u = u(x)$ is the axial displacement at location $x$, Equation (B.2) in Lagrangian coordinate $x$ becomes

$$\left(1+\frac{du}{dx}\right)^{-1}\frac{E}{\rho_0}\frac{d\varepsilon_x}{dx} = -\Omega^2 (x+u). \tag{B.3}$$

For small strain analysis, $\left|\frac{du}{dx}\right| << 1$, and substituting $\varepsilon_x = \frac{du}{dx}$, Equation (B.3) becomes

$$\frac{E}{\rho_0}\frac{d^2u}{dx^2} = -\Omega^2 (x+u),\ 0 < x < L, \tag{B.4a}$$

where $L$ is the length of the non-whirling undeformed rod. Assuming a clamped boundary condition at $x = 0$

$$u(0) = 0 \tag{B.4b}$$

and free boundary condition at $x = L$, i.e. $\sigma(L) = 0$,

$$EA_0\left[\frac{du}{dx}\right]_{x=L} = 0, \tag{B.4c}$$

where $A_0$ is the uniform cross-sectional area of the rod. Equations (B.4) are the governing equations of steady motion for a prismatic whirling rod.

### *B.2 Analytical Solution*

Equation (B.4a) is a second order linear ordinary differential equation with two Boundary Conditions (B.4b,c). The general solution for Equation (B.4a) is

$$u(x) = a\cos(kx) + b\sin(kx) - x,$$

where $k = \Omega\sqrt{\frac{\rho_0}{E}}$. By applying the Boundary Condition (B.4b),

$$a = 0.$$

By applying the Boundary Condition (B.4c),

$$b = \frac{1}{k\cos(kL)}.$$

Hence, the analytical solution of Equations (B.4) becomes

$$u(x) = \frac{\sin(kx)}{k\cos(kL)} - x.$$

The above derivation in B.1 is taken from Inman (2001). The analytical solution in B.2 can be referred to Bhuta and Jones (1963a).

# Appendix C

## Derivation of Classical Approach for Axial Natural Frequencies of Stationary Rods

### *C.1 Receptance of a Clamped-Free Rod*

The governing equation for the axial vibration of a stationary rod with uniform cross-sectional area $A_0$ may be described by (Inman 2001)

$$\frac{\partial^2 u}{\partial t^2} = \frac{E}{\rho_0}\frac{\partial^2 u}{\partial x^2}, \qquad 0 < x < L,\ t > 0 \tag{C.1}$$

where $u = u(x,t)$ is the axial displacement, $\rho_0$ is the density of the rod, $E$ is the Young's modulus, $x$ is the spatial variable in the axial direction and $t$ is the time variable. The geometric configuration of a stationary rod is depicted in Figure C.1.

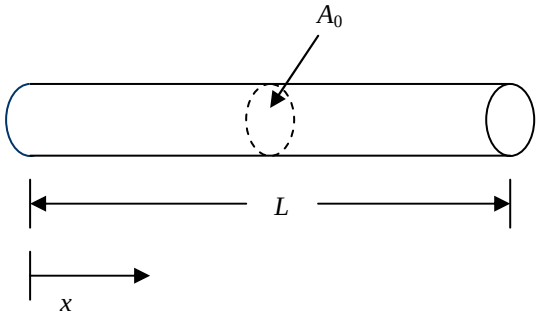


Figure C.1. Geometric configuration of a stationary rod with length $L$ and uniform cross-sectional area $A_0$.

Assume a normal mode of vibration $u(x,t) = U(x)\, e^{j\omega t}$ , then from Equation (C.1),

$$\frac{\partial^2 U}{\partial x^2} + \frac{\rho_0 \omega^2}{E} U = 0. \tag{C.2}$$

Hence $U(x) = a\cos(\kappa x) + b\sin(\kappa x)$, where $\kappa = \omega\sqrt{\frac{\rho_0}{E}}$ , $\omega$ is the axial vibration frequency of the rod, $a$ and $b$ are arbitrary constants.

(i) If the rod is clamped at $x = 0$ and an excitation force $F\,e^{j\omega t}$ is applied axially at $x = L$, then

$$U(0) = 0 \text{ and } EA_0 \left.\frac{\partial U}{\partial x}\right|_{x=L} = F.$$

As a result, from the solution of Equation (C2), $U(x) = \dfrac{F\sin(\kappa x)}{EA_0\kappa\cos(\kappa L)}$.

(ii) If the rod is free at $x = L$ and an excitation force $F\,e^{j\omega t}$ is applied axially at $x = 0$, then

$$EA_0 \left.\frac{\partial U}{\partial x}\right|_{x=0} = F \text{ and } \left.\frac{\partial U}{\partial x}\right|_{x=L} = 0.$$

As a result, from the solution of Equation (C2), $U(x) = -\dfrac{F\cos[\kappa(L-x)]}{EA_0\kappa\sin(\kappa L)}$.

(iii) If the rod is free at $x = 0$ and an excitation force $F\,e^{j\omega t}$ is applied axially at $x = L$, then

$$\left.\frac{\partial U}{\partial x}\right|_{x=0} = 0 \text{ and } EA_0 \left.\frac{\partial U}{\partial x}\right|_{x=L} = F.$$

As a result, from the solution of Equation (C2), $U(x) = -\dfrac{F\cos(\kappa x)}{EA_0\kappa\sin(\kappa L)}$.

Consider the geometric configuration of two smaller sub-structures combined together to form a larger sub-structure in Figure C.2.

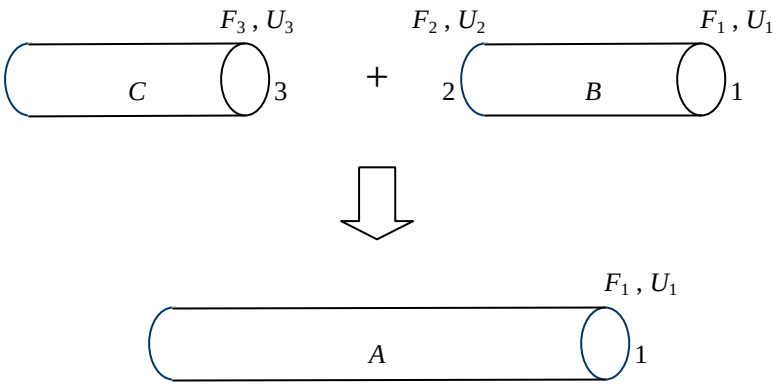


Figure C.2. Geometric configuration of combining two smaller sub-structures *B* and *C* to form a larger sub-structure *A*. Applied forces are $F_1$, $F_2$, $F_3$ with corresponding displacements $U_1$, $U_2$, $U_3$ at locations 1, 2, 3 respectively.

From the receptance approach developed by Bishop and Johnson (1960), receptance $\alpha_{\xi\eta}$ of a structure, for example a rod, is defined as $\alpha_{\xi\eta} = \frac{U}{F}$, where displacement $U$ is at location $\xi$ and applied force $F$ is at location $\eta$. Now in Figure C.2, the addition of two sub-structures $B$ and $C$ by joining location 2 and location 3 gives a receptance at location 1 of a combined sub-structure $A$. If the applied forces are $F_1$, $F_2$, $F_3$ with corresponding displacements $U_1$, $U_2$, $U_3$ at locations 1, 2 and 3 respectively, then

$$U_1 = \beta_{11} F_1 + \beta_{12} F_2 , \tag{C.3}$$

$$U_2 = \beta_{22} F_2 + \beta_{21} F_1 , \tag{C.4}$$

$$U_3 = \gamma_{33} F_3 , \tag{C.5}$$

where $\beta_{\xi\eta}$ is the receptance for sub-structure $B$ with displacement at location $\xi$ and applied force at location $\eta$. Similarly, $\gamma_{\xi\eta}$ is the receptance for sub-structure $C$ with displacement at location $\xi$ and applied force at location $\eta$. Note that displacements in Equation (C.3) and Equation (C.4) produced by different applied forces are additive is only true when the system is linear. Since $U_3 = U_2$, from Equation (C.4) and (C.5), $\gamma_{33} F_3 = \beta_{22} F_2 + \beta_{21} F_1$. But $F_3 = -F_2$, hence

$$F_2 = -\frac{\beta_{21} F_1}{\beta_{22} + \gamma_{33}} . \tag{C.6}$$

Substituting Equation (C.6) into Equation (C.3) and using Maxwell's reciprocal property $\beta_{12} = \beta_{21}$,

$$\alpha_{11} = \frac{U_1}{F_1} = \beta_{11} - \frac{(\beta_{12})^2}{\beta_{22} + \gamma_{33}} , \tag{C.7}$$

where $\alpha_{11}$ is the receptance of the combined structure $A$ with displacement at location 1 and applied force at location 1. For a rod with length $L$ clamped at $x = 0$ and free at $x = L$, it can be viewed as $n$ sub-structures being joined together end-to-end and have a total length equals to $L$, where $n$ is a finite positive integer. If a simple harmonic force is now applied axially at $x = L$, the total receptance of the whole rod can be found by joining two adjacent sub-structures at a time starting from the fixed end to form a larger combined sub-structure until there is only one structure left. To give an example, suppose a clamped-free rod with length $L$ is divided into $n$ sub-rods. Each sub-rod is labelled in such a fashion that sub-rod $i$ is joined by sub-rod $i$–1 at one end and sub-rod $i$+1 at the other end, where $i = 2, 3, \ldots, n-1$. Starting from the fixed end and treating sub-rod 1 as sub-structure $C$, sub-rod 2 as sub-structure $B$ and the resultant sub-rod as

sub-structure $A$ in Figure C.2, together with the results from (i), (ii) and (iii), the receptance $\alpha_{11}$ in Equation (C.7) can be found by substituting

$$\beta_{11} = \beta_{22} = -\frac{\cos(\kappa_2 L_2)}{EA_2\kappa_2 \sin(\kappa_2 L_2)}, \beta_{12} = -\frac{1}{EA_2\kappa_2 \sin(\kappa_2 L_2)}, \gamma_{33} = \frac{\sin(\kappa_1 L_1)}{EA_1\kappa_1 \cos(\kappa_1 L_1)},$$

where $\kappa_j = \omega\sqrt{\frac{\rho_j}{E}}$, $j$ = 1, 2. $\rho_j$ is the constant density of sub-rod $j$, $L_j$ is the length of sub-rod $j$ and $A_j$ is the uniform cross-sectional area of sub-rod $j$. The receptance $\alpha_{11}$ of the resultant sub-structure will become $\gamma_{33}$ in Equation (C.7) for the next two sub-structures integration. The now remaining sub-rods will be renumbered again beginning from 1 and the whole process will repeat itself until there is only one structure left. This classical receptance approach is suitable for uniform cross-sectional area rods as well as tapered rods because each sub-rod $j$ can be approximated by a constant cross-sectional area $A_j$.

## *C.2 Matlab M-file Program on Classical Receptance Method*

```
% This m-file utilises the receptance substructuring approach to solve for the
% natural frequencies of an undamped rod vibrating axially. The bar profile is the
% result obtained from the numerical calculations. It also calls function recept.m.

clear all;
global section_length area youngs_mod density No_of_sections

No_of_sections=100; % Break strained bar into this many equal length sections

density0=7850;          % density in kg/m3.
youngs_mod=200e9;       % modulus of rigidity in Pa.
nu=0.29;                % Poisson ratio.
area0=0.0004;           % uniform cross-sectional area in m2.
length0=1;              % length of the rod in m.
n=10;                   % # of coefficients in the series.

% Input bar strained profile obtained from numerical calculations.
a=[0.244732 0.00001 -0.092261 0.000427 0.008298 0.003533 -0.009395
0.005949 -0.00182 0.000219];
```

```
u=0;
for i=1:No_of_sections
   v=u;
   x=(i-0.5)*length0/No_of_sections;
   y=i*length0/No_of_sections;
   u=0; dudx=0; ux=0; value1=1; value2=1;
   for j=1:n
     dudx=dudx+j*a(j)*value1;
     value1=value1*x;
     value2=value2*y;
     u=u+a(j)*value2;
   end;
   strain=dudx+0.5*dudx*dudx;    % nonlinear strain-displacement relationship.
   area(i)=area0*(1-nu*strain)^2;
   density(i)=density0*area0/(1+dudx)/area(i);
   section_length(i)=(length0/No_of_sections)+(u-v);
end;

% Frequency range omega in rad/sec

w=logspace(3,5,300);

% calculate the total receptance of the rod

for i=1:length(w)
 Recept_total(i)=recept(w(i));
end;

% Resonance frequencies are stored into resonance(j), while the receptance of the
% corresponding resonance is stored in Recept_max(j).

j=0;
for i=2:(length(w)-1)
 if (Recept_total(i-1)<=Recept_total(i))&(Recept_total(i)>=Recept_total(i+1))
   j=j+1;
   resonance(j)=w(i);
   Recept_max(j)=Recept_total(i);
 end;
```

```
end;

% plot Tip Receptance v Frequency.

loglog(w/(2*pi),Recept_total);
xlabel('Frequency (Hz)');
ylabel('Receptance Magnitude (m/N)');
title('Tip Receptance v Frequency (angular velocity = 500rev/s)');
grid on;

function y=recept(w)          % m-file that calculates the receptance

global section_length area youngs_mod density No_of_sections

lambda=sqrt(density(1)/youngs_mod)*w;
Recept_sum=tan(lambda*section_length(1))/(youngs_mod*area(1)*lambda);

for i=2:No_of_sections
  lambda=sqrt(density(i)/youngs_mod)*w;
  Recept_00=-1/(youngs_mod*area(i)*lambda*tan(lambda*section_length(i)));
  Recept_0L=-1/(youngs_mod*area(i)*lambda*sin(lambda*section_length(i)));
  Recept_sum=Recept_00-(Recept_0L^2)/(Recept_00+Recept_sum);
end;

y=abs(Recept_sum);
```

Further information on receptance approach can be directed to Hestermann *et al*. (1996).

# Appendix D

## Derivation of the Linear Coupled Model for Vibrating Rotating Annuli

The derivations on the in-plane displacements of rotating annuli are based on the previous works from Biezeno and Grammel (1954) and Bhuta and Jones (1963b). Consider an annular plate rotating with a constant angular velocity Ω in Eulerian coordinates ($R$,Θ) with thickness $y(R)$ depicted in Figure D.1.

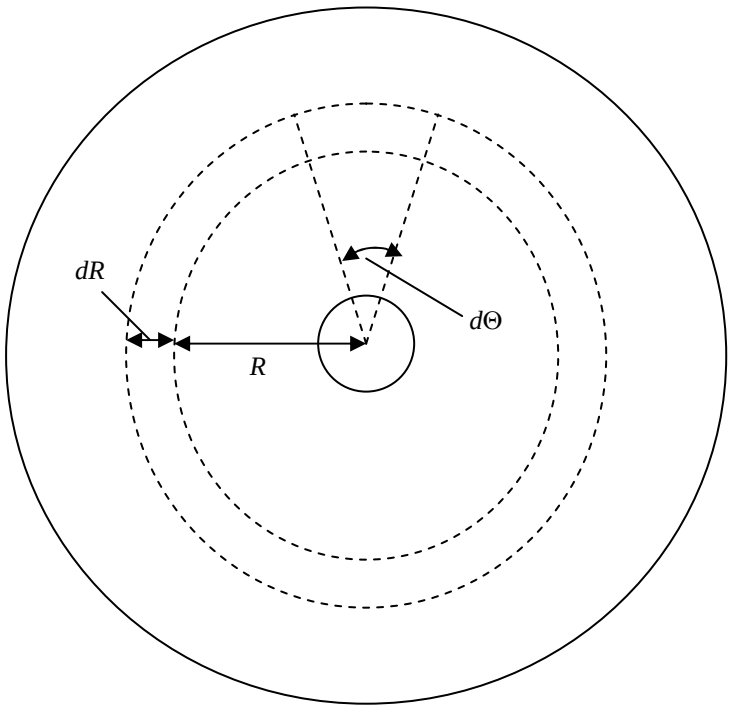


Figure D.1. A view of an annular plate depicted in Eulerian coordinates ($R$,Θ).

An infinitesimally small element at radial distance $R$ subjected to body forces $F_R$ and $F_\Theta$ in $R$ and Θ directions respectively is taken from the annular plate in Figure D.1. A free body diagram of such an element is magnified in Figure D.2.

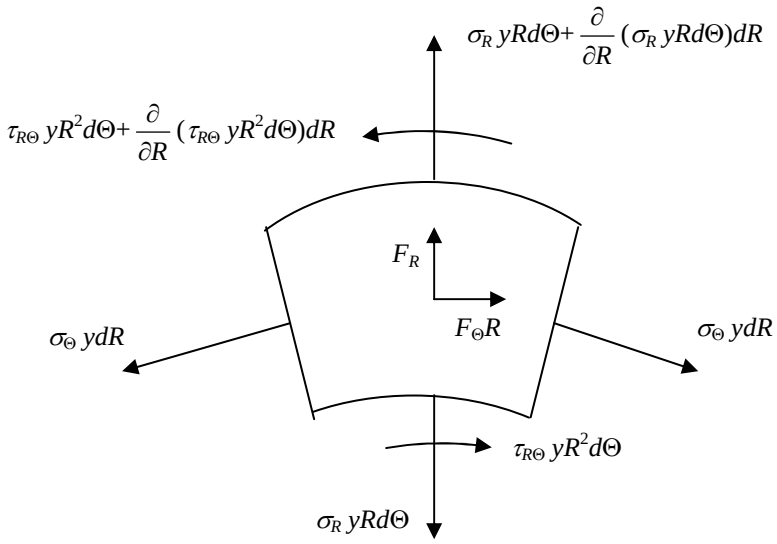


Figure D.2. A magnified view of an infinitesimally small element taken from Figure D.1.

Suppose the infinitesimally small element in Figure D.2 is subjected to normal stresses $\sigma_R$ and $\sigma_\Theta$ in $R$ and $\Theta$ directions respectively and a shear stress $\tau_{R\Theta}$ in the $\Theta$ direction on the surface perpendicular to the $R$ axis, then by summing forces in the radial direction $R$,

$$\frac{\partial}{\partial R}(\sigma_R\, yRd\Theta)dR - 2\sigma_\Theta\, y \sin\left(\frac{d\Theta}{2}\right)dR = F_R\,.$$

Since $|\, d\Theta\, | << 1$, $\sin\left(\frac{d\Theta}{2}\right) \approx \frac{d\Theta}{2}$. Hence the above equation becomes

$$\frac{\partial}{\partial R}(\sigma_R\, yRd\Theta)dR - \sigma_\Theta\, yd\Theta dR = F_R\,,$$

or

$$\frac{\sigma_R}{y}\frac{dy}{dR} + \frac{\partial \sigma_R}{\partial R} + \frac{\sigma_R - \sigma_\Theta}{R} = f_R\,, \qquad \text{(D.1a)}$$

where $F_R$ is the radial body force in Eulerian coordinates and $f_R$ is the radial body force per unit volume in Eulerian coordinates. By summing moment about the centre of the annular plate,

$$\frac{\partial}{\partial R}(\tau_{R\Theta}\, yR^2 d\Theta)dR = F_\Theta R,$$

or

$$\frac{\tau_{R\Theta}}{y}\frac{dy}{dR} + \frac{\partial \tau_{R\Theta}}{\partial R} + \frac{2\tau_{R\Theta}}{R} = f_\Theta\,, \qquad \text{(D.1b)}$$

where $F_\Theta$ is the circumferential body force in Eulerian coordinates and $f_\Theta$ is the circumferential body force per unit volume in Eulerian coordinates. Equations (D.1) are the governing equations for rotating discs in Eulerian coordinates ($R$, $\Theta$). Equations (D.1) can be transformed into Lagrangian coordinates ($r$,$\theta$) by using the relationship $R = r + u(r, t)$ and the approximation $\frac{dR}{dr} \approx \left(1+\frac{\partial u}{\partial r}\right)$. For small strain analysis, $\left|\frac{\partial u}{\partial r}\right| << 1$ and $\left|\frac{u}{r}\right| << 1$, Equations (D.1) become

$$\frac{\sigma_r}{y}\frac{dy}{dr}+\frac{\partial \sigma_r}{\partial r}+\frac{\sigma_r-\sigma_\theta}{r}=f_r\,, \tag{D.2a}$$

$$\frac{\tau_{r\theta}}{y}\frac{dy}{dr}+\frac{\partial \tau_{r\theta}}{\partial r}+\frac{2\tau_{r\theta}}{r}=f_\theta\,, \tag{D.2b}$$

where $\sigma_r$ is the radial normal stress in Lagrangian coordinates, $\sigma_\theta$ is the circumferential normal stress in Lagrangian coordinates, $\tau_{r\theta}$ is the circumferential shear stress acting in the $\theta$ direction on the surface perpendicular to the $r$-axis in Lagrangian coordinates, $f_r$ is the radial body force per unit volume in Lagrangian coordinates and $f_\theta$ is the circumferential body force per unit volume in Lagrangian coordinates. It is known that from 2-D Hooke's law and axisymmetric linear strain-displacement relationships,

$$\sigma_r=\frac{E}{1-\upsilon^2}\left[\frac{\partial u}{\partial r}+\upsilon\frac{u}{r}\right],\ \sigma_\theta=\frac{E}{1-\upsilon^2}\left[\frac{u}{r}+\upsilon\frac{\partial u}{\partial r}\right],\ \tau_{r\theta}=G\left[\frac{\partial v}{\partial r}-\frac{v}{r}\right] \tag{D.3a,b,c}$$

and the body forces per unit volume

$$f_r=\rho_0\,a_r\,,\ f_\theta=\rho_0\,a_\theta\,, \tag{D.3d,e}$$

where $u$ is the Lagrangian radial displacement, $v$ is the Lagrangian circumferential displacement, $a_r$ is the Lagrangian radial acceleration, $a_\theta$ is the Lagrangian circumferential acceleration and $\rho_0$ is the constant density of the isotropic material of the annulus. If $\mathbf{r}$ denotes the position vector starting from the centre of the annulus to a given point in the annular plate, then $\mathbf{r} = (r + u)\mathbf{e}_r + v\mathbf{e}_\theta$, where $\mathbf{e}_r$ and $\mathbf{e}_\theta$ are the unit vectors in radial and circumferential directions respectively. Since

$$\boldsymbol{\Omega} = \Omega\,\mathbf{e}_z\,,\ \dot{\mathbf{e}}_r = \boldsymbol{\Omega}\times\mathbf{e}_r = \Omega\,\mathbf{e}_\theta \text{ and } \dot{\mathbf{e}}_\theta = \boldsymbol{\Omega}\times\mathbf{e}_\theta = -\Omega\,\mathbf{e}_r\,,$$

where dots denote the time derivatives, it follows that

$$\mathbf{a} = a_r\,\mathbf{e}_r + a_\theta\,\mathbf{e}_\theta = \ddot{\mathbf{r}}$$

$$= [\,\ddot{u} - 2\Omega\dot{v} - \Omega^2(r+u) - v\dot{\Omega}\,]\mathbf{e}_r + [\,\ddot{v} + 2\Omega\dot{u} - \Omega^2 v - (r+u)\dot{\Omega}\,]\mathbf{e}_\theta\,.$$

Thus

$$a_r = \ddot{u} - 2\Omega\dot{v} - \Omega^2(r+u) - v\dot{\Omega}, \tag{D.3f}$$

$$a_\theta = \ddot{v} + 2\Omega\dot{u} - \Omega^2 v - (r+u)\dot{\Omega}. \tag{D.3g}$$

Substituting Equations (D.3) into Equations (D.2) and assuming constant angular velocity $\Omega$,

$$\frac{\partial^2 u}{\partial r^2} + \left(\frac{1}{y}\frac{dy}{dr} + \frac{1}{r}\right)\frac{\partial u}{\partial r} + \left(\frac{\upsilon}{ry}\frac{dy}{dr} - \frac{1}{r^2}\right)u = (1-\upsilon^2)\frac{\rho_0}{E}\left[\frac{\partial^2 u}{\partial t^2} - 2\Omega\frac{\partial v}{\partial t} - (r+u)\Omega^2\right], \tag{D.4a}$$

$$\frac{\partial^2 v}{\partial r^2} + \frac{1}{r}\frac{\partial v}{\partial r} - \frac{v}{r^2} = \frac{\rho_0}{G}\left[\frac{\partial^2 v}{\partial t^2} + 2\Omega\frac{\partial u}{\partial t} - v\Omega^2\right]. \tag{D.4b}$$

By assuming a parallel annulus with constant thickness $y$, Equations (D.4) become

$$\frac{\partial^2 u}{\partial r^2} + \frac{1}{r}\frac{\partial u}{\partial r} - \frac{u}{r^2} = (1-\upsilon^2)\frac{\rho_0}{E}\left[\frac{\partial^2 u}{\partial t^2} - 2\Omega\frac{\partial v}{\partial t} - (r+u)\Omega^2\right],$$

$$\frac{\partial^2 v}{\partial r^2} + \frac{1}{r}\frac{\partial v}{\partial r} - \frac{v}{r^2} = \frac{\rho_0}{G}\left[\frac{\partial^2 v}{\partial t^2} + 2\Omega\frac{\partial u}{\partial t} - v\Omega^2\right],$$

which is the Bhuta and Jones' model. By using the relation $v(r, t) = r\vartheta(r, t)$, Equations (D.4) become

$$\frac{\partial^2 u}{\partial r^2} + \left(\frac{1}{y}\frac{dy}{dr} + \frac{1}{r}\right)\frac{\partial u}{\partial r} + \left(\frac{\upsilon}{ry}\frac{dy}{dr} - \frac{1}{r^2}\right)u = (1-\upsilon^2)\frac{\rho_0}{E}\left[\frac{\partial^2 u}{\partial t^2} - 2\Omega r\frac{\partial \vartheta}{\partial t} - (r+u)\Omega^2\right],$$

$$\frac{\partial^2 \vartheta}{\partial r^2} + \left(\frac{1}{y}\frac{dy}{dr} + \frac{3}{r}\right)\frac{\partial \vartheta}{\partial r} = \frac{\rho_0}{G}\left[\frac{\partial^2 \vartheta}{\partial t^2} + \frac{2\Omega}{r}\frac{\partial u}{\partial t} - \vartheta\Omega^2\right],$$

which is the Biezeno and Grammel's model. Notice that the Biezeno and Grammel's model takes the thickness profile $y = y(r)$ of a stationary annulus into account, while Bhuta and Jones's model keep the thickness $y$ to be uniform. In addition, both models treat the material density as a uniform quantity.

# Appendix E

## Existence and Uniqueness of Solutions for Two-Point Boundary Value Problems

Let $\Lambda[u] = a_0(x)u'' + a_1(x)u' + a_2(x)u$ be a linear second order differential expression with continuous coefficients, $B_1[u] = a_{11}u(x_1) + a_{12}u'(x_1) + b_{11}u(x_2) + b_{12}u'(x_2)$, and $B_2[u] = a_{21}u(x_1) + a_{22}u'(x_1) + b_{21}u(x_2) + b_{22}u'(x_2)$ be two boundary functions with boundaries at $x = x_1$ and $x = x_2$ . Now consider the following nonhomogeneous boundary value problem

$$\Lambda[u] = f(x), \tag{E.1a}$$

$$B_1[u] = c_1, \tag{E.1b}$$

$$B_2[u] = c_2, \tag{E.1c}$$

where $c_1$ and $c_2$ are constants, and the associated homogeneous boundary value problem

$$\Lambda[\eta] = 0, \tag{E.2a}$$

$$B_1[\eta] = 0, \tag{E.2b}$$

$$B_2[\eta] = 0. \tag{E.2c}$$

Since Equations (E.2) have either a nontrivial solution or the trivial solution only, the following theorem is established:

Theorem. If Equations (E.2) has a nontrivial solution, then Equations (E.1) has a solution if $f(x)$, $c_1$, $c_2$ satisfy certain conditions. If this is the case, then Equations (E.1) has infinitely many solutions. If, however, Equations (E.2) has the trivial solution only, then Equations (E.1) has a unique solution for any $f(x)$, $c_1$, $c_2$.

Proof. Suppose $\Lambda[\eta] = 0$ has two linearly independent solutions $\eta_1$ and $\eta_2$. Hence the general solution can be written in the form $\eta = \alpha_1\eta_1 + \alpha_2\eta_2$ and $\Lambda[u] = f(x)$ will have the general solution $u = u_0 + \alpha_1\eta_1 + \alpha_2\eta_2$ , where $u_0$ is a particular solution of $\Lambda[u] = f(x)$. In order to satisfy the boundary conditions of Equations (E.1), the following system of equations must be solved,

$$B_1[u] = B_1[u_0] + \alpha_1 B_1[\eta_1] + \alpha_2 B_1[\eta_2] = c_1,$$

$$B_2[u] = B_2[u_0] + \alpha_1 B_2[\eta_1] + \alpha_2 B_2[\eta_2] = c_2.$$

These two linear nonhomogeneous equations for $\alpha_1$, $\alpha_2$ have the form

$$\alpha_1 B_1[\eta_1] + \alpha_2 B_1[\eta_2] = c_1 - B_1[u_0], \tag{E.3a}$$

$$\alpha_1 B_2[\eta_1] + \alpha_2 B_2[\eta_2] = c_2 - B_2[u_0], \tag{E.3b}$$

with the coefficient determinant $\Delta = \begin{vmatrix} B_1[\eta_1] & B_1[\eta_2] \\ B_2[\eta_1] & B_2[\eta_2] \end{vmatrix}$. The following two cases arise:

(1) $\Delta \neq 0$. In this case, Equations (E.3) have a unique solution $\alpha_1$, $\alpha_2$ and the solution of Equations (E.1) exists and is uniquely determined. Since $\eta = \alpha_1 \eta_1 + \alpha_2 \eta_2$, from the boundary conditions in Equations (E.2),

$$\alpha_1 B_1[\eta_1] + \alpha_2 B_1[\eta_2] = 0, \tag{E.4a}$$

$$\alpha_1 B_2[\eta_1] + \alpha_2 B_2[\eta_2] = 0. \tag{E.4b}$$

Hence the above system has the trivial solution only because $\Delta \neq 0$, which implies Equations (E.2) has the trivial solution only.

(2) $\Delta = 0$. In this case, Equations (E.4) have a nontrivial solution $\alpha_1$, $\alpha_2$. Hence Equations (E.2) have a nontrivial solution. In general, Equations (E.3) have no solution. However, there are values of $c_1 - B_1[u_0]$ and $c_2 - B_2[u_0]$ for which the system may have a solution and whenever a nonhomogeneous system of linear equations with a vanishing coefficient determinant has a nontrivial solution (i.e. if the equations are linearly dependent) then it has infinitely many solutions.

Example: Solve $y'' + y = 0$, with boundary conditions

(i) $y(0) = 0$ and $y(\pi) = 1$,

(ii) $y(0) = 0$ and $y\left(\frac{\pi}{6}\right) = 1$,

(iii) $y(0) = 0$ and $y(\pi) = 0$.

Solution: The general solution of the differential equation is $y(x) = A\sin(x) + B\cos(x)$, where $A$ and $B$ are arbitrary constants to be determined from the boundary conditions.

(i) No solutions.

(ii) $A = 2$ and $B = 0$. Unique solution.

(iii) Infinitely many solutions.

The above discussions are taken from Sagan (1989). For further consultancy on existence and uniqueness of solution for heat and wave equations, readers may visit the same reference.